

12-2011

Adsorption and Diffusion of Light Hydrocarbons in DDR Zeolite

Adam Vidoni

Follow this and additional works at: <http://digitalcommons.library.umaine.edu/etd>

 Part of the [Polymer Science Commons](#)

Recommended Citation

Vidoni, Adam, "Adsorption and Diffusion of Light Hydrocarbons in DDR Zeolite" (2011). *Electronic Theses and Dissertations*. 1562.
<http://digitalcommons.library.umaine.edu/etd/1562>

This Open-Access Thesis is brought to you for free and open access by DigitalCommons@UMaine. It has been accepted for inclusion in Electronic Theses and Dissertations by an authorized administrator of DigitalCommons@UMaine.

**ADSORPTION AND DIFFUSION OF LIGHT
HYDROCARBONS IN DDR ZEOLITE**

By

Adam Vidoni

B.S.Ch.E, Bucknell University 2004

A THESIS

Submitted in Partial Fulfillment of the

Requirements for the Degree of

Doctor of Philosophy

(in Chemical Engineering)

The Graduate School

The University of Maine

December, 2011

Advisory Committee:

Douglas Ruthven, Professor of Chemical Engineering, Advisor

William DeSisto, Professor of Chemical Engineering

Michael Mason, Professor of Chemical Engineering

Brian Frederick, Professor of Chemistry

Harry Deckman, Senior Scientific Advisor, ExxonMobil Research

THESIS ACCEPTANCE STATEMENT

On behalf of the Graduate Committee for Adam Vidoni, I affirm that this manuscript is the final and accepted thesis. Signatures of all committee members are on file with the Graduate School at the University of Maine, 42 Stodder Hall, Orono, Maine.

Douglas Ruthven, Professor

Date:

LIBRARY RIGHTS STATEMENT

In present this statement in partial fulfillment of the requirements for an advanced degree at The University of Maine, I agree that the Library shall make it freely available for inspection. I further agree that permission for “fair use” copying of this thesis for scholarly purposes may be granted by the Librarian. It is understood that any copying or publication of this thesis for financial gain shall not be allowed without my written permission.

Signature:

Date:

**ADSORPTION AND DIFFUSION OF LIGHT
HYDROCARBONS IN DDR ZEOLITE**

By Adam Vidoni

Thesis Advisor: Dr. Douglas M. Ruthven

An Abstract of the Thesis Presented
in Partial Fulfillment of the Requirements for the
Degree of Doctor of Philosophy
(in Chemical Engineering)
December, 2011

This thesis reports the results of an experimental study aimed at characterizing the transport properties of DDR crystals (a pure silica zeolite analog) by the “zero length column” technique. This material is potentially useful as a size selective molecular sieve adsorbent for separation of $\text{CH}_4 - \text{CO}_2$ in the upgrading of low grade natural gas (or bio-gas) as well as for the separation of $\text{C}_3\text{H}_6 - \text{C}_3\text{H}_8$ for production of polypropylene. In both these applications pure silica zeolites (such as DDR) have important practical advantages over the traditional cationic zeolites since they are hydrophobic and have low catalytic activity.

Intracrystalline diffusivities of CH_4 in DDR were measured for the single component system and in the presence of an excess of CO_2 . In contrast to the predictions from recent molecular simulations the experimental data show that the diffusivity of methane is increased (rather than decreased) by the presence of CO_2 . This is as expected from transition state theory if CH_4 and CO_2 are competitively adsorbed. In contrast the data for C_2H_6 (and C_2H_4) show no significant difference in diffusivity in the presence of

CO₂, suggesting non-competitive adsorption. This result can be explained if it is assumed that C₂ hydrocarbon molecules occupy preferentially the window sites. The equilibrium isotherms provide tentative support for this hypothesis.

Some of the samples showed evidence of significant surface resistance to mass transfer (in addition to intracrystalline diffusional resistance). This led to a further development of the mathematical model used to analyze the ZLC response curves and hence to an extension of the ZLC technique to allow the simultaneous measurement of both the surface rate coefficient and the intracrystalline diffusivity.

A detailed study of CO₂ equilibrium on several different samples of both DDR and silicalite (another pure silica zeolite) was also undertaken in order to determine the effect of surface hydroxyl content.

ACKNOWLEDGEMENTS

The present study was made possible, first of all, thanks to the support and guidance of my thesis advisor Dr. Douglas Ruthven. The funding was provided by a GOALI grant from NSF which is gratefully acknowledged. Even then I could not have accomplished this project without his guidance, knowledge and advice. I consider myself to be truly fortunate to be able to work for and with such a great person and engineer. I would also like to thank the rest of my committee for their support and guidance through my at U.Maine.

I am sincerely grateful to the staff of the Chemical Engineering Department for their advice and help with the construction of the ZLC apparatus, especially Keith Hodgins, Nick Hill, Jon Spender and Amos Cline. I am also grateful to Robert Marriott (Alberta Sulphur Research Laboratory) for providing the large ZLC cell.

Gratitude for helping me with my work is also due to my colleagues at the ExxonMobil laboratory in Annandale, NJ. I may have only been there for five months, but their guidance and advice gave me several years' worth of experience. In particular I would like to thank Harry Deckman and Peter Ravikovitch for their advice and assistance with all aspects of this work. Thanks are also due to Dave Calabro, Kathy Lee, Steve Cundy, Mobae Afeworki and Clarence Chase for their tolerance of my steady stream of inquiries during my time as an intern at the ExxonMobil Laboratory.

Sincere thanks to my parents, sister and family for being there throughout all of my endeavors. I would like to extend my gratitude onto my grandparents as well. Two men in particular: my maternal grandfather for being the biggest cheerleader for the education of myself and my cousins; and to my paternal grandfather. I never met him,

but he passed on this advice “Get an education; it’s the one thing that can’t be taken away from you”. Pending approval of this thesis, I will be his third grandchild to earn a doctorate.

Lastly I would like thank my adopted extended family in the greater Orono-Bangor area: Pat and Doug Ruthven for their lively living room conversation, and finally, to the Cassidy family for providing me with a second family on this side of the country.

TABLE OF CONTENTS

ACKNOWLEDGEMENTS.....	iii
LIST OF TABLES.....	ix
LIST OF FIGURES.....	xi
LIST OF SYMBOLS.....	xv

Chapter

1. INTRODUCTION.....	1
1.1. Methane Demand and Resources.....	1
1.2. Current Technology and Possible Alternatives.....	2
1.3. Aims and Scope of Present Project.....	3
2. HIGH SILICA ZEOLITES.....	5
2.1. Zeolite Background and History.....	5
2.2. Zeolite Structures.....	7
2.3. Zeolites Used for Natural Gas Purification	9
2.4. Olefin/Paraffin Separations.....	10
3. PREVIOUS STUDIES OF ADSORPTION AND DIFFUSION IN DDR.....	11
3.1. Equilibrium Isotherms.....	11
3.2. Intracrystalline Diffusion Measurements.....	11
3.3. Membrane Permeation Measurements.....	12
3.4. Molecular Simulations.....	15

4. EFFECT OF SURFACE HYDROXYLS ON ADSORPTION OF CO ₂ IN HIGH SILICA ZEOLITES.....	19
4.1. Introduction.....	19
4.2. Experimental Procedure.....	21
4.3. Results & Discussion.....	23
4.3.1. Henry Constants.....	31
4.3.2. Heats of Adsorption.....	35
4.3.3. Correlation of Adsorption with Hydroxyl Content.....	38
4.3.4. Saturation Capacity and Intracrystalline Pore Volume.....	43
4.4. Conclusions.....	45
5. ZLC METHOD.....	47
5.1. General Principle of the ZLC Method.....	47
5.2. Advantages and Limitations of the ZLC Technique.....	49
5.3. Mathematical Model.....	51
5.3.1. Long Time Asymptote Analysis.....	54
5.3.2. Intermediate Time Curve Analysis.....	56
5.4. Extended model.....	58
5.4.1. Experimental Verification.....	62
5.4.2. New Model Discussion.....	64

5.5. Experimental ZLC System.....	66
5.6. Experimental ZLC Procedure.....	67
5.6.1 Single Component ZLC Method.....	67
5.6.2 Binary System/ Counter-Current ZLC Method.....	67
5.6.3 Effect of Pressure Drop.....	68
6. ADSORPTION AND DIFFUSION OF METHANE WITHIN DDR ZEOLITES IN COMPETITION WITH CO ₂	70
6.1. Current DDR-Methane Diffusivity Data	70
6.2. CH ₄ /CO ₂ Competitive Diffusion ZLC Experimental Methods	72
6.3. CH ₄ /CO ₂ Competitive Diffusion Results and Discussion.....	79
6.3.1. Diffusivity Data.....	79
6.3.2. Equilibrium Data.....	85
6.3.3. Diffusion of Methane in Presence of CO ₂	86
6.4. DDR-Methane Conclusions.....	91
7. DIFFUSION OF ETHANE AND ETHYLENE IN DDR ZEOLITES IN COMPETITION WITH CO ₂	93
7.1. Analysis of ZLC Response Curves.....	93
7.2. Diffusion of Ethane in DDR.....	96
7.3. Diffusion of Ethylene in DDR.....	100
7.4. Analysis of L Values: Surface Resistance.....	103
7.5. Ethane and Ethylene Henry Constants.....	107
7.6. Ethane and Ethylene Results Discussion.....	109
7.7. Conclusions.....	111

8. DIFFUSION OF PROPYLENE IN DDR ZEOLITES IN COMPETITION	
WITH CO ₂	113
8.1. Propane/Propylene Results and Discussion.....	113
8.2. Propane/Propylene Conclusions.....	120
9. CONCLUSIONS AND RECOMMENDATIONS.....	121
9.1. General Considerations.....	121
9.2. Effect of Hydroxyl Concentration on CO ₂ Adsorption.....	122
9.3. Extended ZLC Model Incorporating Surface Resistance.....	123
9.4. Adsorption and Diffusion of Methane Within DDR in	
Competition with CO ₂	124
9.5. Adsorption and Diffusion of Ethane, Ethylene and Propylene within	
DDR in Competition with CO ₂	125
9.6. Modified MFI Zeolites, Adsorption and Diffusion with Light	
Alkanes.....	126
9.7. Recommendations.....	127
REFERENCES.....	129
APPENDIX A. ZLC RESPONSE FOR A CYLINDRICAL PARTICLE.....	134
APPENDIX B. CHARACTERIZATION OF MODIFIED	
SILICALITE ADSORBENTS.....	136
BIOGRAPHY OF THE AUTHOR.....	146

LIST OF TABLES

Table 4.1 Hydroxyl Densities of DDR & MFI Samples.....	24
Table 4.2 Comparison of Henry Constants, obtained using three different Methods.....	35
Table 4.3 Isosteric Heats of Adsorption and Zero-loading Heats of Adsorptions....	38
Table 4.4 Calculated Saturation Capacities for CO ₂ Adsorption	44
Table 5.1 Parameters Derived from ZLC Response Curves Comparing L and L'	62
Table 6.1 Details of DDR Crystals.....	72
Table 6.2 Summary of Parameters Derived from ZLC Response Curves.....	76
Table 6.3 Summary of Diffusivities and Henry Constants for CH ₄ -DDR.....	79
Table 6.4 Parameters Giving Temperature Dependence of D and K according to Eqs. 6.1 and 6.2.....	82
Table 6.5 Comparative Data for Diffusion of CH ₄ in 8-ring Zeolites.....	84
Table 6.6 Diffusivity Ratio and Product of Diffusivity and Henry Constants Trending with Temperature.....	88
Table 6.7 Data showing Apparent Activation Energy of Diffusion for Methane in Both Sorbates Purged by Both He and CO ₂	90
Table 7.1 Parameters Derived from Representative ZLC Response Curves.....	96
Table 7.2 Comparison of Diffusional Time constants for Ethane in DDR I at 298K.....	96
Table 7.3 Analysis of L' Values for DDR I, 2.4 mg Sample.....	106

Table 7.4 Summary of Kinetic and Equilibrium Parameters for C ₂ H ₆ and C ₂ H ₄ in DDR.....	108
Table 7.5 Comparison of KD (m ² s ⁻¹) for Methane and Ethane in DDR II.....	111
Table 8.1 Parameters giving Temperature Dependence of D and K.....	118
Table B.1 Resulting Kinetic and Equilibrium Data for Methane and Ethane.....	138
Table B.2 Resulting Kinetic and Equilibrium Data for Propane and Butane.....	138
Table B.3 Published Values for Henry Constants of Ethane and Propane in Silicalite.....	140
Table B.4 Published values for Diffusivity for Methane, Ethane and Propane in Silicalite	140

LIST OF FIGURES

Figure 2.1 Molecular Structures of Select Zeolites.....	8
Figure 3.1 Arrhenius Plot Showing Temperature Dependence of Corrected Diffusivities for Light Gases in DD3R Derived From Permeation Measurements	13
Figure 3.2 Temperature Dependence of Permeance of Methane in DD3R.....	14
Figure 3.3 Temperature Dependence of Permeance of CO ₂ in DD3R.....	15
Figure 3.4 Modeled Diffusion of CO ₂ and CH ₄ in DD3R Zeolite.....	17
Figure 3.5 DDR Unit Cell & Cage Structure.....	18
Figure 4.1 TGA Water Equilibrium Isotherms for MFI & DDR Samples.....	20
Figure 4.2 XRD Data for MFI & DDR Samples.....	23
Figure 4.3 NMR Data for MFI & DDR Samples.....	24
Figure 4.4 MFI CO ₂ Adsorption Isotherms	26
Figure 4.5 DDR CO ₂ Adsorption isotherms for DDR Samples	27
Figure 4.6 DDR CO ₂ Adsorption Isotherms Compared to Published Data.....	29
Figure 4.7 Plot Showing General Correlation Between Hydroxyl Concentration and Intercept Offset.....	30
Figure 4.8 Representative Virial Plots	32
Figure 4.9 Representative Langmuir Plots	34
Figure 4.10 van't Hoff Plot for MFI and DDR Samples.....	36
Figure 4.11 Calculated Loading Dependence of the Isosteric Heat of Adsorption	37
Figure 4.12 Variation of Henry Constants with Hydroxyl Density.....	40

Figure 4.13 Correlation of Langmuir Capacity (q_s) with Hydroxyl Density	41
Figure 4.14 Variation of Henry Constant Pre-Exponential Parameter (K_0) with Hydroxyl Concentration for DDR Samples.....	43
Figure 5.1 Schematic Diagram of the ZLC system.....	48
Figure 5.2 ZLC Packed Swagelok Union.....	48
Figure 5.3 Sample ZLC Data Comparing Diffusion and Equilibrium control.....	55
Figure 5.4 Representative ZLC Response Curve for Intermediate Time Analysis.....	58
Figure 5.5 ZLC Response Data with Mass Transfer Surface Resistance Affecting L Value.....	61
Figure 5.6 Relation of $1/L' \nu 1/F$ Showing Offset From Surface Resistance.....	63
Figure 6.1 SEM Photomicrographs of DDR Samples.....	73
Figure 6.2 Representative Data Plots for Methane-He 25 °C	74
Figure 6.3 Comparison of Time Constants for Both Purge Gasses Comparing D/R^2 vs F.....	78
Figure 6.4 Comparison of Time Constants for Both Purge Gasses Comparing $1/LV_s$ vs $1/F$	78
Figure 6.5 Arrhenius Plots Showing Temperature Dependence of Diffusivity in DDR I.....	80
Figure 6.6 Arrhenius Plots Showing Temperature Dependence of Diffusivity in DDR II.....	81
Figure 6.7 Comparison of ZLC Response Curves	83

Figure 6.8 van't Hoff Plots Showing Temperature Dependence of Dimensionless Henry Constants.....	86
Figure 6.9 Representative Plot Describing Energy Levels of CH ₄ in DDR Cage.....	90
Figure 6.10 Plot of the Ratio of Measured Diffusivities vs the Ratio of Measured Equilibrium Constants.....	91
Figure 7.1 Representative ZLC Data for C ₂ H ₆ -He in DDR II.....	95
Figure 7.2 Variation of Experimental Diffusivities of C ₂ H ₆ with Flow Rate.....	97
Figure 7.3 Comparison of Experimental ZLC Response curves of C ₂ H ₆	98
Figure 7.4 Arrhenius Plot Showing Temperature Dependence of Diffusivity for C ₂ H ₆	100
Figure 7.5 Diffusivity Data for C ₂ H ₄ in DDR I.....	101
Figure 7.6 Direct Comparison of ZLC Response curves of C ₂ H ₄	102
Figure 7.7 Arrhenius Plot Showing Temperature Dependence of Diffusivity for C ₂ H ₄	102
Figure 7.8 Relation of 1/L' v 1/F for C ₂ H ₆ in Two Different Samples.....	104
Figure 7.9 van't Hoff plot for C ₂ H ₆ -He and C ₂ H ₆ -CO ₂ in DDR	108
Figure 8.1 Representative ZLC Response Curves for C ₃ H ₆ -He and C ₃ H ₆ - CO ₂	114
Figure 8.2 Representative Intermediate Time Analysis ZLC Data for C ₃ H ₆ in DDR.....	115
Figure 8.3 Arrhenius Plot for C ₃ H ₆ in DDR.....	117
Figure 8.4 van't Hoff plot for C ₃ H ₆ in DDR.....	118

Figure 8.5 Representative ZLC Data for C ₃ H ₈ in DDR Samples.....	119
Figure B.1 Comparative Methane Isotherms at 5 ml/min, 50 °C.....	141
Figure B.2 Comparative Methane Isotherms at 15 ml/min, 50 °C.....	142
Figure B.3 Comparative Ethane Isotherms at 5 ml/min, 50 °C.....	142
Figure B.4 Comparative Ethane Isotherms at 15 ml/min, 50 °C.....	143
Figure B.5 Comparative Propane Isotherms at 5 ml/min, 50 °C.....	143
Figure B.6 Comparative Propane Isotherms at 15 ml/min, 50 °C.....	144
Figure B.7 Comparative Propane Isotherms at 5 ml/min & 15 ml/min, 50 °C	144

LIST OF SYMBOLS

- A virial constant
- b Langmuir equilibrium constant ($K = bq_s$)
- b_0 K_0/q_s (Eq. 4.5)
- c sorbate concentration
- c_0 initial value of c at which sample is equilibrated
- D intracrystalline diffusivity
- D_0 thermodynamically corrected diffusivity or limiting value of D at low loading
- D_∞ pre-exponential factor
- E_A diffusional activation energy
- f^\ddagger partition function for transition state
- f_g^\ddagger partition function free gas phase
- F flow rate
- h Planck's constant
- $-\Delta H_0$ limiting heat of adsorption at zero coverage
- $-\Delta H$ isosteric heat of adsorption (q_{st}) at finite loading
- $-\Delta H_{ads}$ heat of adsorption
- k surface mass transfer coefficient defined by Eqn. 5.21, Boltzmann constant
- K Henry constant
- K' Apparent Henry Constant
- K_∞ Pre-exponential factor (Eq.4.3)
- ℓ lattice spacing parameter (Eq 6.3)

ℓ column bed length
 L dimensionless parameter defined in Eq. 5.7
 L' apparent dimensionless parameter defined in Eq. 5.19
 n lattice spacing parameter (Eq 6.3)
 N_{ads} Number of moles adsorbed
 p sorbate partial pressure
 p_o saturation vapor pressure
 q sorbate loading
 q_s saturation capacity
 q_R value of q just inside external surface of particle
 q_{surf} value of q at external surface (in equilibrium with fluid concentration c).
 Note: that if there is no surface resistance $q_{\text{surf}} = q_R$
 Q Parameter defined in Eq. 5.5
 Q_r apparent loading of crystal
 q_{st} saturation loading of crystal
 r radial coordinate,
 r_c zeolite crystal radius
 R equivalent radius of zeolite crystals; Gas constant
 t_{diff} half-time for internal diffusion
 t_{surf} half time for surface resistance control
 T temperature
 v interstitial gas velocity
 V potential energy difference between transition state and gas phase (Eq. 6.3)
 V_s volume of zeolite crystal sample

V_g volume of free gas in sample cell

ΔU internal energy of adsorption

X mole fraction

Greek

β_n nth root of Eq. 5.8

η parameter defined in Eq. 5.5

τ parameter defined in Eq. 5.5

ε voidage of adsorbent bed

CHAPTER 1

INTRODUCTION

1.1 Methane Demand and Resources

The continuing rise in demand for energy has stimulated research to find alternative more efficient and environmentally friendly approaches to energy production. One such approach involves expanding the extraction and use of natural gas (and other methane rich waste gas streams) for both power generation and transportation fuel. Most of the high quality gas reservoirs have been or are currently being exploited so, in the future, we will have to rely increasingly on lower grade fields in which the methane is diluted by impurities such as CO₂ and/or H₂S. Indeed some larger gas fields have CO₂ contents as high as 60% but because of the volume of the deposits commercial exploitation still appears to be attractive. However, the economic viability of recovering methane from such low grade sources is critically dependent on the separation cost. These same components are also present in landfill gases and most other waste gases so similar considerations apply to these potential sources.

Removal of H₂S to very low concentration levels is obviously essential from both safety and environmental considerations but the requirements for CO₂ removal are less severe since CO₂ acts merely as a diluent that reduces the calorific value. Current pipeline specifications allow up to about 3% CO₂. Because of safety issues the focus of the present study is on CO₂ separation although the possibility of also extending adsorption processes to H₂S removal should be kept in mind.

1.2 Current Technology and Possible Alternatives

Current technology for upgrading natural gas depends on an amine based (liquid phase absorption) process. This system becomes economically attractive only at a very large scale making such processes viable only for the largest land based gas fields, and even then the process cost is substantial. The exploitation of smaller and more remote fields, including deep ocean fields, will require a separation process that is economic at smaller scales. Cryogenic processes such as cryogenic distillation or “controlled freeze zone” (CFZ) offer one possible approach; but the cost, weight and power requirements of the refrigeration system are severe disadvantages. Although such processes can produce a high purity product they are generally uneconomic for production of fuel gas.

Selective adsorption or membrane separation processes have also been considered and developed to pilot plant scale but so far such processes have not proved to be economic except in particular situations. This limited success has indicated the great potential of zeolitic adsorbents but further study is needed to determine how they can be modified for maximum efficacy. Not only must the capacity and separation factor(s) be high enough to yield the required product purity but the material must be robust and durable under operational conditions. Earlier approaches used adsorbents such as 5A zeolite (See for example MacLean, 1987)¹ which selectively adsorbs CO₂ in preference to CH₄. The selectivity of such adsorbents depends on the stronger-higher energy (equilibrium) adsorption of the quadrupolar CO₂ molecules in preference to the non-polar CH₄ molecules resulting from the presence of the exchangeable cations (Na⁺ or Ca⁺⁺)

within the structure. However, the presence of these cations leads to deterioration of the adsorbent by acid attack as well as to catalytic reactions such as the production of COS: this has proved to be a significant problem that could be resolved only by rigorous dehydration of the feed gas.

More recently the possibility of using cation free silicon zeolites has been considered. These materials show very little equilibrium selectivity but, with the correct pore size, an efficient kinetic separation is in principle possible. Although CO₂ has a higher molecular weight than methane its critical molecular diameter (3.3Å) is significantly smaller than that of methane (3.8Å)² so in pores of this diameter a substantial difference in diffusivity is to be expected due to greater steric hindrance of the larger methane molecules. Two possible structures that fulfill this requirement are DD3R and Si CHA. Alternatively by suitable treatment it may be possible to reduce the effective pore size of a larger pore (but relatively cheap) material such as silicalite to the required dimensions.

1.3 Aims and Scope of the Present Project

This thesis covers research that was undertaken as part of an NSF funded GOALI project in an effort to supplement recent studies of DDR adsorbents and membranes conducted at the ExxonMobil research laboratory in Clinton NJ^{3,4,5,6}. These studies found that DDR zeolite membranes had a very high perm-selectivity (and a correspondingly high kinetic selectivity for a DDR adsorbent) for CO₂/CH₄ and C₃H₆/C₃H₈ separations. Both these separations are commercially important, the former in connection with the recovery of methane from low grade natural gas deposits and from bio-gas and the latter

in connection with the recovery of propylene from cat cracker off-gas. To build on data obtained from permeance and uptake measurements, a more detailed study of intracrystalline diffusion of these molecules was deemed prudent.

In the present research project the diffusion of C_1 , C_2 and C_3 hydrocarbons as both single components and in combination with CO_2 were studied using the zero length column technique over a wide range of conditions on two different samples of DDR crystals. Additionally, the effect of hydroxyl functional groups (which are inherent to the zeolite crystalline structure) on CO_2 sorption was studied in both silicalite and DDR.

A brief review of the structures of these materials is given in Chapter 2, and some of the more relevant previous studies of adsorption and permeation are reviewed in Chapter 3. CO_2 isotherm measurements are presented in detail in Chapter 4. The ZLC technique is described in Chapter 5 and results of the ZLC measurements are presented and discussed in Chapters 6-8, with general conclusions and recommendations in Chapter 9.

Along with the present studies of DDR, Professors Sholl and Nair (at Georgia Institute of Technology) have been examining the feasibility of modified silicalite adsorbents. To contribute to their current studies, a series of ZLC measurements was carried out on their samples; these data are summarized in Appendix B.

CHAPTER 2

HIGH SILICA ZEOLITES

This chapter presents a short review of the structures of some important zeolites, including those covered by the present study, as well as brief comments on the important industrial separations underlying this research.

2.1 Zeolite Background and History

The term “zeolite” is used to categorize a large family of crystalline aluminosilicates that are distinguished by having open microporous crystalline structures. The structural regularity and uniformity of the pore dimensions confer some remarkable and practically important adsorptive properties on these materials, notably the ability to separate mixtures of small molecules according to differences in their molecular dimensions (size selective molecular sieving). Zeolites were first discovered as naturally occurring minerals found in volcanic tuffs but remained scientific curiosities for more than a century. During the second world war, to overcome the shortage of high octane aviation gasoline, Professor R.M. Barrer suggested that natural chabazite (from the Bay of Fundy) might be used to selectively adsorb linear paraffins from regular gasoline in order to increase the octane number (as well as lowering the freezing point). However, this idea was never developed beyond small scale laboratory trials.

The first commercial use of zeolites came in the 1950's when a synthetic zeolite (5A) for Oxygen-Nitrogen separations was developed. Type A zeolite was first

synthesized by R.M. Milton and his colleagues at the Union Carbide laboratories in Tonawanda, N.Y.^{7,8} Numerous process applications of zeolite A and other synthetic zeolites were developed during the following years including air separation^{9,10} and the separation of linear and branched hydrocarbons^{11,12}, as originally suggested by Barrer.

Zeolites are built up from SiO₂ and AlO₂-tetrahedra connected together in a wide array of different regular arrangements, forming frameworks with different symmetries and channel dimensions. In order to maintain charge balance, these structures contain one loosely held (therefore exchangeable) monovalent cation for each Al atom in the structure. Depending on the conditions of the synthesis of the zeolites and the presence of various “templates”, the structure can vary with consequent differences in the shape and size of the intracrystalline pores. About 60 different zeolite structures are currently known¹³, differing in their Si/Al ratio, channel dimensions and geometry.

The earliest synthetic zeolites (Types A and X) have Si/Al ratios approaching 1.0. More recently many silica rich zeolites have been produced including a number of pure silica forms (Si/Al → ∞). These materials are more desirable for certain industrial applications as they have higher thermal and hydrothermal stability as well as reduced catalytic activity, compared to the traditional Al rich zeolites.

The first pure silica zeolite to be synthesized was silicalite (the Si analog of HZSM-5)¹⁴. The synthesis of other pure silica zeolite structures such as ITQ-29 (the analog of Zeolite A), Si-CHA (the analog of natural chabazite) and DD3R¹⁵, which is the main focus of this thesis, is more recent. Several excellent reviews of zeolite structures are available – see for example Breck², Barrer¹⁶ and Cejka¹⁷. Only zeolites relevant to the present study are discussed here.

2.2 Zeolite Structures

Several different structures are described below. The connecting lines represent oxygen, the angled points represent silicon. Structure A represents Zeolite A and Structure B represents Chabazite. Chabazite and Zeolite-A are common small pore zeolites that have been extensively studied. Zeolite-A is cubic and has a three-dimensional isotropic pore network constricted by symmetric 8-membered oxygen windows. Chabazite is rhombohedral and also has an approximately isotropic three-dimensional pore structure constrained by 8-membered rings but, unlike zeolite A, the 8-membered rings are distorted with maximum and minimum diameters of approximately $3.7 \times 4.1 \text{ \AA}$. compared to Zeolite A with a window of about $4.3 \times 4.6 \text{ \AA}$ ¹³.

The MFI framework (structure C) is more complex. The pores are constricted by ten-membered rings of larger diameter – approximately 6.0 \AA . The pore network is essentially two-dimensional, consisting of a perpendicular array of intersecting straight and sinusoidal channels. There are no pores along the third direction (the long dimension of the crystals). To diffuse in that direction molecules must move between straight and alternating sinusoidal channels. The structure is therefore anisotropic with slower diffusion along the length of the crystal by a factor of 4.4 ¹⁸ compared to the other dimensions.

DDR is shown in structure D. DDR consists of a network of 19-hedral cages inter-connected through 8 membered windows. Five cages can be seen in the foreground of the image below.

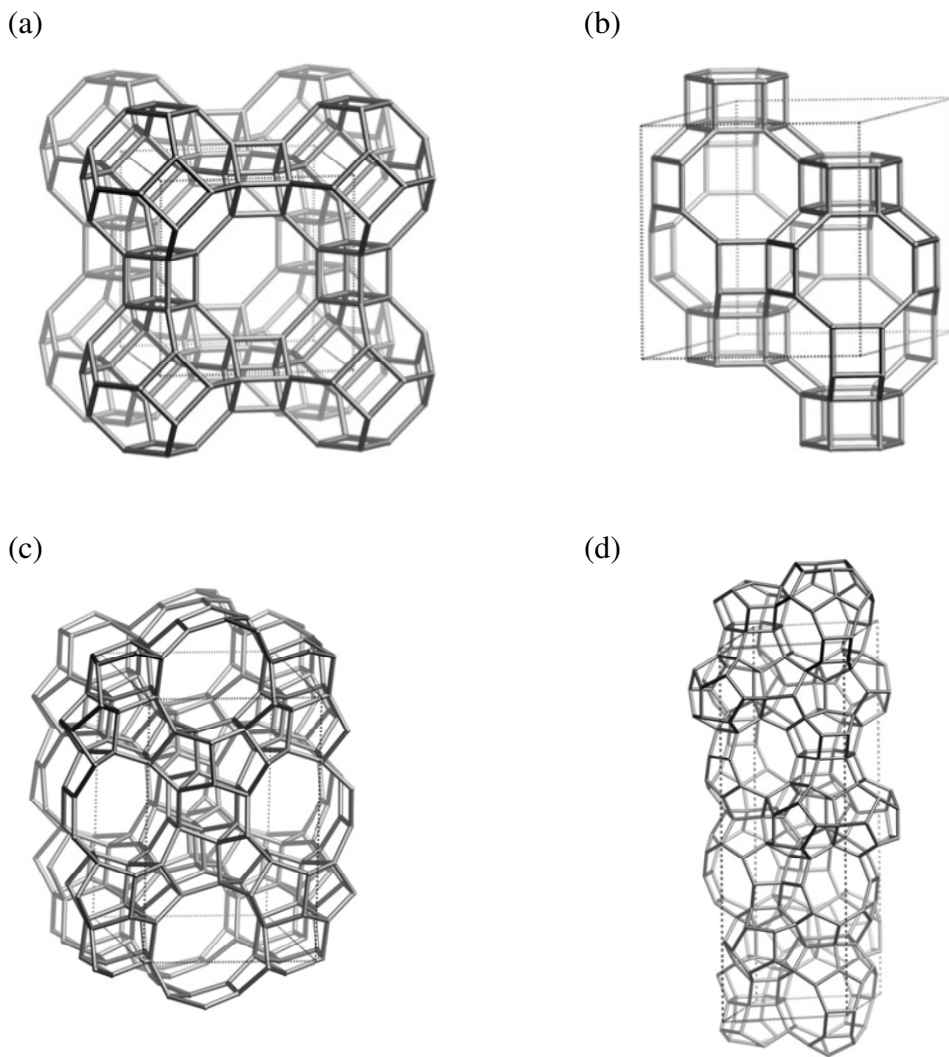


Figure 2.1 Molecular Structures of Select Zeolites. (a) Zeolite-A (b) Chabazite (c) MFI (a.k.a Silicalite) (d) DDR. *Images from Zeolite Atlas¹³.*

2.3 Zeolites Used for Natural Gas Purification

It has been proposed that zeolites could be used for upgrading natural gas through size selective membrane processes¹⁸. An important issue with this application is that water and H₂S, which are often present in natural gas, can quickly degrade most zeolites. One way to avoid this problem is to use highly siliceous zeolites, such as silicalite or DDR, which are much less reactive.

DDR or DD3R, which is short for Decadodecasils 3R, was first developed in the mid-80's by Geis¹⁵ who developed the synthesis and established the crystal structure of this material. The pore system comprises relatively large (19-hedral) cages interconnected through 8-ring windows with aperture approximately 3.6 x 4.4 Å. This window size makes DDR an attractive candidate for CO₂/CH₄ separations as the critical window diameter (0.3.6 Å) falls between the critical diameters of methane (0.38 Å) and carbon dioxide (0.33 Å)⁴, as required for size selective molecular sieve separation.

MFI (a.k.a silicalite, a.k.a. HZSM-5) is well known zeolite that has been widely studied and is therefore reasonably well understood. Since both silicalite and DDR3 have similar compositions and pore size it is to be expected that the sorbate-sorbent interactions for silicalite and DDR will be similar, at least under equilibrium conditions. Collaborators in the Nair research group at the Georgia Institute of Technology have modified MFI crystals by replacing the hydroxyls (which are inherent to the MFI structure) with different functional groups. Such functional groups include butanol, hexanol and phenyldiamine. The idea is to modify the size of the pore to an aperture that

is similar to that of DD3R, thereby making it a viable candidate for CO₂/CH₄ separations. The procedure for making these zeolites with integrated functional groups is described in detail elsewhere¹⁹.

2.4 Olefin/Paraffin Separations

The adsorptive separation of light olefins from the corresponding paraffins (C₂H₄/C₂H₆ and C₃H₆/C₃H₈) has attracted much attention in recent years as a potentially attractive route to the recovery of pure C₂H₄ and C₃H₆ (the feedstock for polyolefin production) from catalytic cracker off-gases. Earlier attempts to develop such processes were based on equilibrium selective separation over cationic zeolites. Coke formation resulting from polymerization of the olefins by these adsorbents proved to be a critical obstacle. Kinetic (molecular sieve) separations over pure silica zeolites with the correct pore dimensions appear to offer a more promising approach²⁰. Recent studies have shown that both Si-CHA and DDR have very high kinetic selectivity for C₃H₆/C₃H₈ separation^{21,22}. Although several patents have been issued it is not clear whether or not such processes have been developed beyond the laboratory scale.

CHAPTER 3

PREVIOUS STUDIES OF ADSORPTION AND DIFFUSION IN DDR

Due to its potential for industrial application in a number of important separation processes, DDR has attracted much research in recent years including equilibrium isotherm measurements, diffusion studies, membrane permeation measurements and molecular simulation studies. Since some of these studies are directly relevant to the present work a short review of some of the more relevant results is given in this chapter.

3.1 Equilibrium Isotherms

Equilibrium isotherms for methane and carbon dioxide in DDR, measured over wide ranges of temperature and pressure, have been reported by van den Bergh et al.^{23,24,25} Extensive data for other light gases are also given in van den Bergh's thesis. The same research group, under the direction of Prof. Kapteijn at Delft Technical University, has also published detailed equilibrium data for the C₂ and C₃ hydrocarbons in DDR²⁶. A detailed study of the effect of hydroxyl content on the equilibrium adsorption of CO₂ was carried out as part of the present research and is reported in Chapter 4 of this thesis.

3.2 Intracrystalline Diffusion Measurements

Although permeation through DDR membranes has been studied in some detail and intracrystalline diffusivities derived from such measurements have been

published^{5,6,23} only a few direct measurements of intracrystalline diffusion in DDR have been reported. Hedin et al.²⁷ measured self-diffusion of CH₄ and C₂H₄ in DDR crystals at 300K by the PFGNMR (pulsed field gradient NMR) method. Frequency response measurements for both CO₂ and CH₄ in DDR crystals have been reported by Chance⁶ and Deckman et al.⁵ but more detailed information, including the effect of CO₂ on the intracrystalline diffusion of methane is required. This is the main focus of the present research, the results of which are summarized in Chapters 6-8.

3.3 Membrane Permeation Measurements

An experimental study of DDR membranes including detailed characterization of both the kinetic and equilibrium behavior was carried out by Clark et al⁵. More recently the thesis of van den Bergh²³ provides an extensive report of his measurements of the permeation of several light gases (including CO₂ and CH₄) through a similar DDR membrane for both single component and binary systems. Diffusivities derived from single component permeation measurements are shown as an Arrhenius plot in Figure 3.1.

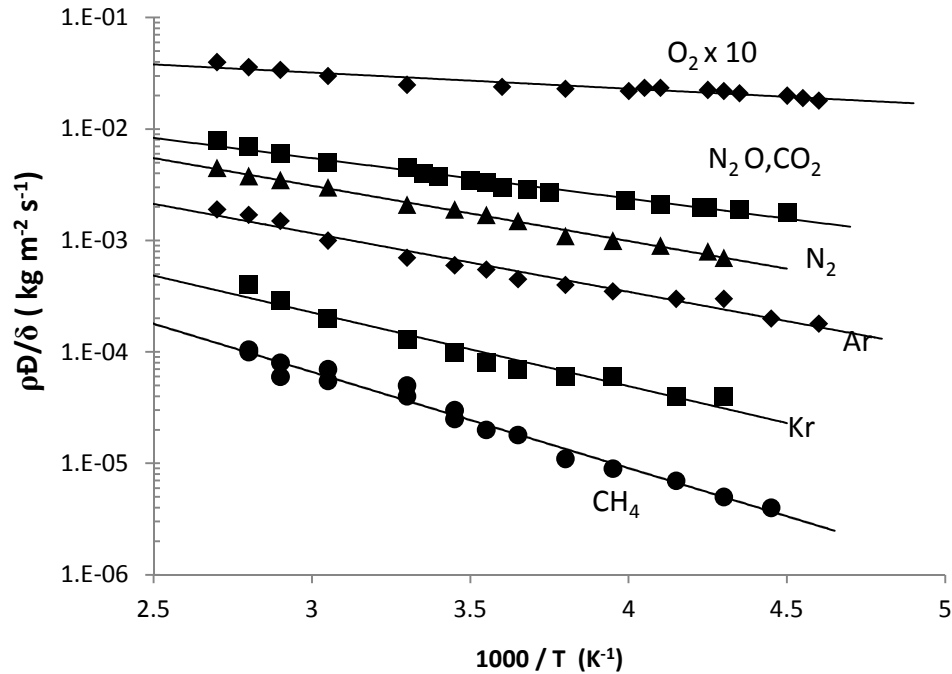


Figure 3.1. Arrhenius Plot Showing Temperature Dependence of Corrected Diffusivities for Light Gases in DD3R Derived From Permeation Measurements. (From van den Bergh Thesis)²³.

It is evident that at temperatures greater than 300K the diffusivity of CO₂ exceeds that of methane by more than an order of magnitude, suggesting the possibility of an efficient kinetic separation. Although the reported data are mainly for single component permeation the thesis also includes some studies of binary mixtures such as CH₄-CO₂. Examples are shown in Figures 3.2 and 3.3

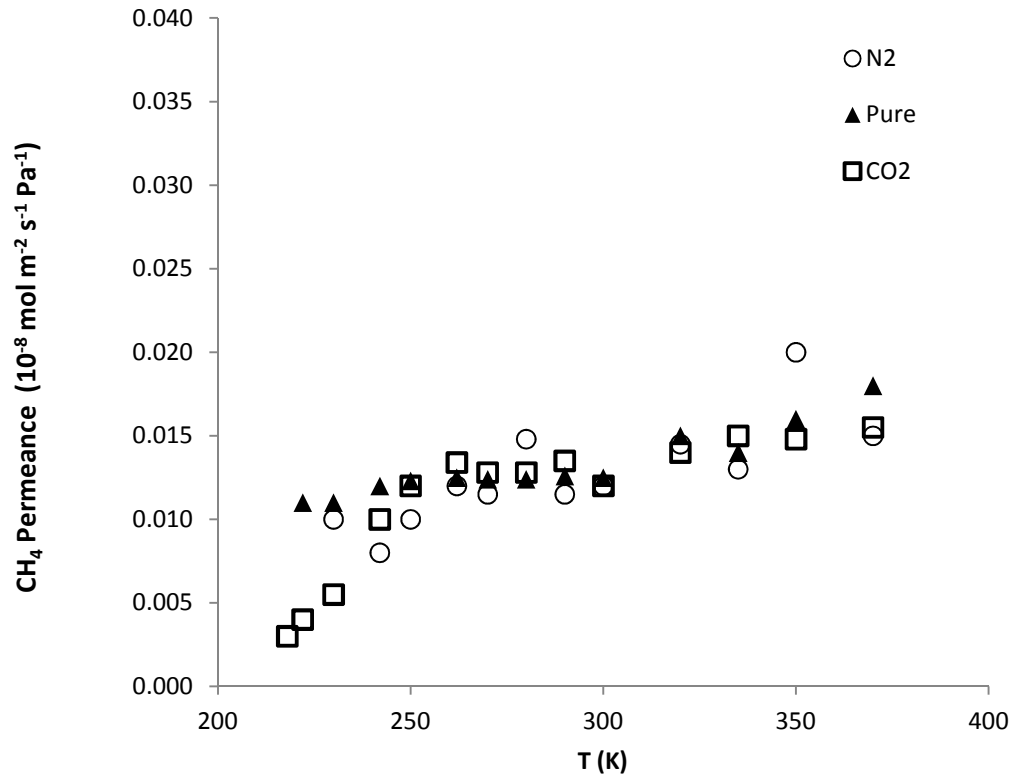


Figure 3.2. Temperature Dependence of Permeance of Methane in DD3R. As single component and in equimolar mixtures with N₂ or CO₂. (From van den Bergh Thesis)²³.

These data suggest that at higher temperatures, the permeance of methane in DDR is not significantly affected by the presence of CO₂ although at lower temperatures it is somewhat decreased. The effect of methane on the permeance for CO₂ is shown in Figure 3.3.

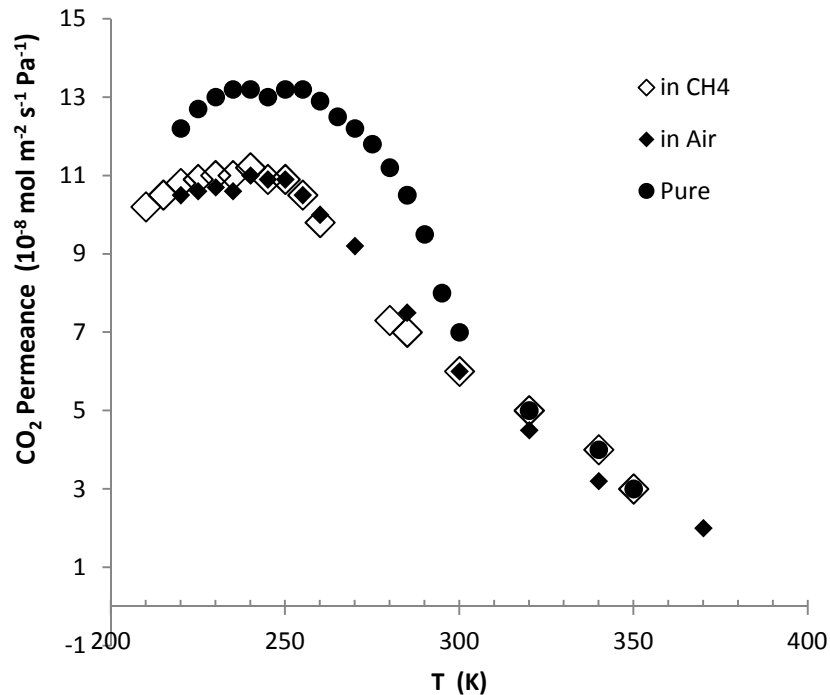


Figure 3.3. Temperature dependence of Permeance of CO₂ in DD3R. As pure component and in equimolar mixture with methane or air. (From van den Bergh Thesis)²³.

Evidently at lower temperatures the permeance of CO₂ is significantly reduced by the presence of methane but this effect becomes minimal above about 300K. Van den Bergh's data thus suggest that, within the relevant temperature range, the perm-selectivity for the mixture should be close to that predicted from the ratio of the single component permeances.

3.4 Molecular Simulations

The earliest molecular simulations of the diffusion of methane and CO₂ in DDR were carried out by Krishna and van Baten^{28,29}. However, their predicted intracrystalline

single component diffusivities for both CH₄ and CO₂ were very much larger than the experimentally measured values. It was later shown that this large error arises from the great sensitivity to the assumed repulsive force field and that the standard Lennard-Jones 6-12 potential does not work well for systems in which there is strong steric hindrance.

A more reliable simulation was later published by Sholl and Jee³⁰ (2009) in which the repulsive forces were adjusted to match the experimental diffusivity values at low loading. Some of their results are reproduced in figure 3.4.

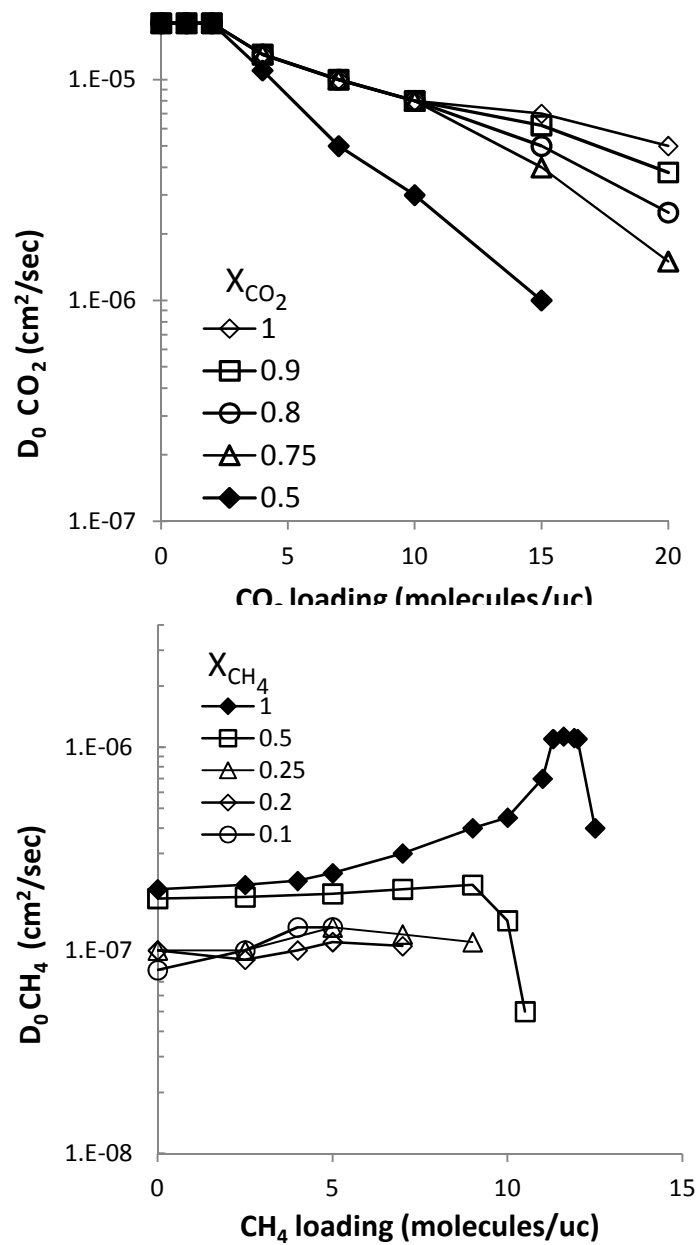


Figure 3.4. Modeled Diffusion of CO₂ and CH₄ in DD3R zeolite. Top figure shows the effect of CH₄ concentration on the diffusion of CO₂; the bottom figure shows the effect of CO₂ concentration on the diffusion of CH₄. (From Jee & Sholl, 2009)³⁰.

The simulation results suggest that the mutual diffusion effect depends substantially on the loading level and the composition of the adsorbed phase. Perm-

selectivities based on the binary ($\text{CH}_4\text{-CO}_2$) diffusivities are somewhat greater than the ratio of the single component permeances since, according to the simulation results, the diffusion of methane appears to be retarded by the presence of CO_2 . In contrast the effect of CH_4 on the diffusion of CO_2 appears to be minimal except at high loadings when the mole fraction of methane is high. This was explained by the preferential occupation of the 8-membered ring windows by CO_2 which was predicted from the equilibrium (Monte Carlo) simulations. An image of the DDR unit cell and an individual cage is shown in figure 4.5.

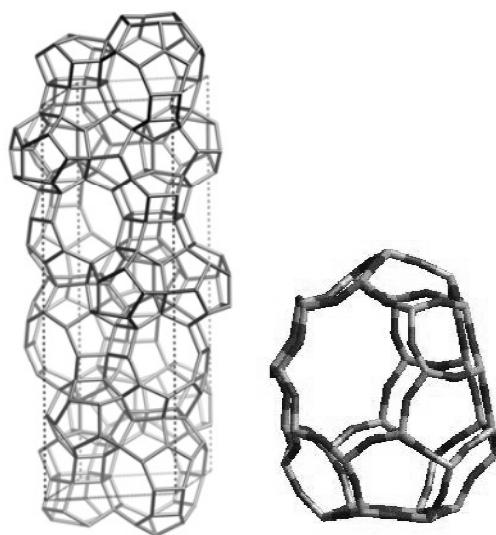


Figure 3.5. DDR Unit Cell & Cage Structure. Image on left is the DDR unit cell comprised of interconnected cages. Image on right is depiction of individual of DDR cage structure. The 8-membered window is site of preferential occupation of CO_2 molecules as theorized by Sholl et al. *Image from Zeolite Atlas¹³.*

CHAPTER 4

EFFECT OF SURFACE HYDROXYLS ON ADSORPTION OF CO₂ IN HIGH SILICA ZEOLITES

Depending on the method of synthesis, the high silica zeolites generally contain a significant proportion of surface hydroxyls. When utilizing such materials for the separation of gas streams containing CO₂ it is therefore important to understand how and to what extent the adsorption of CO₂ is affected by the hydroxyl content of the zeolite. The present study involving the measurement of equilibrium isotherms for CO₂ on several differently synthesized (with different hydroxyl content) samples of silicalite and DDR was undertaken in order to clarify this issue. The experimental work was carried out at the ExxonMobil Laboratory (Clinton, NJ) between June and October 2008.

4.1 Introduction

Because of their high thermal and hydrothermal stability, small pore high silica zeolites such as silicalite (high-Si MFI), silicon chabazite and DD3R offer considerable promise as size selective adsorbents^{7,31,32,33,34,35,36}. In particular, the small pore size of DD3R offers the possibility of a size selective (molecular sieve) separation of CO₂ (minimum diameter ≈ 3.3 Å) from methane (molecular diameter ≈ 3.8 Å) with much higher separation factors than are available for equilibrium based separations, thus potentially offering an alternative to energy intensive processes such as cryogenic distillation and amine absorption. The possible application of DD3R for separation of

CO₂ from natural gas or from the off-gas from bio-processing facilities has therefore attracted much attention.

These adsorbents are generally prepared by a templated synthesis that results in partial hydroxylation of the internal surface. It is evident that this may affect the adsorptive behavior, especially for polar or quadrupolar molecules such as water or CO₂. This effect, for water, is illustrated in figure 4.1 which shows the experimental (TGA) isotherms for several different high silica zeolite samples with different levels of hydroxyl content.

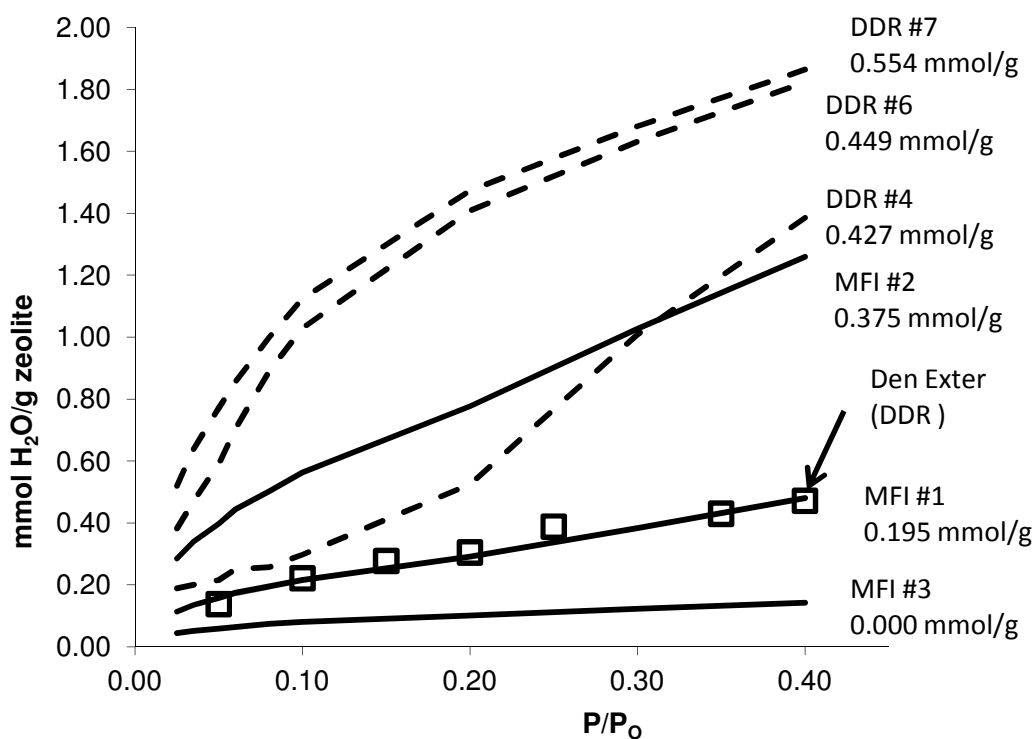


Figure 4.1 TGA Water Equilibrium isotherms for MFI & DDR Samples. Temperature is 77K, different hydroxyl contents indicated on the figure.

The isotherm for water on DD3R, reported by den Exter et al.³² is also included for comparison. The hydroxyl content of their sample was not reported but the close

similarity of their isotherm to that for the MFI sample with 0.195 mmole/g of hydroxyls suggests a similar hydroxyl content. It is clear that for both silicalite and DDR materials there is a general correlation between the affinity for water and the hydroxyl content. However, the available isotherm data are not sufficiently extensive to allow a detailed analysis. The present study was undertaken in order to establish whether similar effects occur for the adsorption of CO₂ on these adsorbents and to determine the magnitude of any such effects.

4.2 Experimental Procedure

A range of different samples prepared by different methods and therefore with different levels of surface hydroxylation, were studied. MFI Sample #1 was prepared using a TEOS:TPAOH (Tetraethyl orthosilicate: Tetrapropyl ammonium hydroxide) ratio of 1:0.36⁸, MFI Sample #2 was prepared using a higher TPAOH ratio. MFI Sample #3, was prepared using fluoride synthesis in order to create a hydroxyl concentration approaching zero. DDR Sample #4 was produced using methyltropinum iodide as a template and it was allowed to crystallize for 18 hours at 160 °C. DDR Sample #5 was templated with 1-Adamantanamine & Ethyldenedamine at 160 °C for 48 hours. DDR Sample #6 was also templated with methyltropinum iodide, but at 170 °C for 48 hours. DDR Sample #7 was templated using methyltropinum iodide, at 160 °C, but for 90 hours.

The crystals were first evaluated using SEM in order to check the crystallinity and determine crystal size, which ranged from 500 nm to 20 µm for the different samples. Smaller crystal sizes were preferred in order mitigate diffusion effects and measure

equilibrium behavior. The structural integrity of all samples was confirmed by XRD and the hydroxyl contents were measured by NMR. XRD data were collected using a PANalytical X'pert system at 0.1° increments at 10 seconds per point. The NMR Data were collected by H^1 (proton) NMR, using a 500 MHz magnet at 2400 scans per second.

Adsorption equilibrium isotherms widely used to understand the interaction of a sorbate with a solid sorbent. Isotherms correlate the pressure (or partial pressure) of the sorbate gas with the adsorbed phase loading (at equilibrium). As the pressure in the gas phase is increased, more sorbate is adsorbed on the surface. Isotherms are generated by incrementally increasing the pressure in the system and measuring the amount of sorbate adsorbed; the resulting data are plotted as amount adsorbed (amount per mass of sorbent) against pressure (or partial pressure). The resulting isotherm plot has an initial linear portion at low pressures; this is referred to as the Henry's law region. The slope of this line is the Henry constant which measures the affinity of the sorbent for the sorbate. Beyond the Henry's Law region the isotherm becomes nonlinear but, in general, the loading still increases monotonically with increasing pressure.

CO_2 adsorption equilibrium isotherms were measured using an *Autosorb I* system (Quantachrome Instruments). The *Autosorb* operates on a pure gas volumetric basis and measures excess adsorption isotherms. Helium is used to determine the system volume (approximately 10 ml). At room temperature He is not significantly adsorbed but it does penetrate the intracrystalline pores, so the volume of He "adsorbed" will be only very slightly greater than the intracrystalline pore volume. The measured excess adsorption isotherms were therefore re-calculated to absolute isotherms using the crystallographic pore volumes. However, in the relevant pressure range this correction is trivial. All

molecules within the crystal are thus considered as “adsorbed”. Further details have been given by Neimark and Ravikovitch³⁷. CO₂ isotherms were measured for several differently prepared samples of silicalite and DD3R containing different levels of residual hydroxyls. The results, which are summarized below, suggest that both the saturation capacity and the affinity (for CO₂) are influenced by the hydroxyl content. These effects appear to be more pronounced for DD3R than for silicalite but this may be simply because the level of hydroxyl in the DD3R sample was higher.

4.3 Results and Discussion

The XRD measurements showed that all samples conform to the MFI or DDR structures and have high crystallinity. The patterns were compared with those reported in the zeolite atlas¹³ and, for all samples, there was a good match. Representative patterns are shown in figure 4.2.

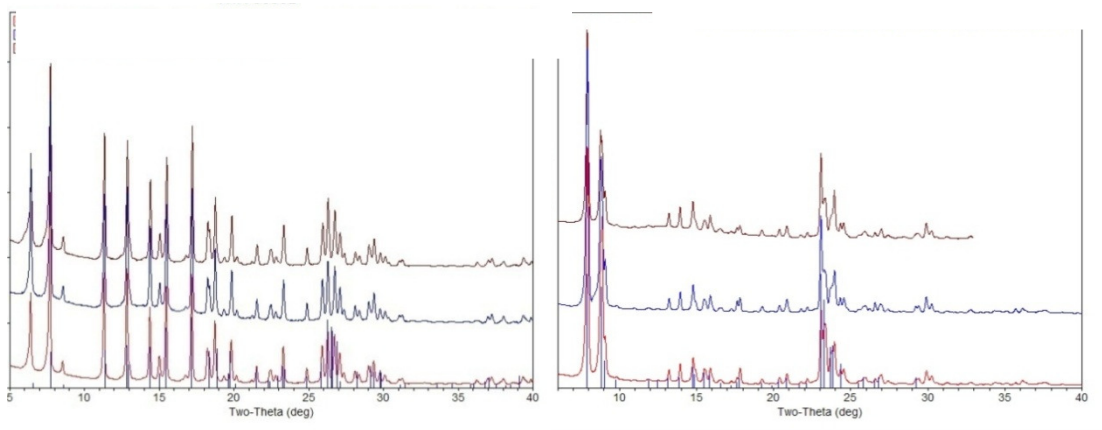


Figure 4.2 XRD Data for MFI & DDR Samples. Confirming crystalline structures for DDR (Left) and MFI (Right).

The NMR spectra, shown in figure 4.3, show considerable differences in the hydroxyl content, as expected. The hydroxyl densities, estimated by integration of the peaks between 4 ppm and 0 ppm, are summarized in Table 4.1 together with other relevant details of the adsorbent properties. (The broad resonances greater than 4 ppm are excluded).

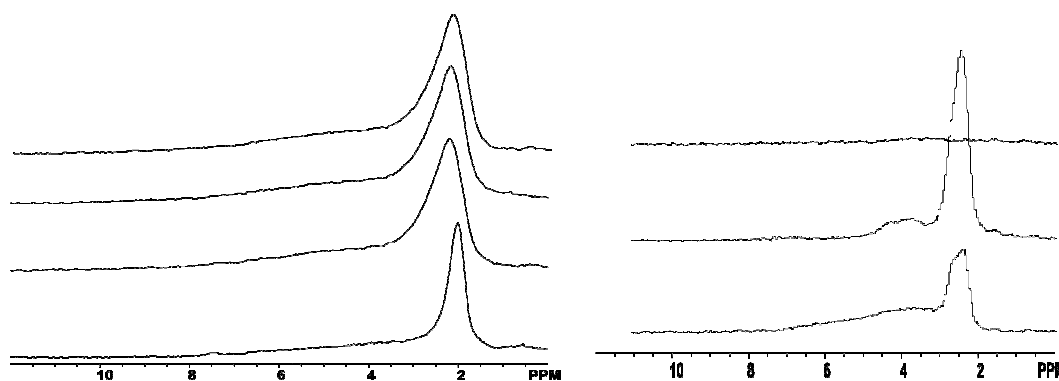


Figure 4.3 NMR spectra for DDR & MFI Samples. DDR (Left) and MFI (Right).

Table 4.1 Hydroxyl Densities of DDR & MFI Samples.

Sample #	Physical Characteristics			Hydroxyl Conc.
MFI	BET SA (m² / g)	Mean Crystal Size (μm)	Si/Al Ratio	Non-acidic, (mmol/g)
1	405.27	0.5	∞	0.195
2	437.28	0.2	∞	0.375
3	397.24	20	1728	0.000
Sample #	Physical Characteristics			Hydroxyl Conc.
DDR	BET SA (m² / g)	Mean Crystal Size (μm)	Si/Al Ratio	Non-acidic, (mmol/g)
4	-	5	380	0.672
5	-	20	∞	0.427
6	-	30	>1000	0.449
7	-	30	950	0.554

The experimental isotherms for CO₂ are shown in figures 4.4 and 4.5, plotted on linear scales. The isotherms for the three MFI samples are all quite similar, as may be seen from figure 4.4. Differences between the DDR samples (figure 4.5) are more pronounced. The isotherms for sample 4, which has the highest hydroxyl content, are consistently higher than the other samples. The isotherms for samples 5 and 7 are similar but the capacities are substantially smaller than those for sample 4, Sample 6 is intermediate.

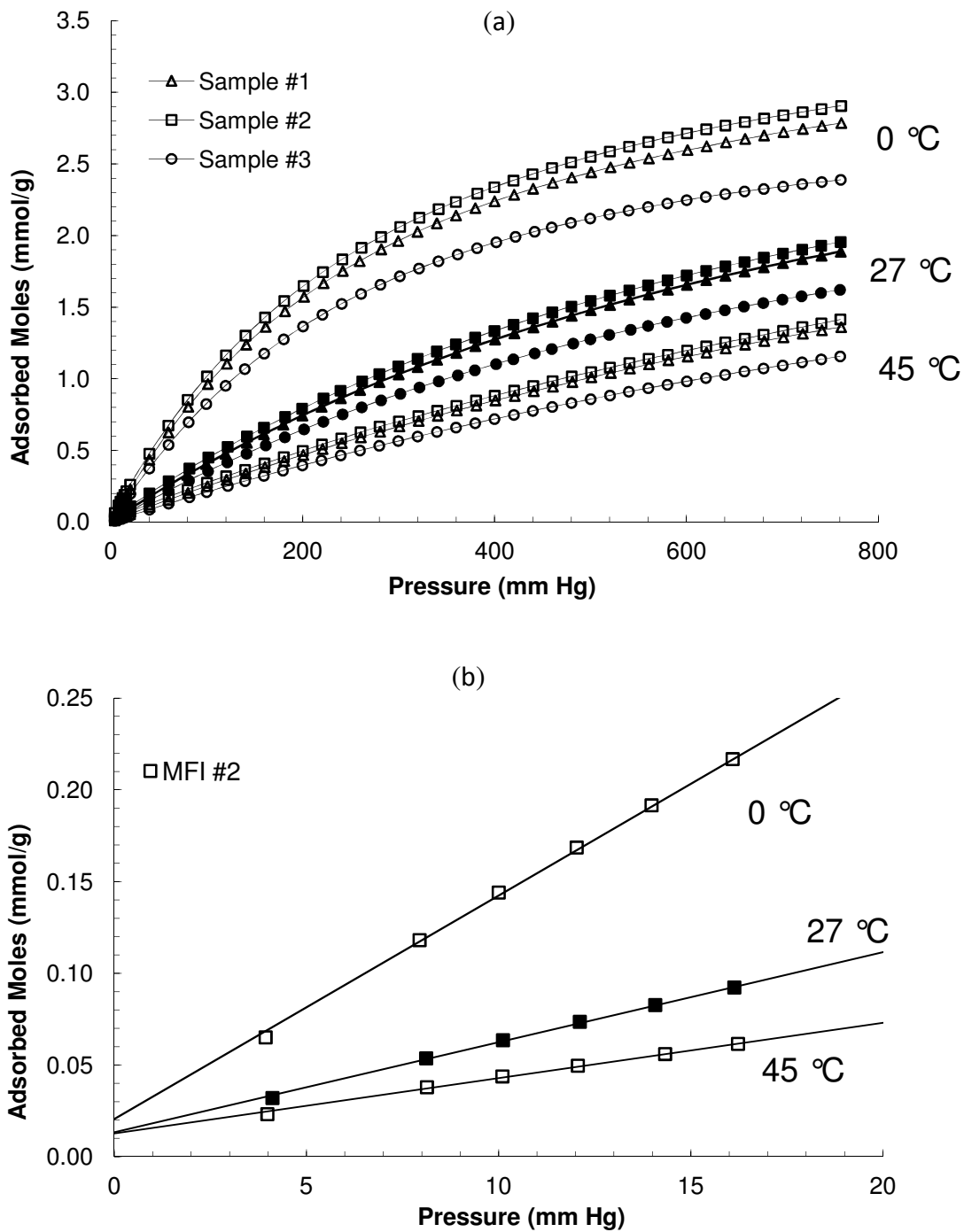


Figure 4.4 MFI CO₂ Adsorption isotherms. (a) Entire Curve (b) low loading for sample #2

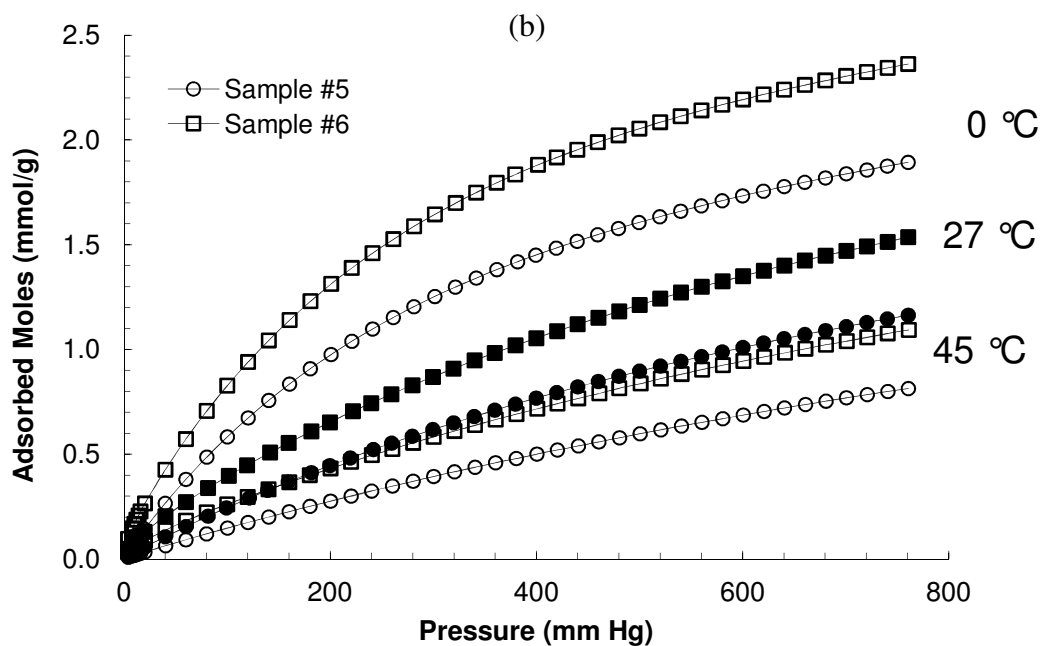
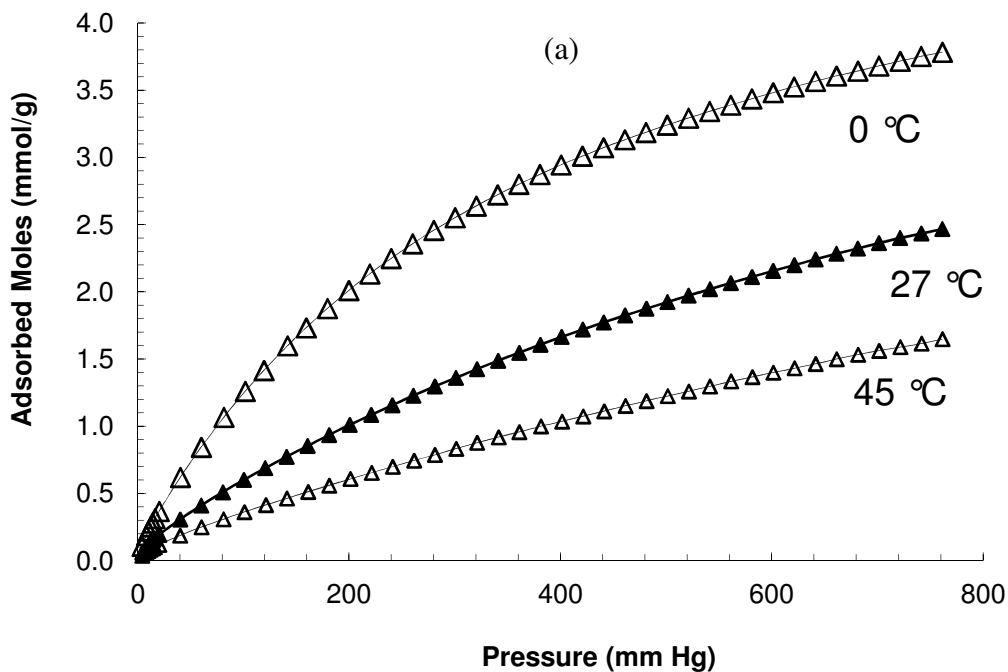


Figure 4.5 DDR CO₂ Adsorption isotherms for DDR Samples. (a) Sample 4
(b) Samples 5 & 6.

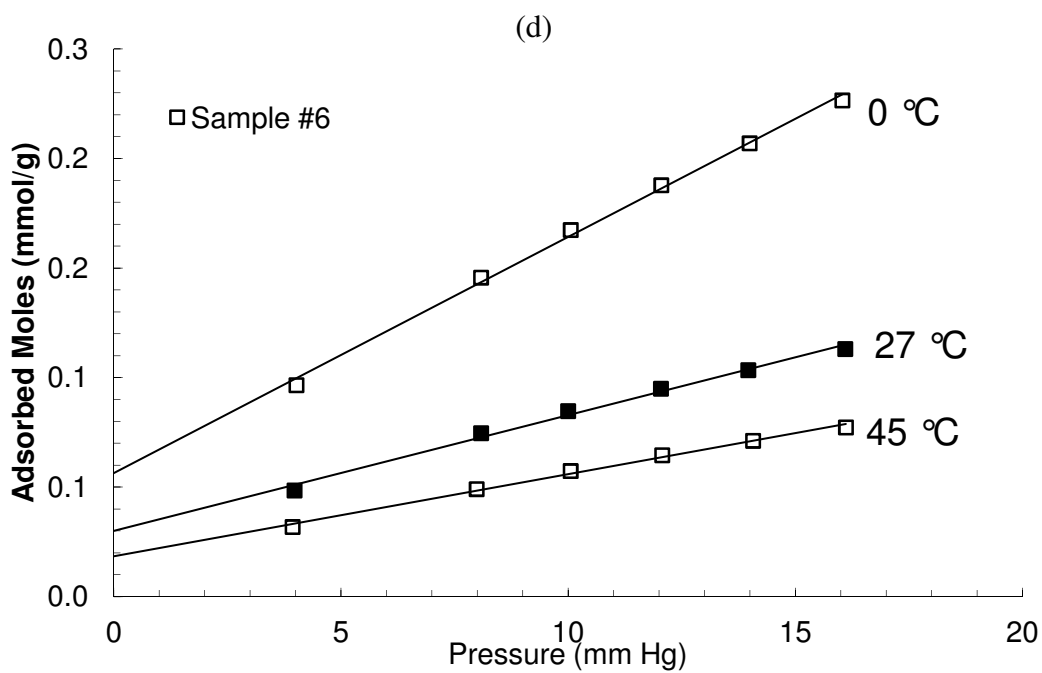
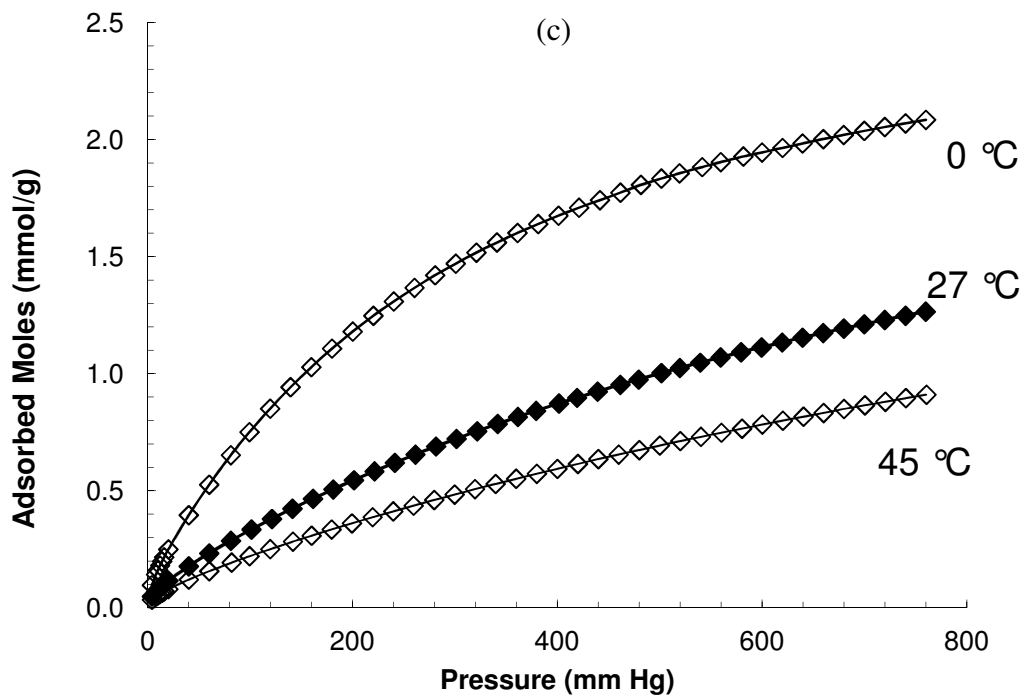


Figure 4.5 (continued) DDR CO₂ Adsorption isotherms for DDR Samples.
 (c) Sample 7 (d) sample 6 at low loading.

Figure 4.6 shows a comparison of our isotherms at 273K and 300K with the isotherms of Himeno et al.³⁸ and Van den Bergh^{23,24}. The van den Bergh sample appears to be similar to our sample 6 while the Himeno sample is similar to our lower loading samples (5 and 7).

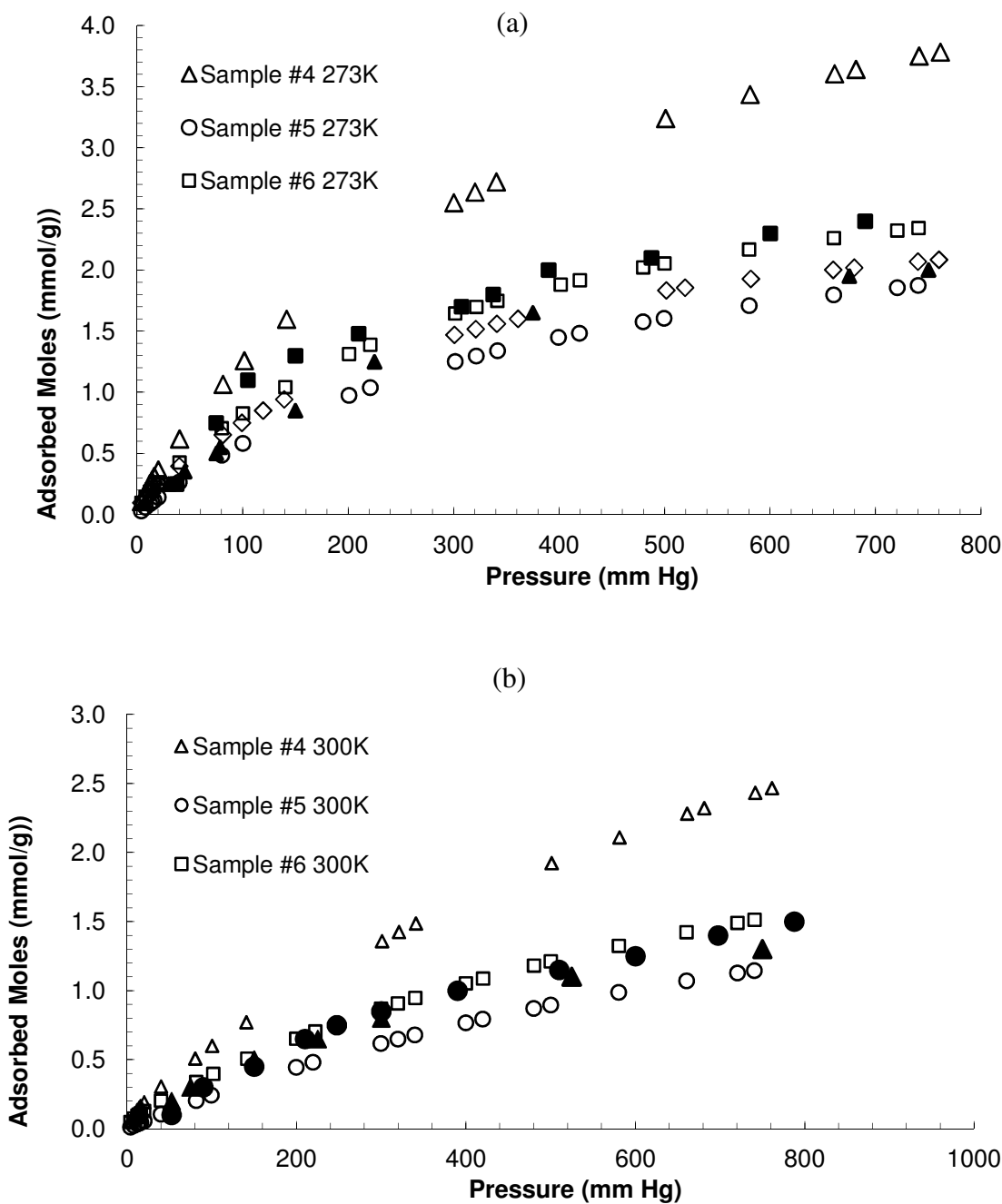


Figure 4.6 DDR Adsorption Isotherms Compared to Published Data. (a) Measured at 273 K (b) Measured at 300 K.

For some of the samples a linear plot of the isotherm (q vs p) showed a small positive intercept at zero pressure, as shown in figures 4.4b and 4.5b, suggesting a small proportion of very strongly held CO_2 . These intercepts appear to correlate, in a general way, with the hydroxyl content of the samples, as may be seen from figure 4.7. Such a relationship is to be expected if the hydroxyls provide favorable adsorption sites for CO_2 but the data points are not sufficiently numerous to establish the quantitative form of this correlation. This behavior might correspond to a dual-site Langmuir isotherm with a few very strong sites, the model used by van den Bergh et al.^{23,24} for correlation of their equilibrium data. However, more extensive data in the low pressure region (< 4 Torr) would be needed to confirm this.

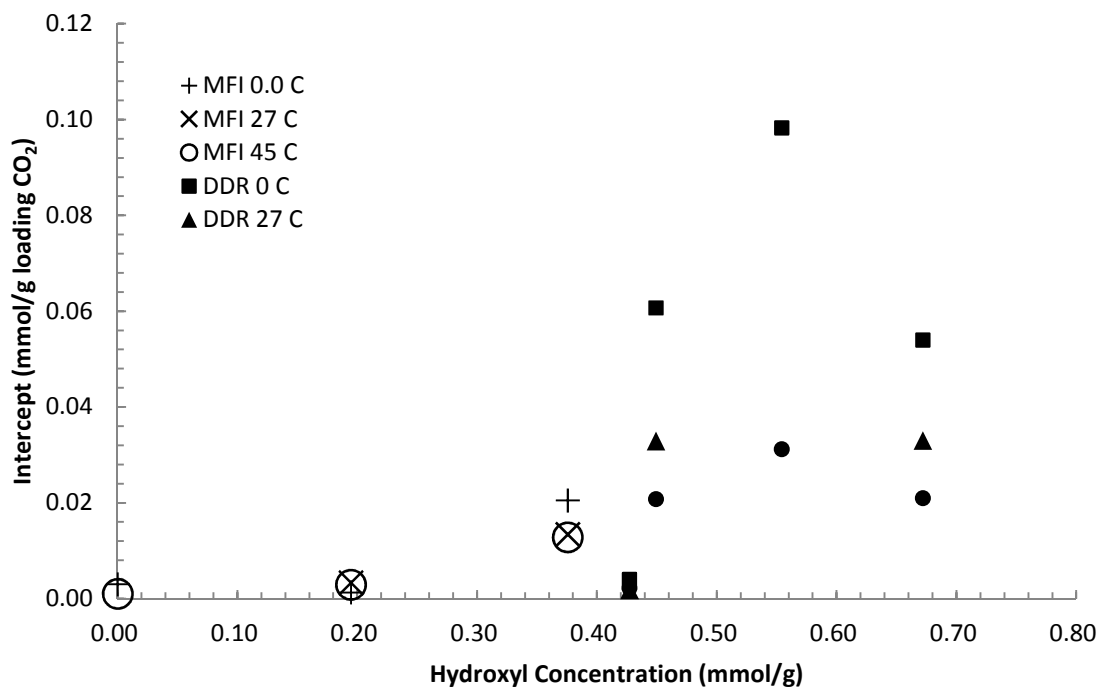


Figure 4.7 Plot Showing General relationship Between Hydroxyl Concentration and Intercept Offset (or foot).

For further analysis of the isotherms the values of the intercepts for each data point were subtracted in order to correct the zero pressure point to the origin. Such a procedure amounts to neglecting the small fraction of irreversibly adsorbed molecules in order to apply thermodynamic analysis to the major fraction of the (reversibly) adsorbed phase.

4.3.1 Henry Constants

Approximate values for the Henry constants were estimated from the initial slopes of the isotherms. It may be shown that, for physical adsorption, regardless of the specific nature of the surface, the isotherm, at low loading, should approach the limiting form of the virial isotherm³⁹:

$$Kp = q \exp(Aq) \quad (4.1)$$

where A is the first order virial coefficient. A plot of $\log(p/q)$ vs q should therefore approach a straight line with intercept $-\log(K)$. This allows for simple extrapolation of sorbate-sorbent interactions at low loadings. More accurate values of the Henry constant (K) were therefore extracted from such “virial plots”, as suggested by Barrer and Davies⁴⁰. Representative examples are shown in figure 4.8.

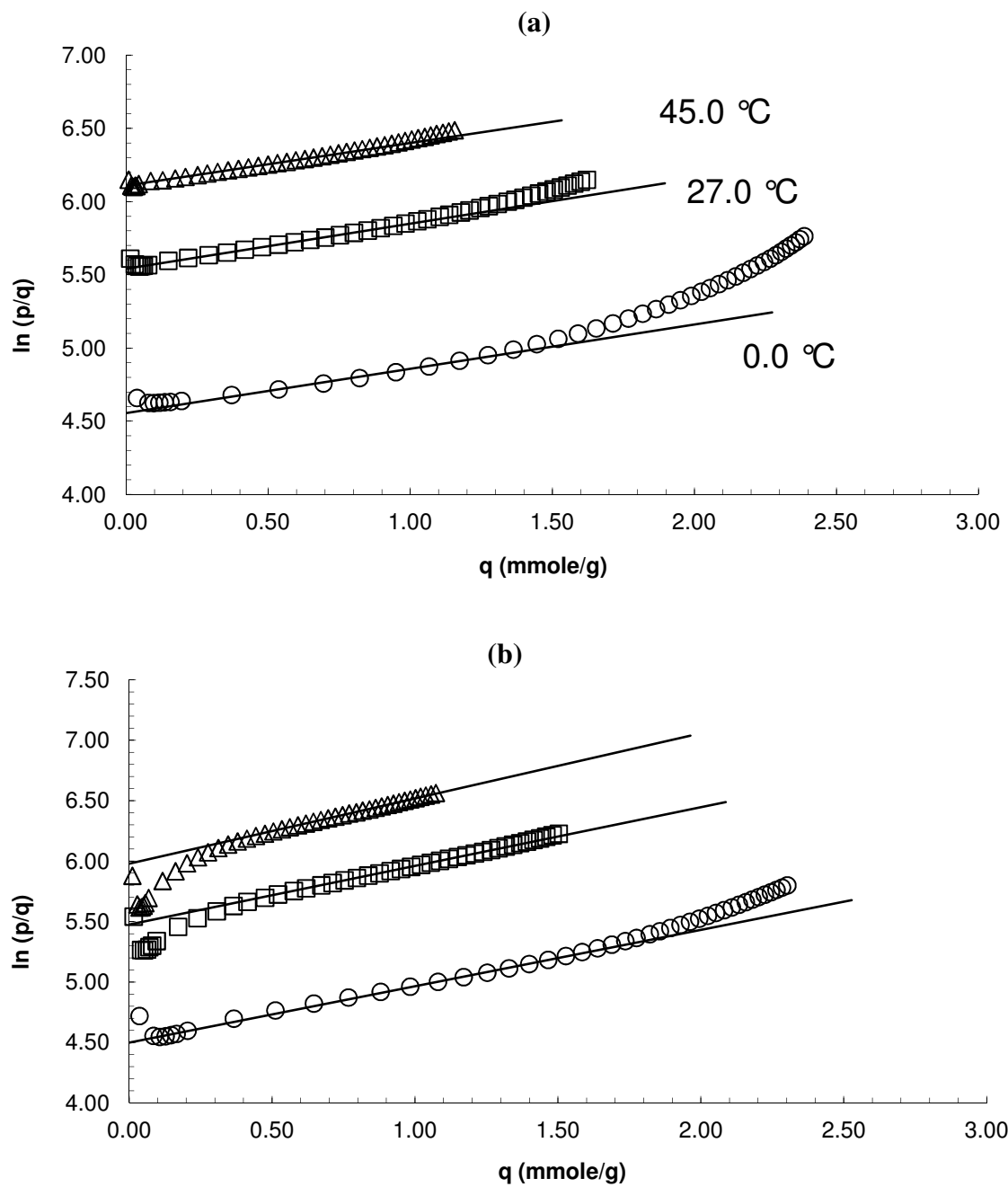


Figure 4.8 Representative Virial Plots. (a) MFI (b) DDR.

Henry constants were also extracted from plots of $1/q$ vs $1/p$ according to the Langmuir model, which may be written in the linearized form:

$$\frac{1}{q} = \frac{1}{q_s} + \frac{1}{K} \frac{1}{p} \quad (4.2)$$

This simple model provides a surprisingly good fit of most of the isotherms (see for example figure 4.9).

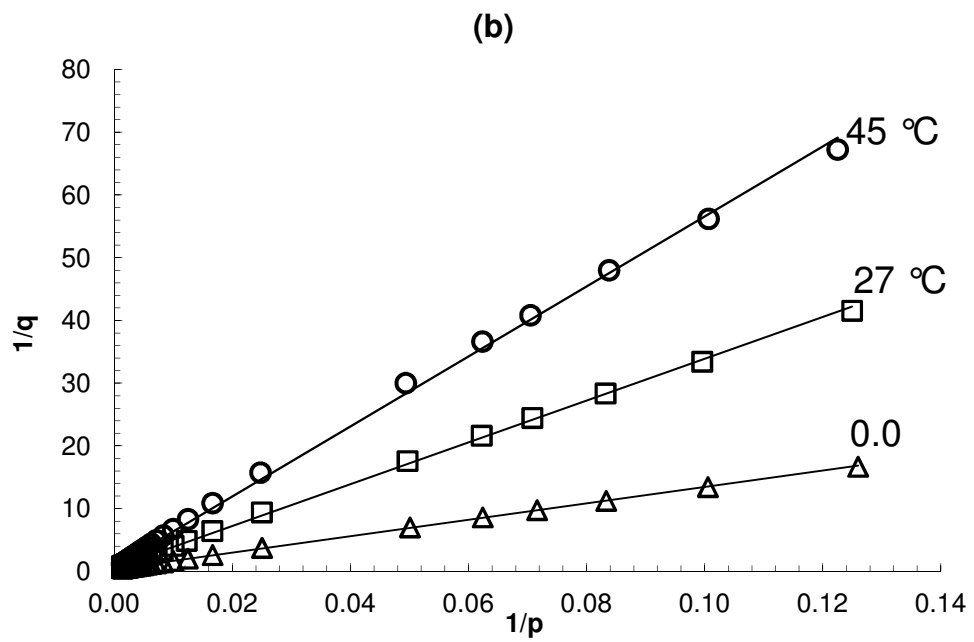
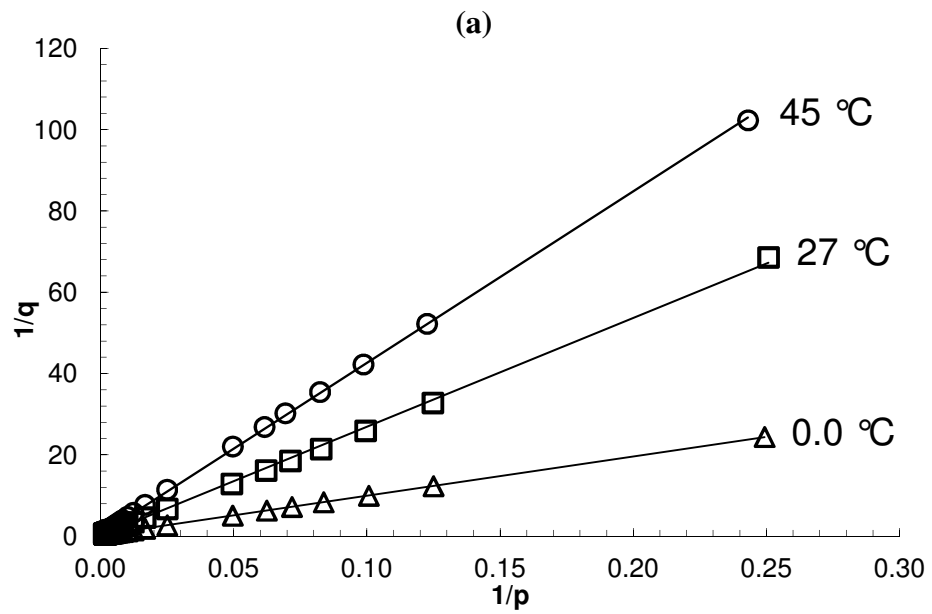


Figure 4.9 Representative Langmuir Plots. (a) MFI (b) DDR.

4.3.2 Heats of Adsorption

The Henry constants calculated from the three different approaches were quite consistent (see Table 4.2) and their temperature dependence conforms to the van't Hoff equation:

$$K = K_{\infty} \exp\left(\frac{-\Delta H_0}{RT}\right) \quad (4.3)$$

Table 4.2 Comparison of Henry Constants, Obtained using three different methods.

Table Showing Results of Henry Constants, Determined from different methods									
MFI	Henry Constant CO ₂								
Sample #	Initial Slope (0.0 °C)	Virial Plot (0.0 °C)	Langmuir Plot (0.0 °C)	Initial Slope (27.0 °C)	Virial Plot (27.0 °C)	Langmuir Plot (27.0 °C)	Initial Slope (45.0 °C)	Virial Plot (45.0 °C)	Langmuir Plot (45.0 °C)
1	0.0114	0.0124	0.0112	0.0045	0.0045	0.0045	0.0027	0.0027	0.0029
2	0.0122	0.0132	0.0119	0.0045	0.0049	0.0051	0.0030	0.0028	0.0032
3	0.0097	0.0105	0.0097	0.0039	0.0039	0.0039	0.0022	0.0022	0.0022

DDR	Henry Constant CO ₂								
Sample #	Initial Slope (0.0 °C)	Virial Plot (0.0 °C)	Langmuir Plot (0.0 °C)	Initial Slope (27.0 °C)	Virial Plot (27.0 °C)	Langmuir Plot (27.0 °C)	Initial Slope (45.0 °C)	Virial Plot (45.0 °C)	Langmuir Plot (45.0 °C)
4	0.0159	0.0160	0.0169	0.0081	0.0064	0.0095	0.0049	0.0034	0.0032
5	0.0070	0.0074	0.0072	0.0028	0.0027	0.0029	0.0016	0.0016	0.0015
6	0.0103	0.0111	0.0109	0.0050	0.0042	0.0056	0.0035	0.0025	0.0040
7	0.0146	0.0158	0.0155	-	-	-	0.0048	0.0035	0.0060

as may be seen from figure 4.10. Limiting heats of adsorption at zero loading ($-\Delta H_0$) were calculated from the slopes of these plots, which are closely linear, and these values are compared with the corresponding isosteric heats of adsorption at finite loadings, calculated from the Clausius-Clapeyron equation:

$$\ln \frac{p_2}{p_1} = \frac{\Delta H}{R} \left(\frac{1}{T_1} - \frac{1}{T_2} \right) \quad (4.4)$$

where (p_1, T_1) and (p_2, T_2) represent points at a constant loading. The limiting values are summarized in Table 4.3 and the variation of heat of adsorption with loading is shown in figure 4.11.

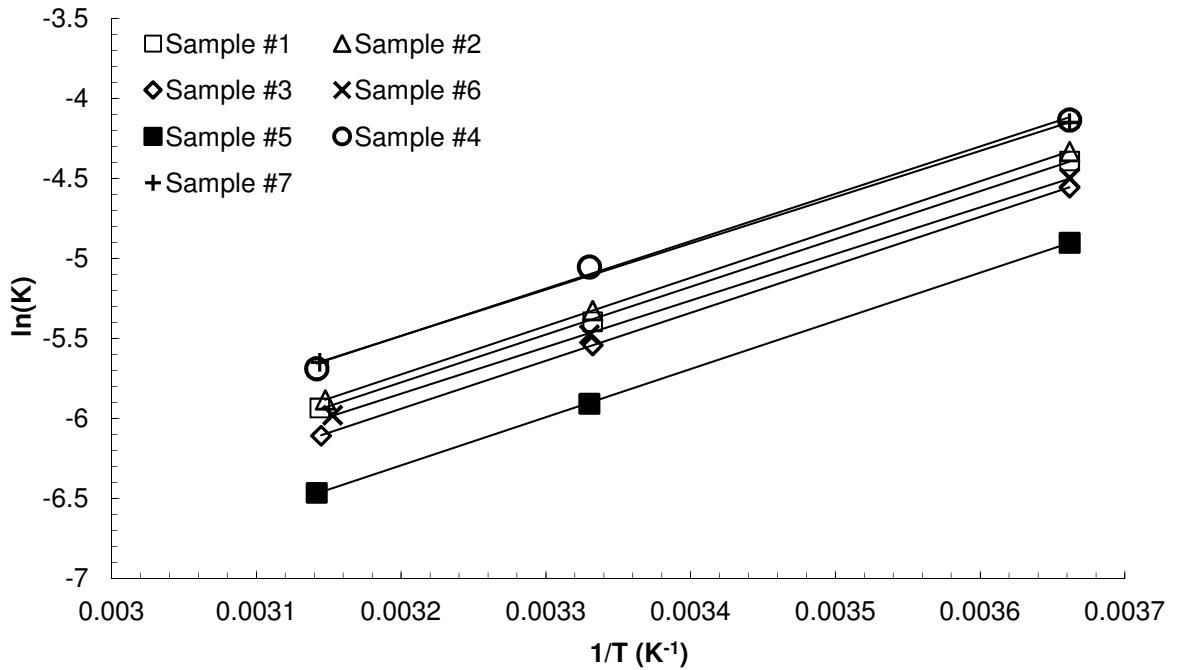


Figure 4.10 van't Hoff plots for MFI and DDR samples. Shows linear relationship, this allows for easy extraction of the heat of adsorption at zero loading. Henry constants from Virial method of calculation.

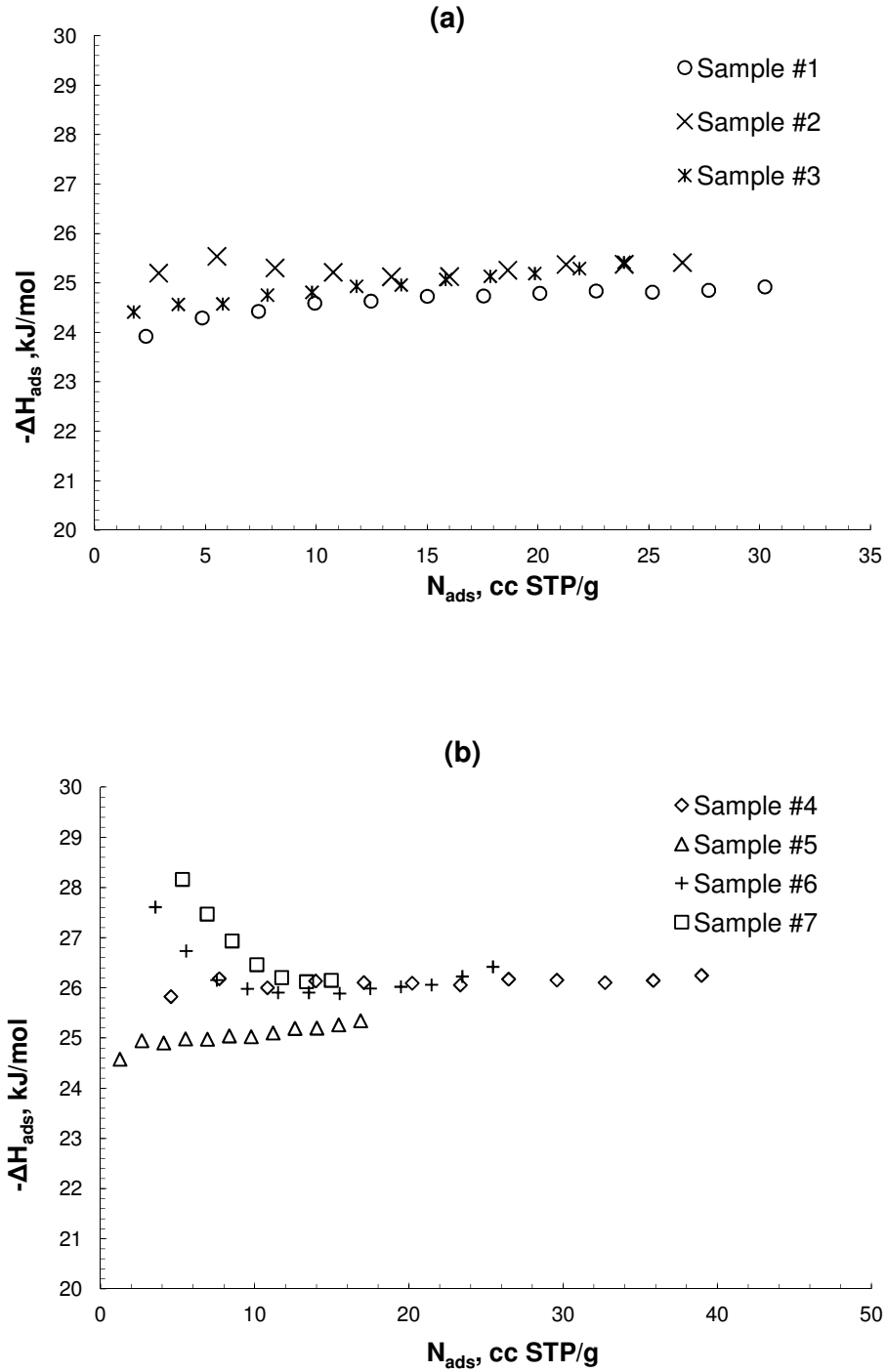


Figure 4.11 Calculated Loading Dependence of the Isothermic Heat of Adsorption. (a) MFI (b) DDR.

For MFI the heat of adsorption (≈ 25 kJ/mole) is essentially the same for all samples and independent of loading. The values for DDR are slightly higher (≈ 26

kJ/mole), with some evidence of higher values at low loadings for some but not all of the samples. This pattern is commonly seen and can be attributed to two different sites⁴¹. Van den Bergh⁽⁷⁾ gives values of 23.7 and 28.5 kJ/mole (for CO₂-DD3R) based on the single site Langmuir and dual site Langmuir models respectively.

Table 4.3 Isothermic Heats of Adsorption and Zero-loading Heats of Adsorption.

MFI	Heats of Adsorption CO ₂	
Sample #	Clausius Clapyeron (kJ/mol)	Van't Hoff Zero-Loading (kJ/mol)
1	23.9	24.8
2	25.2	25.5
3	24.4	25.1
DDR	Heats of Adsorption CO ₂	
Sample #	Clausius Clayperon (kJ/mol)	Van't Hoff Zero-Loading (kJ/mol)
4	25.8	24.6
5	24.6	25.3
6	27.6	24.2
7	28.2	24.0

4.3.3 Correlation of Adsorption with Hydroxyl Content

The correlation between the Henry constants and Langmuir capacities with the hydroxyl content was examined and the results are shown in figures 4.12 and 4.13. For MFI the hydroxyl contents were all relatively small (< 0.4 mmole/g) and, at least at this level, there appears to be no clear correlation between either the Henry constant or the Langmuir capacity and the hydroxyl content. This is consistent with the data from the intercepts which, for MFI, were always close to zero. In contrast the data for DD3R show

a strong dependence of both the Henry constant and the saturation capacity on the hydroxyl content. This is consistent with the low pressure behavior which, for the DD3R samples, shows significant intercept offsets (or a “foot”) which correlate well with the hydroxyl content (as shown in figure 4.7). However, although the correlation of the q_s values with hydroxyl content (Figure 4.13) appears convincing it is important to remember that the q_s values derived from Langmuir plots of the isotherm data are not necessarily physically meaningful. A more detailed analysis would be needed before definite conclusions can be drawn.

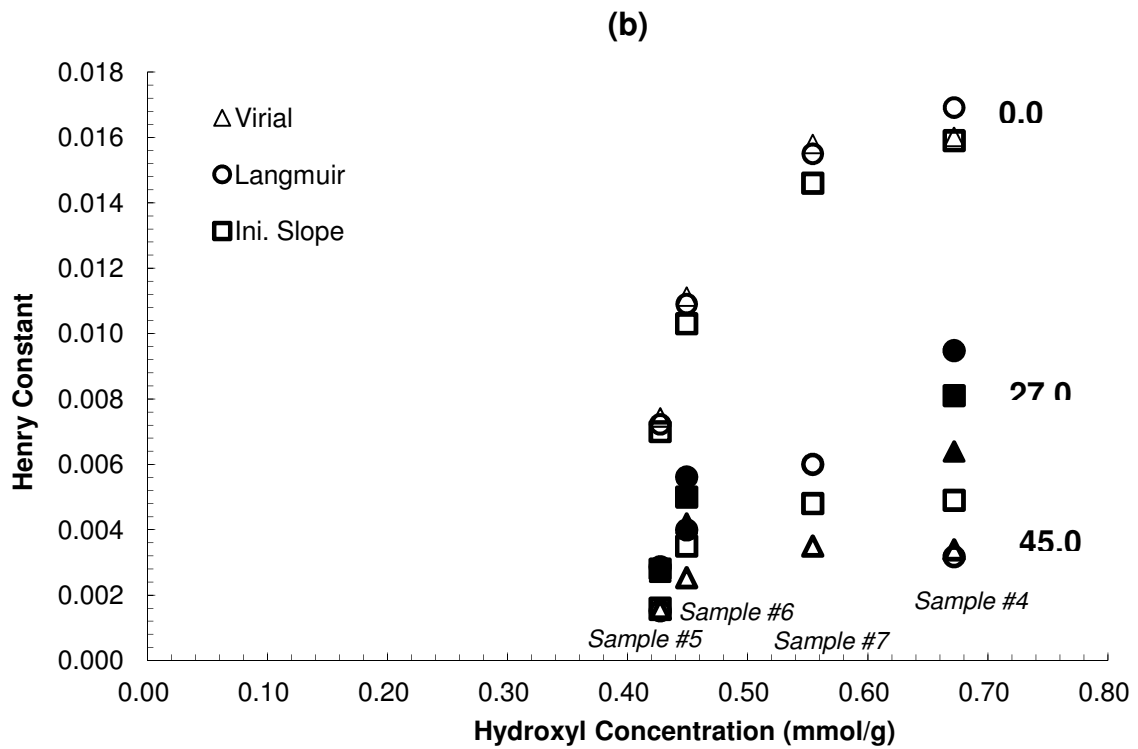
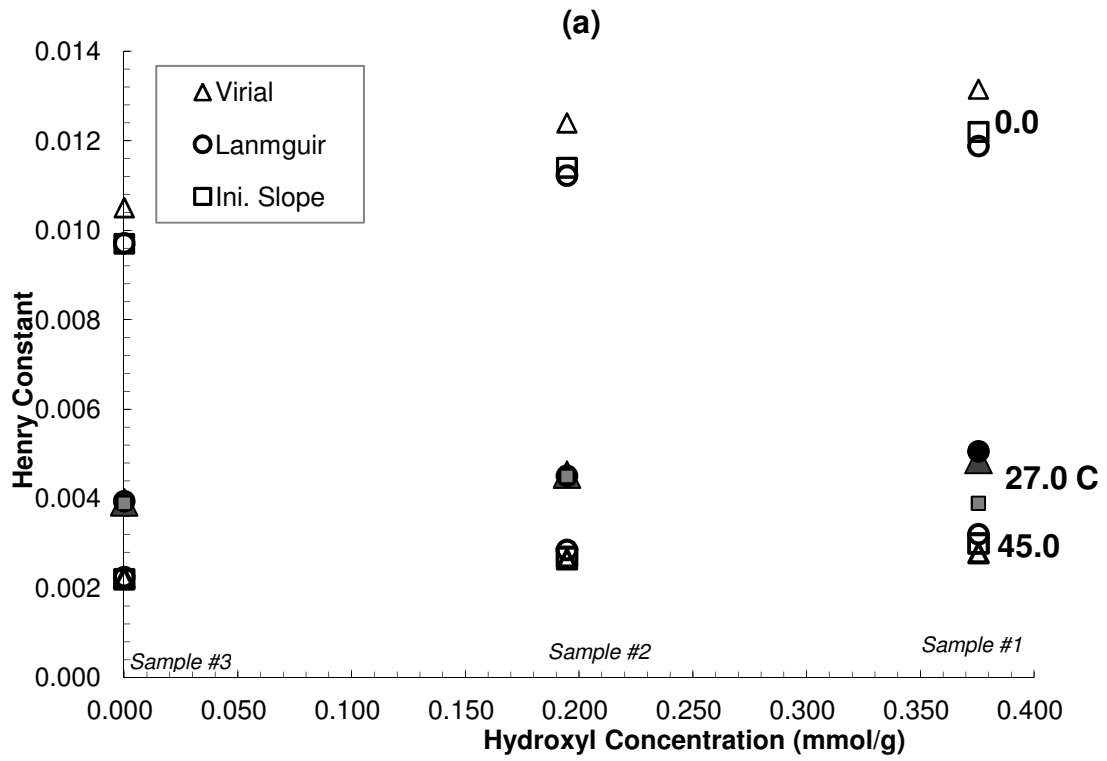


Figure 4.12 Variation of Henry Constants with Hydroxyl Density. (a) MFI Samples (b) DDR Samples.

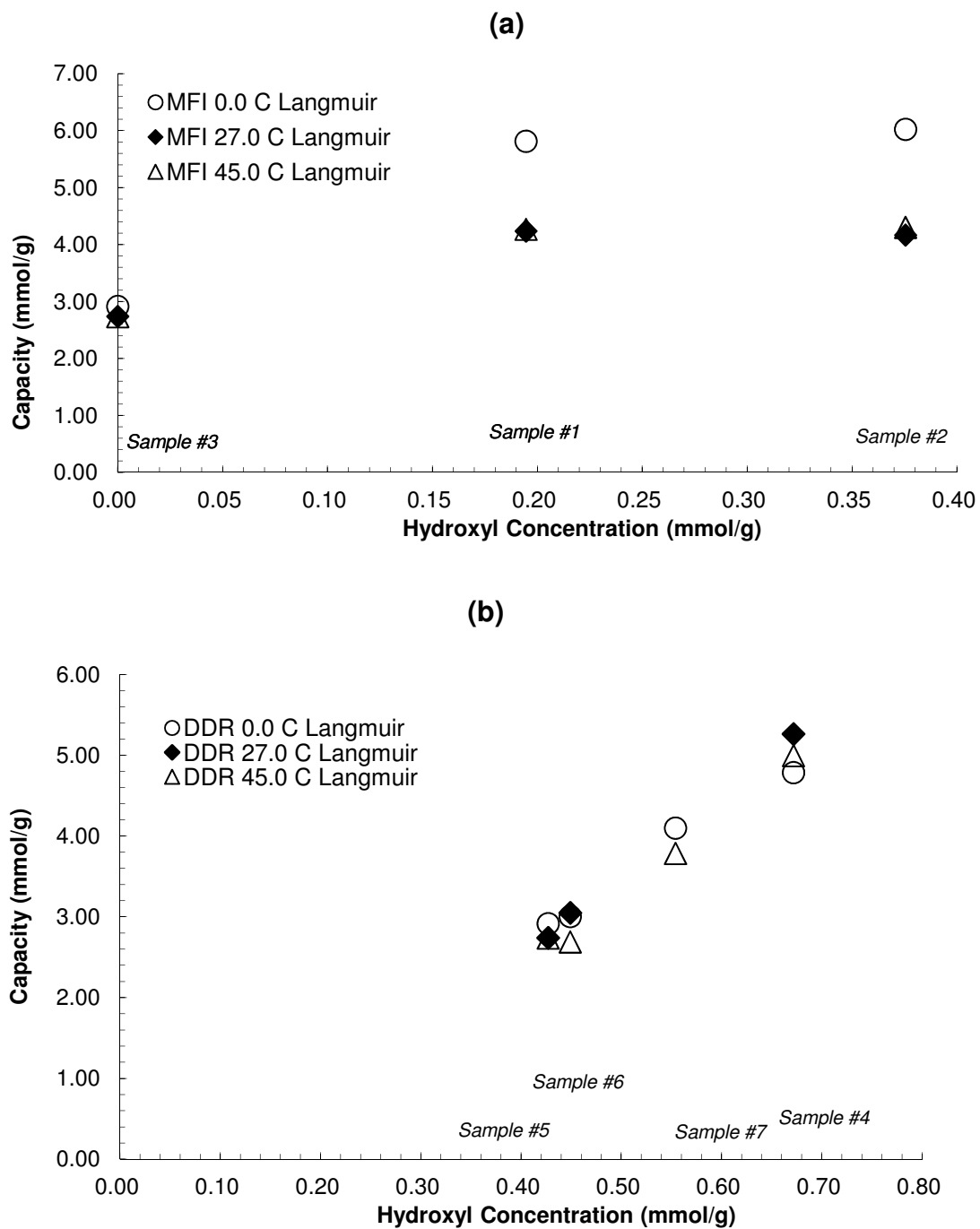


Figure 4.13 Correlation of Langmuir Capacity (q_s) with Hydroxyl Density. (a) MFI Samples (b) DDR Samples.

According to the Langmuir model the Henry constant is related to the Langmuir equilibrium constant by $K = bq_s$ where q_s is independent of temperature and the temperature dependence of b follows a van't Hoff equation (Eq 4.3). We therefore have:

$$K \exp\left(\frac{\Delta H_0}{RT}\right) = b_0 q_s \quad (4.5)$$

where $b_0 q_s = K_0$ (at reference temperature T_0). If, in accordance with the Langmuir model, all sites are equivalent in all four DDR samples, then the Henry constant data shown in figure 4.12b should be reduced to a single straight line when plotted in the form $K \exp(\Delta H_0/RT)$ vs q_s . Such a plot is shown in figure 4.14 from which it appears that the experimental data for DD3R do indeed conform approximately to this simple model. The data therefore suggest that the observed increase in the Henry constant with hydroxyl density arises from a substantial increase in the CO_2 site density, rather than from the creation of a few very strong sites.

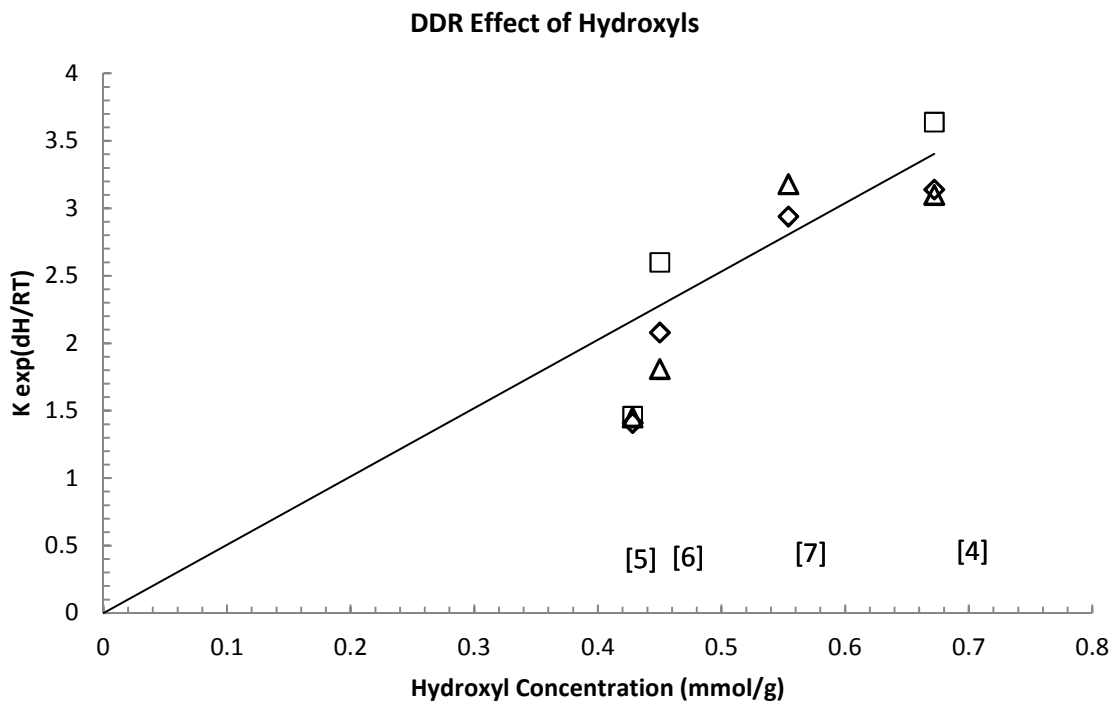


Figure 4.14 Variation of Henry Constant Pre-Exponential Parameter (K_0) with Hydroxyl concentration for DDR samples. Sample numbers are indicated.

4.3.4 Saturation Capacity and Intracrystalline Pore Volume

The saturation capacities derived from the isotherms are compared in Table 4.4 with the values estimated from the specific pore volumes (0.185 ml/g for MFI and 0.15 ml/g for DD3R derived from N_2 adsorption at 77K)^{42,43} and the liquid density or van der Waals co-volume for CO_2 (42.7ml/mole). For DD3R the saturation capacity for CO_2 at 20 atm derived by Jee and Sholl³⁰ from a GCMC simulation is also included. It is worth noting that these capacities (for DD3R) are significantly smaller than the value estimated from the crystallographic interior volume of the large (19-hedral) cages (0.35nm³ per cage, 6 cages per unit cell), the unit cell volume (6.8nm³) and the crystal density

(1.71g/ml), which yield a specific pore volume of 0.18ml/g and a corresponding saturation capacity of 4.2 mmole/g.

Table 4.4 Calculated Saturation Capacities for CO₂ Adsorption.

	MFI Capacity (mmol/g)	DDR (mmol/g)
Liquid ρ	4.3	3.62
Van Der Waals	4.45	3.63
GCMC (Sholl)	-	3.12
Langmuir*	2.7 - 6.0	2.7-5.3

*See figure 4.13.

The Langmuir model provides only an approximate representation of the equilibrium isotherms for most zeolitic systems and results derived from such an analysis must therefore be treated with caution. Nevertheless, for these systems, the Langmuir saturation capacities are comparable with the values estimated directly from the pore volumes, thus suggesting that they are at least approximately correct. For DD3R the lowest of the Langmuir saturation capacities (corresponding to the low hydroxyl samples, 5 and 6) are similar to the GCMC value and somewhat smaller than the pore volume based estimates while the highest values (for the higher hydroxyl samples) are larger than the pore volume based estimates. They are also larger than the saturation capacity estimated for total filling of the large cages (4.2 mmole/g.).

It is remarkable that, for DD3R, a modest increase in the hydroxyl density (from 0.43 to 0.67 mmole/g) leads to an increase in the saturation capacity from about 3 to 5 mmole/g. The variation in hydroxyl content corresponds to 0.52 – 0.8 hydroxyls per large cage or about 3 -5 hydroxyls per unit cell. The observed increase in CO₂ saturation capacity with hydroxyl content, which corresponds to a change from 20 to 37 CO₂

molecules per unit cell, cannot therefore be attributed, on any reasonable stoichiometric basis, to a variation in the number of surface sites due to the presence of the hydroxyls. The explanation may be that the presence of hydroxyl defects allows the CO₂ molecules to access regions of the structure which are inaccessible in a perfect crystal. The total specific intracrystalline pore volume is about 0.25 ml/g which would correspond to a saturation capacity of about 6 mmoles/g or about 43 CO₂ molecules per unit cell which is larger than the highest of the Langmuir q_s values (≈ 5 mmole/g. for sample 4).

4.4 Conclusions

The adsorption equilibrium isotherms for CO₂ (a small quadrupolar molecule) on high silica MFI and DD3R zeolites are of similar form but they show some striking differences, especially with respect to the effect of hydroxyl content. The MFI surface appears to be quite homogeneous and is evidently not significantly perturbed by the presence of hydroxyls, at least at levels less than 0.4 mmole/g (as indicated by Henry constants). Heats of adsorption are essentially independent of loading (≈ 25 kJ/mole) regardless of hydroxyl content. The isotherms conform closely to the Langmuir model and the saturation capacities of the different samples are similar but appear to show some dependence on temperature.

Two of the DD3R samples show some evidence of energetic heterogeneity since the heat of adsorption increases at low loading. The isotherms for these samples also show a significant “foot” (corresponding to a small fraction of highly favorable sites) the magnitude of which correlates approximately with the hydroxyl content. The isotherms,

when corrected for the “foot”, conform well to the simple Langmuir model. The saturation capacities are essentially independent of temperature but show a correlation with the hydroxyl content. For the sample with the highest hydroxyl content the Langmuir saturation capacity is about 5 mmole/g, which is greater than the capacity estimated from total filling of the large (19-hedral cages) but less than the estimated capacity for complete filling of the intracrystalline pore space.

The heats of adsorption for all four DDR samples are similar but the Henry constants are significantly different and, in conformity with the Langmuir model, they appear to correlate approximately linearly with the saturation capacities. This implies that the effect of the hydroxyls is to increase the number of sites with no significant effect on the “strength” of each site. Although clearly supported by the experimental data such behavior seems surprising as it implies that an increase in hydroxyl density from 0.43 to 0.67 mmole/g leads to an increase from about 2.7 to 5.3 mmole/g in the CO₂ saturation capacity! This may suggest that the hydroxylated samples, as a result of structural defects, allow CO₂ to access interior regions of the framework which are normally inaccessible.

The hydroxyl content of the silicalite samples varied between 0 and 0.375 mmoles/g whereas, for the DD3R samples the corresponding range was 0.43 to 0.67 mmoles/g. One cannot therefore exclude the possibility that the observed differences in behavior between MFI and DD3R simply reflect the difference in the levels of hydroxyl content, rather than any intrinsic difference. However, based on the magnitude of the effects observed for DD3R, this seems somewhat unlikely.

CHAPTER 5

ZLC METHOD

The intracrystalline diffusion measurements reported in this thesis were all made by the ZLC technique. This approach was introduced in 1988 by Eic and Ruthven⁴⁴ to provide a reliable and reproducible macroscopic technique that would avoid the intrusion of heat transfer limitations and other extracrystalline effects that make it difficult to derive reliable intracrystalline diffusivities from direct gravimetric or volumetric measurements of uptake rates. The technique has been developed and refined over the years and has been widely applied to study many different systems. This chapter presents a review of both the underlying theory and the experimental practice as well as a detailed description of the experimental system used in the present studies.

5.1 General Principle of the ZLC Method

Put simply, the ZLC technique measures the desorption rate from a small sample (typically about 3 mg) that has been pre-equilibrated with the sorbate and then purged, at a steady flow rate with a non-adsorbing carrier gas such as He. Desorption rather than adsorption is measured in order to take advantage of the greatly enhanced detector sensitivity when the baseline is zero. A schematic diagram showing a typical ZLC system is shown in Figure 5.1 and the ZLC cell is shown in Figure 5.2.

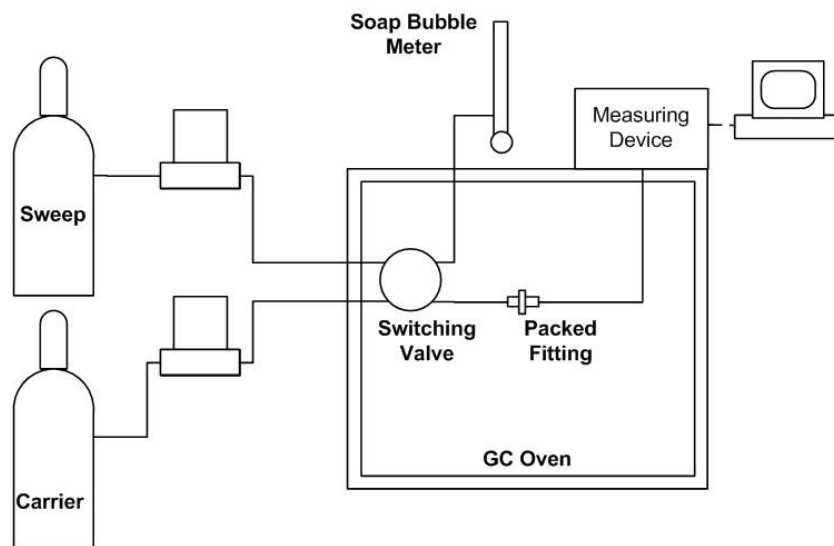


Figure 5.1 Schematic Diagram of the ZLC System.

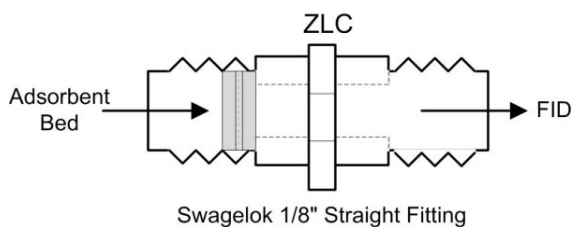


Figure 5.2 ZLC Packed Swagelok Union.

Two limiting situations can be visualized depending on the purge flow rate or, more specifically, on the dimensionless parameter $L = FR^2/3KV_sD$. At sufficiently low flow rates ($L \ll 1.0$) the adsorbed phase is always at equilibrium with the purge stream. In this situation the desorption rate is controlled entirely by equilibrium and, depending on the initial loading level, the ZLC desorption curve will directly yield the Henry constant. For higher initial loadings the equilibrium isotherm can be extracted from the response curve. At sufficiently high flow rates ($L > 10$) the desorption rate is controlled by diffusion out of the particle (or less commonly by mass transfer resistance at the particle surface). Under these conditions, provided that the measurement is performed at

low concentrations (within the Henry's law region), analysis of the ZLC response curve yields both the Henry constant and the time constant for intracrystalline diffusion (D/R^2) or, under conditions of surface resistance control, the surface mass transfer time constant ($3k/R$).

A very small sample of adsorbent is used in order to minimize the intrusion of extracrystalline resistance to heat and mass transfer. However, for weakly adsorbed species with low Henry constants and comparatively low heats of adsorption larger adsorbent samples (approximately 20 mg) can be used. This has the advantage of improving the accuracy of the values derived for the Henry constants.

5.2 Advantages and Limitations of the ZLC Technique

The method requires a sensitive detector capable of following the concentration of sorbate in the effluent stream over several orders of magnitude. A rapid response and stable baseline are also necessary.

The main advantage of the ZLC technique is that, by making measurements at high purge flow rates, extracrystalline resistance to heat and mass transfer may be essentially eliminated and, in contrast to other chromatographic methods, axial dispersion has no impact. The absence of significant extracrystalline resistances can be confirmed simply by varying the sample quantity and any influence from surface resistance can then be determined from replicate measurements over a range of purge flow rates.

In its original embodiment the ZLC technique measures the limiting transport diffusivity at zero loading which should correspond to the limiting value of the

thermodynamically corrected diffusivity (D_0). However, obvious extensions of the technique allow the measurement of self diffusivities at any desired loading level (tracer ZLC) utilizing isotopically labeled molecules to differentiate between sorbate and purge. Another variant is the measurement of diffusion in a counter-flow system (CCZLC in which one component is adsorbing while another species desorbs). In the present study a number of experiments were carried out in the CCZLC mode in order to assess the impact of an excess of CO_2 on the diffusion of methane.

The method is useful for measuring relatively rapid diffusion processes but it is of course essential that the diffusion time (R^2/D) is substantially larger than the response time of the detector (as well as response time of switching valve and dead volume of cell). This places a limit on the maximum diffusivity that can be measured with any given size of crystal. Simultaneous determination of the diffusional time constant and the Henry constant is possible over a wide range of conditions, but for weakly adsorbed species the accuracy with which the Henry constant can be determined declines. This can often be compensated for by using a larger sample of adsorbent but this may introduce extracrystalline resistances to mass and heat transfer, thereby reducing the accuracy of the diffusion measurements.

The method also breaks down for very strongly adsorbed species since, for such species, it may be difficult (or even impossible) to achieve a combination of loading level and purge flow rate that will yield sufficiently large L values and a sufficiently high concentration level to allow the desorption curve to be followed accurately.

5.3 ZLC Mathematical Model

The mathematical model that is generally used to analyze ZLC response curves is based on the following assumptions:

- Equilibrium between sorbate concentration at the particle surface ($r = R$) and in the surrounding gas in accordance with Henry's law ($q_R = Kc$).
- Perfect mixing of fluid surrounding the particle(s) with negligible hold-up in the fluid phase. This implies that each particle is always exposed to the same fluid concentration at its external surface.
- Fickian diffusion in a spherical particle with constant D ; as described by equation 5.1

$$\frac{\partial q}{\partial t} = D \left(\frac{\partial^2 q}{\partial r^2} + \frac{2}{r} \frac{\partial q}{\partial r} \right) \quad (5.1)$$

Initial Conditions:

- Particle is initially at equilibrium with a fluid phase sorbate concentration c_0 .

i.e For $t < 0$, purge stream contains concentration c_0 :

$$q(r) = q(R) = q_0 = Kc_0 \quad (5.2)$$

- For $t > 0$, purge contains no sorbate.

Boundary Conditions:

The sorbate concentration in the effluent stream (c) is determined by the rate at which sorbate diffuses out of the solid. Equilibrium is established rapidly at particle

surface. Combining the boundary conditions and the model assumptions, equation 5.3 can be reduced to equation 5.4

$$\left(\frac{\partial q}{\partial r}\right)_{r=0} = 0; q(R,t) = Kc(t) \quad (5.3)$$

$$-D\left(\frac{\partial q}{\partial r}\right)_R \cdot \frac{3V_s}{R} = Fc = \frac{Fq}{K} \quad \text{or} \quad -D\left(\frac{\partial q}{\partial r}\right)_R = \frac{FR}{3KV_s} \cdot q \quad (5.4)$$

In dimensionless form these equations become:

$$\frac{\partial Q}{\partial \tau} = \frac{2}{\eta} \frac{\partial Q}{\partial \eta} + \frac{\partial^2 Q}{\partial \eta^2} \quad (5.5)$$

where $Q = q/q_0$, $\eta = r/R$, $\tau = Dt/R^2$.

$$\eta = 1; -\left(\frac{\partial Q}{\partial \eta}\right)_{\eta=1} = \frac{FR^2}{3KV_s D} Q_{\eta=1} = LQ_{\eta=1} \quad (5.6)$$

$$\text{where } L = \frac{FR^2}{3KV_s D} ; F = \text{Flow Rate, } V_s = \text{Volume of Sample} \quad (5.7)$$

The above equation simply expresses the fact that the rate of diffusion out of the solid is equal to the rate at which sorbate flows out of the cell. The solution to this set of equations is given by Crank (*Mathematics of Diffusion*)⁴⁵:

$$\frac{c}{c_0} = \sum_{n=1}^{\infty} \frac{2L}{\beta_n^2 + L(L-1)} e^{\left(-\beta_n^2 \frac{D}{R^2} t\right)} \quad (5.8)$$

where β is given in the roots of equation 5.9, and L is defined in Equation 5.10, K is the dimensionless Henry constant and D/R^2 is the diffusion time constant.

$$\beta_1 \cot \beta_1 + L - 1 = 0 \quad (5.9)$$

$$L = \frac{\varepsilon v r_c^2}{3(1-\varepsilon)KDl} = \frac{1}{3} \frac{\text{Purge flowrate}}{\text{Crystal volume}} \frac{r_c^2}{KD} \quad (5.10)$$

Note that in the long time region only the first term of the summation is significant so Eq.5.8 becomes:

$$\frac{c}{c_o} = \frac{2L}{\beta_1^2 + L(L-1)} e^{\left(-\beta_1^2 \frac{D}{R^2} t\right)} \quad (5.11)$$

In the diffusion controlled system, the ZLC response curve therefore approaches the linear asymptote defined by Eq. 5.11.

$$\ln\left(\frac{c}{c_o}\right) \approx \ln\left[\frac{2L}{\beta_1^2 + L(L-1)}\right] - \left(\beta_1^2 \frac{D}{R^2}\right)t \quad (5.12)$$

The parameter L determines whether the system is equilibrium controlled or diffusion controlled. That is to say, if it is diffusion controlled then the rate limiting step is the diffusion of the sorbate out of the micropores. This occurs when the flow rate is sufficiently high so that when a sorbate molecule migrates to the external surface of the particle it is immediately swept away, maintaining the surface concentration close to zero. Conversely, equilibrium control occurs when the flow rate of the sweep stream is

sufficiently low. The sorbate then has sufficient time to equilibrate, and the concentration throughout the adsorbent is uniform and very close to the equilibrium level.

5.3.1 Long Time Asymptotic Analysis

Given these two different regimes, both diffusivity and equilibrium can be determined. Furthermore, within the diffusion controlled regime, both the equilibrium and diffusion parameters can be determined. When L is large ($L > 10$), $\beta_1 \approx \pi$ and Eq. 5.12 reduces further to:

$$\ln \frac{c}{c_0} = \ln \left[\frac{2L}{\pi^2 + L(L-1)} \right] - \pi^2 \frac{Dt}{R^2} \quad (5.13)$$

The concentration is normalized using the initial concentration, and plotted against time on a semi-log plot, that is $\ln(c/c_0)$ v t . The slope and intercept of a plot of $\ln(c/c_0)$ vs t thus yield D/R^2 and L (from which K can be calculated using Eq.5.10). Knowing the sample mass, density and mean particle radius the intraparticle diffusivity (D) and the adsorption equilibrium constant (K) can then be immediately obtained. Even if the initial sorbate loading lies somewhat beyond the linear region of the isotherm the linear analysis is justified because, in the asymptotic region, the loading approaches zero. However, under such conditions the value derived for K (from the intercept) will not be reliable.

A more accurate estimate of K can be obtained from measurements at low flow rates (such that $L \ll 1$). Under these conditions the ZLC response curve (Eq.5.11) reduces to the very simple exponential form:

$$\frac{c}{c_o} = \exp\left(-\frac{Ft}{KV_s}\right) \quad (5.14)$$

or, allowing for gas phase hold-up within the ZLC cell:

$$\frac{c}{c_o} = \exp\left(-\frac{Ft}{KV_s + V_g}\right) \quad (5.15)$$

In coordinates of $\ln(c/c_o)$ vs t this yields a straight line through the origin of slope $F/(KV_s + V_g)$ from which K is easily obtained. Under most conditions the hold-up in the gas phase was negligible ($KV_s \gg V_g$) so this contribution was neglected. However, this approximation breaks down for weakly adsorbed species (such as methane) at higher temperatures when V_s is small.

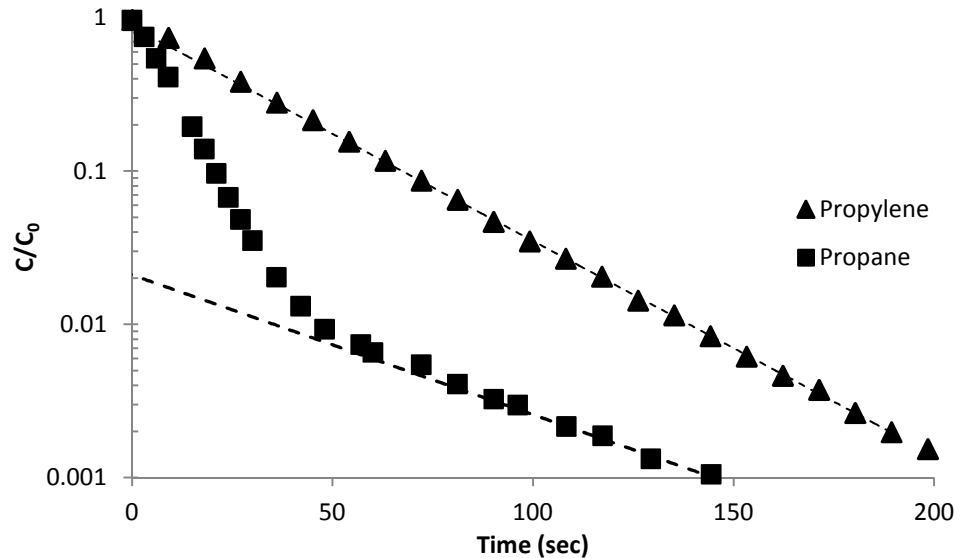


Figure 5.3 Sample ZLC Data Comparing Diffusion and Equilibrium control. Zeolite 4A, 150 °C, 5 ml/min. The propylene data (\blacktriangle) is equilibrium controlled, Propane data (\blacksquare) is diffusion controlled.

A plot showing sample data is given in Figure 5.3. Under the conditions of these experiments propylene diffuses rapidly so the ZLC response is controlled mainly by

equilibrium (Eq. 5.16). Propane diffuses more slowly and shows the form of response typical of diffusion control with the long time linear asymptote given by Eq. 5.13.

It follows from Eq 5.13 that when L is large (diffusion control), the slope of the $\ln(c/c_0)$ vs t plots should be inconsistent with flow rate while the intercept will decrease as F (and therefore L) increases. Measurements at different flow rates should therefore yield a series of parallel asymptotes. Similarly when L is small the desorption curve depends only on the product Ft which corresponds to the total purge gas volume. Under these conditions a plot of $\ln(c/c_0)$ vs Ft will be independent of flow rate thus providing a convenient experimental test for equilibrium control, even under non-linear conditions.

For a linear system adsorption and desorption rates, measured over the same pressure step are the same. The desorption curve is used instead of the adsorption curve because the detector is more sensitive when approaching zero as the baseline, thus yielding more accurate data.

5.3.2 Intermediate Time Curve Analysis

The robustness and reliability of the asymptotic analysis have been confirmed in many previous experimental studies^{46,47,48,49,50}. However, when the sorbate is both weakly adsorbed and fast diffusing it is not always possible to determine the long time asymptote with sufficient accuracy. In the study discussed in chapters 6 and 7 this problem was encountered for some of the measurements with methane, especially in the presence of CO_2 . In that situation an alternative approach based on the “intermediate time approximation” for the ZLC response⁴⁹ is useful. In the short time region (after a time

dictated by the blank response and before the long time asymptote is reached) for sufficiently high values of L (> 20):

$$\frac{c}{c_o} \approx \frac{I}{L} \left[\sqrt{\frac{R^2}{\pi D t}} - 1 \right] \quad (5.16)$$

In this regime a plot of (c/c_o) vs $1/\sqrt{t}$ should yield a straight line with an intercept of $\sqrt{(\pi D/R^2)}$ on the $1/\sqrt{t}$ axis ($x_{\text{int}} = \sqrt{\pi D/R^2}$), thus allowing the direct determination of D/R^2 ; and an intercept of $-1/L$ on the c/c_o axis ($y_{\text{int}} = -1/L$) allowing the determination of L and hence the Henry constant. Representative examples of such plots are shown in figure 5.4. It should be noted that the average x-axis intercept is approximately 0.295, and is independent of flow rate, in conformity with Eq 5.16.

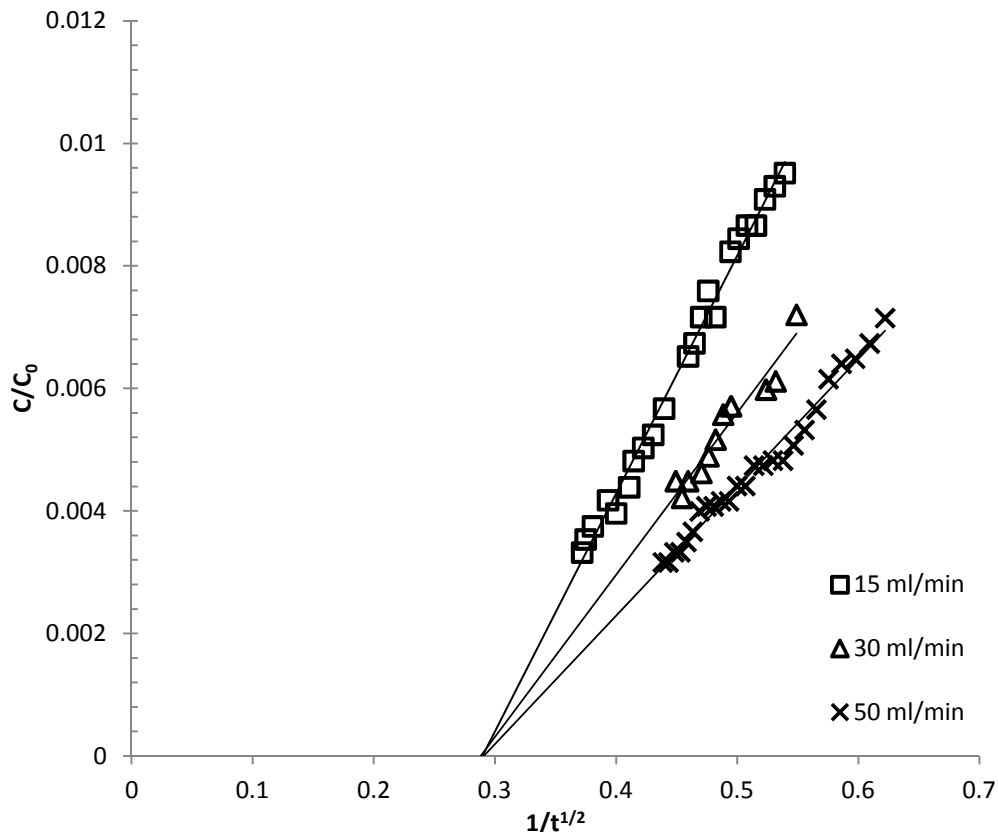


Figure 5.4 Representative ZLC Response Curve for Intermediate Time Analysis. DDR I Methane 75 °C, Plot shows consistency with Eq. 5.16.

An alternative approach would be to use the full solution for the ZLC response as defined by Eq.5.8. However that approach suffers from two significant disadvantages: (i) the initial response (for fast systems) is limited by the detector response time and (ii) the initial part of the ZLC response curve is sensitive to any small deviations from isotherm linearity. Therefore, in this study, the asymptotic analysis was preferred.

5.4 Extended Model

In the course of the analysis of the data for ethane and ethylene which is discussed in detail in chapter 7, puzzling results were initially obtained. In the original ZLC

model^{50,51,52} it was assumed that the desorption rate is controlled entirely by diffusion out of the particle, with equilibrium always maintained with the surrounding fluid at the external surface. For many systems this is a reasonable approximation but recent studies carried out by advanced optical techniques such as interference microscopy (IFM) or infra-red microscopy (IRM)^{53,54,55} have revealed that, in many zeolite crystals, there is significant mass transfer resistance at the external surface so that the sorption rate is actually controlled by the combined effects of internal diffusion and surface resistance. The ZLC model has been modified for the extreme case in which surface resistance is rate controlling⁵⁶ but the more important general situation in which both internal and surface resistances are important has not yet been addressed. Detailed analysis showed that the puzzling data obtained for C₂H₆ and C₂H₄ in DDR was due to the intrusion of significant surface resistance to mass transfer.

When surface resistance is significant Eq. 5.3 remains the same, but Eq. 5.4 becomes:

$$-D \left(\frac{\partial q}{\partial r} \right)_{r=R} = k(q_R - q_{surf}) = \frac{FR}{3KV_s} q_{surf} = \frac{FR}{3V_s} c(t) \quad (5.17)$$

$$\text{Therefore: } Q_R = \frac{q_R}{q_{surf}} = 1 + \frac{FR}{3kKV_s} \quad (5.18)$$

where k is the mass transfer rate coefficient at the surface; in the dimensionless form

Eq.5.5 is replaced by:

$$\eta = 1; \quad - \left(\frac{\partial Q}{\partial \eta} \right)_{\eta=1} = L' Q_{\eta=1}; \quad \frac{1}{L'} = \frac{1}{L} + \frac{D}{kR} \quad (5.19)$$

Since Eq. 5.19 is formally the same as Eq. 5.5 (with L replaced by L') the solutions (Eqs. 5.8 – 5.11) remain the same with L replaced by L' . In the limit of high surface resistance D/kR becomes large and if the purge rate is high enough to satisfy the condition:

$$\frac{3k}{R} \ll \frac{F}{KV_s} \quad (5.20)$$

the concentration profile within the particle becomes flat and the response curve reduces to a simple exponential decay:

$$\frac{c}{c_o} = \frac{3kKV_s}{FR} \exp\left(-\frac{3kt}{R}\right) \quad (5.21)$$

This corresponds to the case of surface resistance control⁵⁷.

It is evident (since L is proportional to F/K) that if a ZLC response curve for a system in which there is significant surface resistance is interpreted in accordance with the original model (assuming negligible surface resistance) the derived value of the parameter L' will be smaller than the true value of L (see Eq. 5.19) with the result that the values of the apparent equilibrium constant (estimated assuming $L' = L$) will be erroneously large and will show an increasing trend with purge flow rate. In contrast the slope of the long time asymptote (provided that $L' > 10$) is essentially independent of L , implying that the diffusional time constant (D/R^2) calculated from the asymptotic slope is not affected by the presence of moderate surface resistance

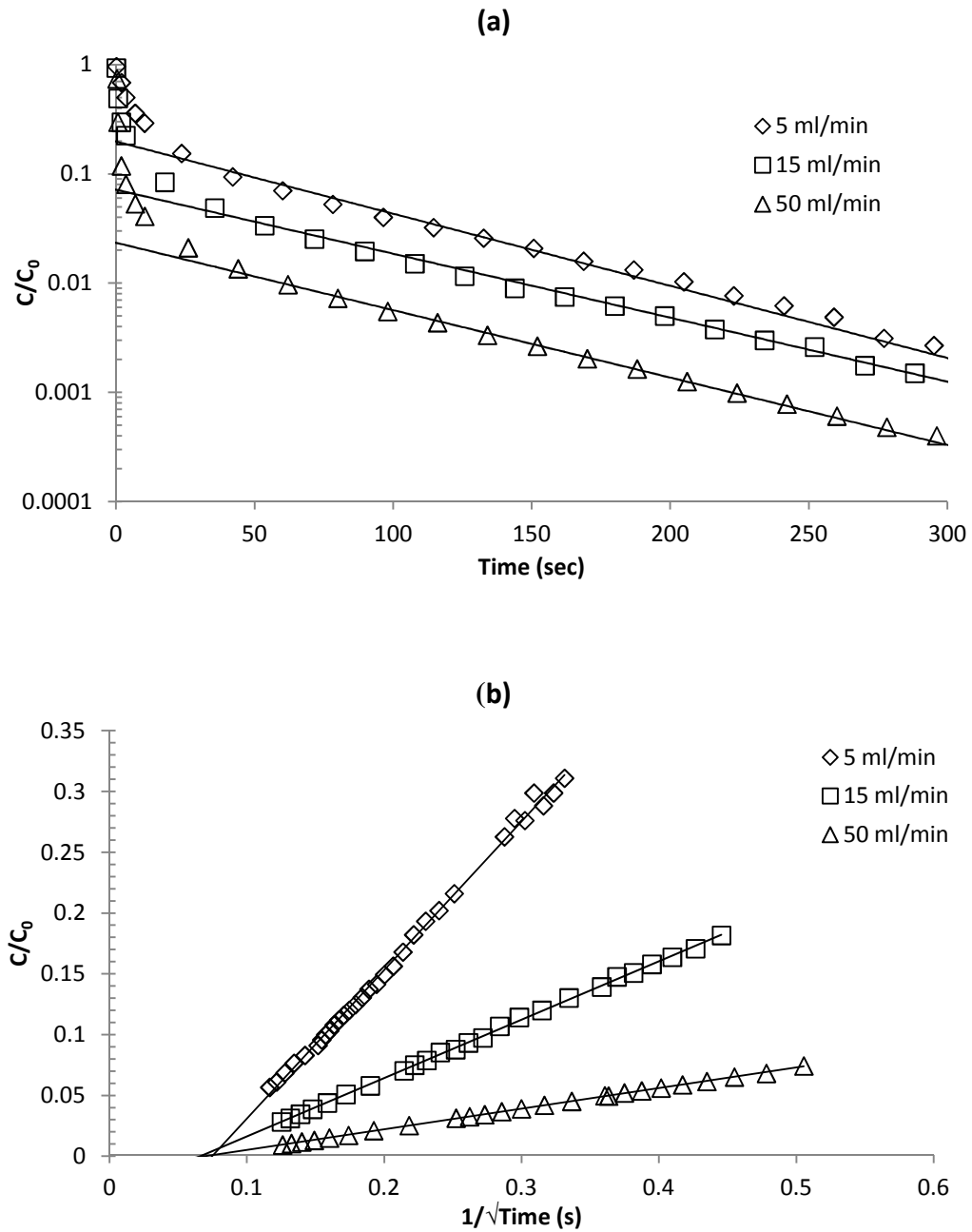


Figure 5.5 ZLC Response Data with Mass Transfer Surface Resistance Affecting L Value. Ethane-He, DDR II 22.1 mg, 75 °C. (a) Represented in long time asymptote form (b) intermediate time analysis.

5.4.1 Experimental Verification

Precisely this pattern of behavior was observed in the experimental study of diffusion of ethane in large crystals (40 μ m diameter) of DD3R discussed in chapter 7. ZLC response curves measured at three different purge flow rates (5,15, 50 ml/min) were used to calculate the diffusional time constants and equilibrium constants in accordance with Eq. 5.8. It is evident from figure 5.5 that the theoretical curves provide an excellent representation of the observed behavior. The parameters L' and D/R^2 were calculated from the slopes and intercepts of the long time asymptotes in accordance with Eq. 5.12, and from the c/c_0 and $1/\sqrt{t}$ intercepts in accordance with Eq. 5.16. The parameter values obtained in both ways were very similar; the average values are summarized in Table 5.1.

Note that the slopes of the long time asymptotes in Fig.5.5(a) are essentially constant and the plots of c/c_0 vs $1/\sqrt{t}$ (Fig.5.5 (b)) show a common intercept on the $1/\sqrt{t}$ axis implying that the diffusivity is independent of flow rate (as it should be).

Table 5.1 Parameters Derived from ZLC Response Curves Comparing L and L'. Ethane in DDR at 348K

F (ml/sec)	L'	L	K'	K	D/R ² (s ⁻¹)
0.097	14	15	120	110	0.0015
0.292	37	49	140	103	0.0015
0.973	78	150	215	112	0.0015

Note: L' is calculated directly from the response curves (Eq.5.12 or 5.16). The values from both these equations are very similar so only the averages are shown. K' is calculated from L' according to Eq. 5.6 assuming $L' = L$. L and K are calculated from L' via Eq. 5.19 with $D/KR = 0.0065$, the value derived from the intercept of figure 5.2.

The variation of L' with flow rate, shown in figure 5.6a, conforms to Eq. 5.19, thus allowing the values of K and the surface rate coefficient (k) to be derived from the slope and intercept of such linear plots.

For comparison the ZLC data for CH_4 in the same sample of DDR crystals at 323K are also included in Figure 5.6. For that system the K values calculated from the traditional model (assuming intracrystalline diffusion control with negligible surface resistance) are independent of flow rate ($L' = L$) and the plot of $1/L'$ vs $1/F$ passes through the origin. It appears that, although surface resistance is significant for ethane it is insignificant for the smaller methane molecule.

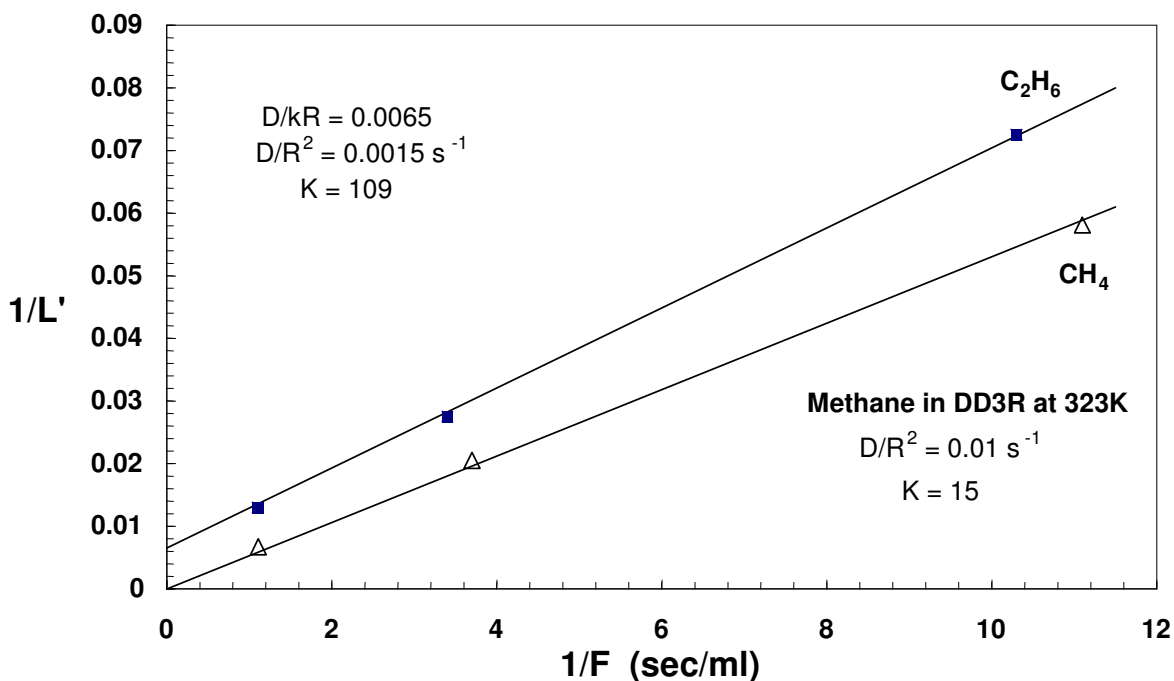


Figure 5.6 Relation of $1/L'$ vs $1/F$ Showing Offset From Surface Resistance, Ethane in DDR at 348 K

5.4.2 New Model Discussion

The new model provides a clear and consistent interpretation of the ZLC response curves for ethane in DDR. More importantly, it provides additional insight into the ZLC technique and a practically useful extension of that technique to allow the detection and measurement of surface resistance.

For ethane in DDR the surface resistance is quite small. To put the magnitude of the surface resistance into context, the half time for surface resistance control is given by $t_{\text{surf}} = (R/3k)\ln 2$ while the half time for internal diffusion is given by $t_{\text{diff}} = 0.03(R^2/D)$ so the ratio $t_{\text{diff}}/t_{\text{surf}} \approx 0.13(kR/D)$. With $D/Rk = 0.0065$ this gives $t_{\text{diff}}/t_{\text{surf}} \approx 20$ so, by normal criteria, the system would be considered to be diffusion controlled. Nevertheless, unless it is properly accounted for in the mathematical model, even this small contribution leads to a strong variation of the apparent K value with flow rate, as may be seen from Table 5.1.

By considering the time constants for the different rate processes (surface resistance, internal diffusion and convective washout of the bed) it is possible to delineate three different kinetic regimes:

1.
$$\frac{3k}{R} \gg \frac{F}{KV_s} \gg \frac{15D}{R^2}$$

In this regime surface resistance is small and convective washout is fast ($L \gg 5$) so the ZLC response is controlled by internal diffusion, as in the original ZLC model.

$$2. \quad \frac{3k}{R} \ll \frac{F}{KV_s} \ll \frac{15D}{R^2}$$

In this regime internal diffusion is rapid while surface resistance is large so that the ZLC response curve is controlled by surface resistance, as in the surface control model⁵⁷.

$$3. \quad \frac{3k}{R} \approx \frac{F}{KV_s} \gg \frac{15D}{R^2}$$

This is the regime covered by the present measurements for ethane-DDR. The desorption rate is controlled mainly by internal diffusion. The slope of the long time asymptote provides an accurate estimate of (D/R^2) but the intercept of the long time asymptote is significantly affected by surface resistance. Within this regime it is possible to determine reasonably accurate values for both the surface rate coefficient and the internal diffusivity as well as the equilibrium constant, provided that measurements are carried out over a sufficiently wide range of purge rates and, under the experimental conditions, the equilibrium isotherm is accurately linear.

The robustness of the derivation of diffusional time constants from the asymptotic slope of a plot of $\ln(c/c_0)$ vs time is clearly demonstrated^{51,52,57}. The experimental data confirm that the diffusivity values derived from the long time asymptote are not significantly impacted by the presence of surface resistance. In contrast, even modest surface resistance has a significant effect on the intercept of the long time asymptote. If the ZLC response curves are interpreted according to the

traditional model this leads to erroneously high apparent values for the Henry constant which will show a regularly increasing trend with purge flow rate. Variation of the purge flow rate thus provides a useful experimental test for the presence of significant surface resistance.

5.5 Experimental ZLC System

The ZLC system used for the experimental studies reported in subsequent chapters is built around a Hewlett-Packard 5890 gas chromatograph. A VICI 4-1/8"-port, high temperature switch valve is used with one of the outlet ports connected to the ZLC cell. The ZLC cell consists of the zeolite adsorbent sandwiched between two sintered disks held inside a 1/8" Swagelok® straight union, a graphic of the cell is in figure 5.2. The outlet of the cell is connected directly to the FID, the other outlet port is vented through a soap bubble meter which allows for precise metering of flow rates. The entire ZLC apparatus is controlled through a program developed using LABVIEW software. A schematic of the entire ZLC apparatus can be found in Figure 5.1.

The two gas streams fed to the system are controlled by mass flow controllers which in turn are controlled by the LABVIEW program. One input line is the purge or sweep gas, the other input is the feed gas prepared using the mixing system set up in order to create gas mixtures of the required composition. This experimental set-up allows for the combination of: methane, ethane, propane, butane, carbon dioxide and helium.

5.6 Experimental ZLC Procedure

Before the experiment, the sample cell is heated to roughly 200 °C under a helium purge stream for 4 hours in order to drive off any moisture or CO₂ previously introduced to the system. The flow rates of the sorbate carrier stream and purge stream are equalized and the sample is equilibrated with the carrier stream (containing 2-3 % mole fraction of the hydrocarbon sorbate). For methane, equilibration times of 20-30 mins were sufficient but longer equilibration times (up to 200 mins) were used for the heavier sorbates. After the equilibration step the valve is switched to expose the ZLC cell to the purge stream. The purge stream picks up the sorbate as it desorbs from the zeolite sample and is carried to the FID to measure concentration, which is recorded as a function of time; the resulting desorption curve can then be used for analysis.

5.6.1 Single Component ZLC Method

The simplest ZLC experiment which is used to determine single component diffusivity and equilibrium values is performed using a non-adsorbing species such as He as carrier and purge. Helium also has the advantage that it diffuses rapidly and has no significant effect on the intracrystalline diffusivity of the sorbate.

5.6.2 Binary System / Counter-Current ZLC Method

The sample is pre-equilibrated with a mixture of CH₄-CO₂ and the sweep stream is pure CO₂ (instead of pure helium). However, to quantify the effect of CO₂ partial pressure the balance of the carrier stream can also be a mixture of both CO₂ and He as

long as the sweep stream contains the same ratio of He:CO₂. It is important to note that the FID sensor performs by measuring the amount of material oxidized in a flame; since CO₂ cannot be oxidized further, the FID is blind to it.

5.6.3 Effect of Pressure Drop

In a traditional ZLC system the quantity of adsorbent within the ZLC cell is very small (typically 2 – 5 mg) so pressure drop through the bed is negligible. However, in order to improve the accuracy with which the equilibrium constants could be measured, larger samples of adsorbent (up to 22 mg) were used in some of the later experiments. It is therefore important to consider whether, for the larger samples, the mathematical model needs to be modified to account for pressure drop through the bed. There are two effects that need to be considered; the variation of gas velocity and the variation of partial pressure through the adsorbent bed. Since the flow rate is controlled by a mass flow controller the molar flow rate will remain constant through the bed, with any variation in gas velocity due to the pressure gradient being exactly compensated by the variation in gas density. The value of c_0 at which the adsorbent particles are pre-equilibrated will vary through the bed but, since the flow rate is constant, the concentration in the gas phase during desorption ($c(t)$) will vary in exactly the same way so that the ratio c/c_0 will be invariant through the bed, even though the absolute value of c varies. Provided that the equilibrium isotherm is linear the desorption curve should therefore not be affected by a pressure gradient.

Direct experimental evidence in support of this conclusion is provided by the agreement observed between the diffusivities measured, under similar conditions, with 2.4 mg and 18.8 mg adsorbent samples – see for example Figures 6.3 and 6.4a.

CHAPTER 6

ADSORPTION AND DIFFUSION OF METHANE WITHIN DDR ZEOLITES IN COMPETITION WITH CO₂

An understanding of diffusion in small pore (molecular sieve) zeolites is important from both practical and theoretical perspectives since such adsorbents offer the possibility of practically useful kinetic separation processes as well as providing model systems for the detailed study of diffusion under sterically restricted conditions. Early size selective (molecular sieve) separations were mostly carried out with cationic 8-ring zeolites such as natural chabazite and Type A^(58,59). From the practical viewpoint such materials suffer from two significant disadvantages; they are strongly hydrophilic and have the potential for catalytic activity, especially at elevated temperatures. These issues can be avoided by the use of pure silica zeolite analogs such as SiCHA and DD3R (the pure silica form of ZSM-58) and, as a result of this advantage these materials have attracted increasing attention in recent years^{60,61,62}. In particular it has been shown that a DD3R membrane has a high perm-selectivity for CO₂/CH₄ making it a promising candidate for application in the purification of low grade natural gas and/or biogas which commonly contain relatively high proportions of CO₂^{20,23}.

6.1 Current DDR-Methane Diffusivity Data

A detailed experimental study of the permeation of light molecules (including CH₄ and CO₂) through a DD3R membrane, supported by a series of careful equilibrium measurements, has recently been reported by van den Bergh et al.^{24,25} Diffusion in DD3R

has also been studied by molecular simulation^{63,64,30} which can provide valuable insight concerning qualitative trends even though the absolute values of the predicted diffusivities are often unreliable. The membrane permeance data and the molecular simulations both suggest a high kinetic selectivity for CO₂/CH₄ (permeance ratio > 100) but a detailed examination of the experimental data, especially the limited permeance data for CH₄-CO₂ mixtures, reveals some interesting and potentially problematic trends. At temperatures in the range 250-300K, where the loading is relatively high, the permeance of CO₂ appears to be reduced in the presence of methane while the permeance of CH₄ is not significantly affected by the presence of CO₂, thus suggesting a reduction in selectivity compared with estimates based on single component data²³. In contrast, the molecular simulations of Jee and Sholl³⁰ suggest that the diffusivity of CH₄ is reduced by the presence of CO₂, suggesting that the perm-selectivity will in fact be greater for the mixture! However, in view of the uncertainty inherent in the molecular simulations, such a conclusion should not be accepted without experimental verification.

Published intracrystalline diffusion measurements for DD3R crystals are limited. The rapid diffusion of CO₂ in DD3R suggested by the permeation data ($D \sim 10^{-10} \text{ m}^2\text{s}^{-1}$ at 300K) has been confirmed by frequency response measurements⁽⁶⁵⁾. Hedin et al⁽²⁷⁾ and Corcoran and Chance^{3,6} have also reported self-diffusivities of $1.5 - 2.0 \times 10^{-12} \text{ m}^2\text{s}^{-1}$ for CH₄ in DD3R (at 301K) as measured by PFGNMR. The high perm-selectivity of DD3R for CO₂/ CH₄ evidently results from a combination of the faster diffusion *and* stronger adsorption of CO₂ relative to CH₄.

In addition to providing single component diffusivity data the ZLC technique is well suited to studying the effect of a second component on intracrystalline diffusion⁴⁷,

^{48,66}. The initial objectives of this study were therefore (a) to provide detailed diffusivity measurements for CH₄ in DD3R, over a range of temperatures, for comparison with the available permeance and PFGNMR diffusivity data and (b) to study the effect of CO₂ on the diffusion of CH₄ in order to confirm, supplement or refute the conflicting information derived from mixed gas permeance measurements and molecular simulations.

6.2 CH₄/CO₂ Competitive Diffusion ZLC Experimental Methods

The experimental study was carried out using the ZLC method described in chapter 5 with two different samples of DD3R crystals of mean equivalent radius 10 μm (DDR I) and 20 μm (DDR II), see figure 6.1. Brief details are given in Table 6.1. Sample DDR I was used without any treatment but sample DDR II was subjected to a proprietary treatment.

Table 6.1 Details of DDR Crystals

	DDR I	DDR II
Avg Crystal Size (μm)	20	40
Si/Al Ratio	950	1662
BET (m²/g)	365	

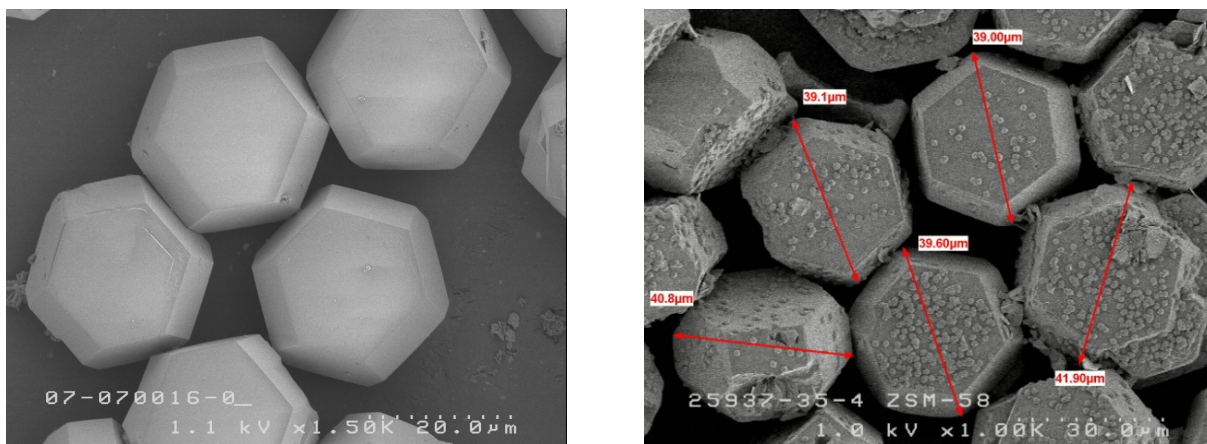


Figure 6.1 SEM Photomicrographs of DDR Samples. Mean diameters: DDR I (left) = 20 μm ; DDR II (right) = 40 μm .

The samples were pre-conditioned by purging with helium for a period of several hours at 250° C and then equilibrated, at the relevant temperature, with a gas stream containing 3% CH_4 in either He or CO_2 . In the initial series of measurements, carried out with DDR I, two different sample quantities of adsorbent were used (2.4 and 18.8 mg) in order to confirm the absence of any bed diffusion or other extracrystalline resistances. In later experiments (with DDR II) a somewhat larger sample (22.1 mg) was used in order to improve the accuracy of the equilibrium data. The large sample was made possible by using a much larger ZLC cell provided by Drs Robert Marriott and Johnathan Lowe of the Alberta Sulphur Research Lab.

Representative ZLC experimental response curves are shown in figure 6.2a. The curves clearly show the asymptotic form predicted from Eq.5.13. with slopes essentially independent of flow rate, as expected for the diffusion controlled regime ($L > 10$). The corresponding diffusivities and equilibrium constants are summarized in Table 6.2. Both the derived diffusivity values (calculated from the slopes of the long time asymptotes) and the dimensionless equilibrium constants (calculated from the intercepts) are

essentially constant ($\pm 10\%$) for the different flow rates in conformity with the mathematical model.

The robustness and reliability of the asymptotic analysis have been confirmed in many previous experimental studies. However, when the sorbate is both weakly adsorbed and fast diffusing it is not always possible to determine the long time asymptote with sufficient accuracy. During the study this problem was encountered especially for some of the measurements with $\text{CH}_4 - \text{CO}_2$ in the smaller samples of DDR I. In this situation the intermediate time approximation for the ZLC response⁴⁹ is useful; utilizing equation 5.16 described in the previous chapter. Examples of such plots are shown in figure 6.2c and the consistency of the kinetic and equilibrium parameters derived from intermediate time plots in comparison with the values derived from the asymptotic analysis is shown in Table 6.2. In all subsequent calculations the average values from the two different methods are used.

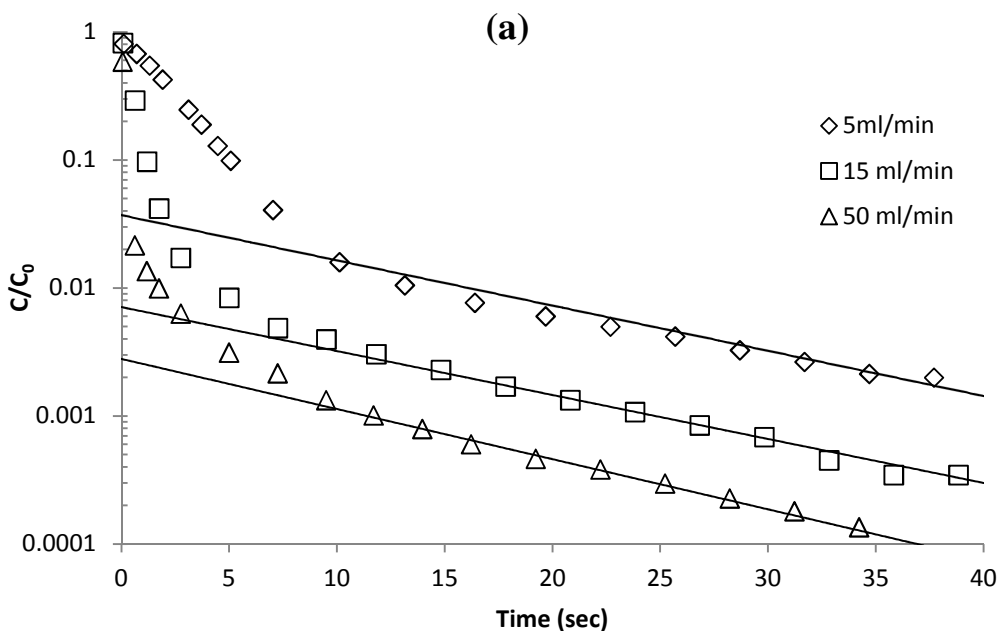


Figure 6.2 Representative Data Plots for Methane-He 25 °C. (a) Long Time Asymptote DDR I, 2.4 mg.

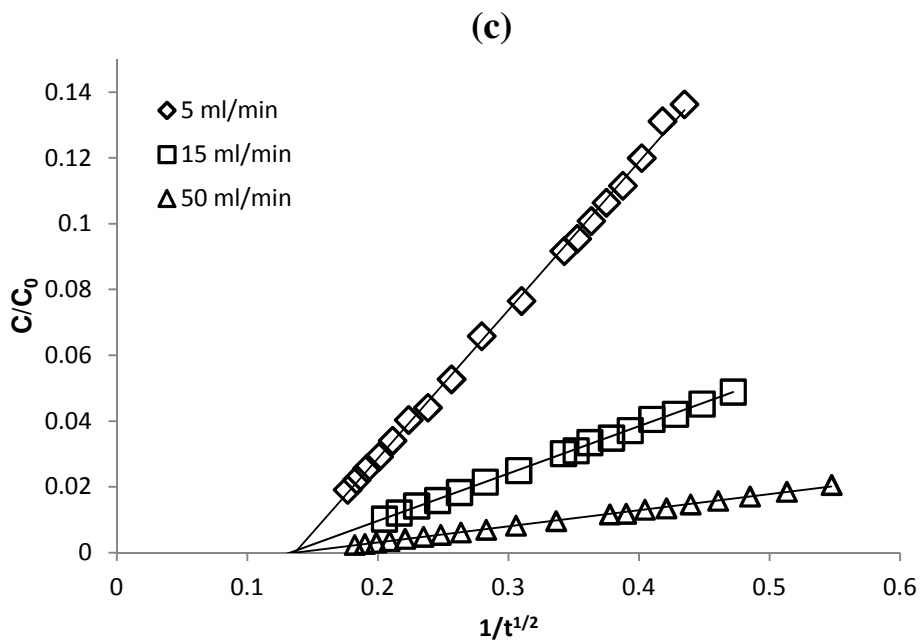
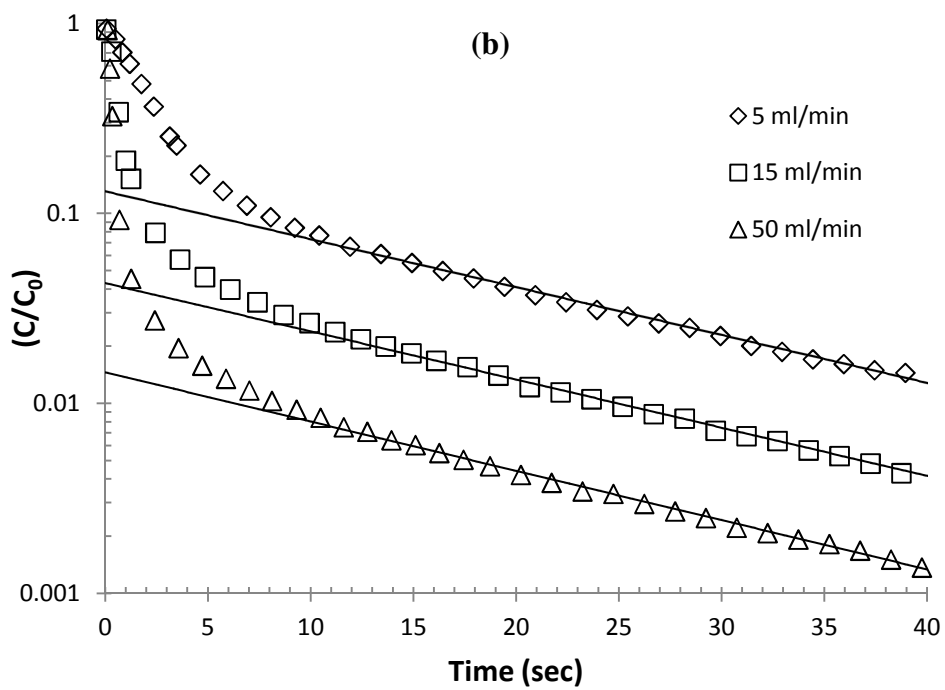


Figure 6.2 (continued...) Representative Data Plots for Methane-He 25 °C (b) Long Time Asymptote, DDR II 22.1mg (c) Intermediate Time Analysis, DDR II 22.1mg.

Table 6.2 Summary of Parameters Derived from ZLC Response Curves. Response Curves can be found figure 6.2.

CH₄-He 298K 2.4mg DDR I – Asymptotic Analysis					
F(ml/min)	Int.	-Slope (s⁻¹)	L	D/R²	K
5	0.028	0.078	71	0.0082	32
15	0.0092	0.089	217	0.0091	30
30	0.0046	0.075	435	0.0077	36
30	0.0044	0.085	455	0.0086	30
50	0.002	0.072	1000	0.0073	28

CH₄-He 298K 22.1 mg DDR II – Asymptotic Analysis					
F(ml/min)	Int.	-Slope (s⁻¹)	L	D/R²	K
5	0.028	0.0563	16	0.0064	24
15	0.0422	0.058	47	0.0061	26
50	0.128	0.056	156	0.0057	24

CH₄-He 298K 22.1 mg DDR II – c/co vs 1/vt Plot					
F(ml/min)	y int.	x int.	L	D/R²	K
5	-0.0592	0.134	17	0.0057	22
15	-0.019	0.133	52	0.0056	22
50	-0.0066	0.136	152	0.0059	24

The model assumes isotropic diffusion in a spherical adsorbent particle. In fact the channel structure of DDR is two-dimensional²⁶ so, in an ideal DDR crystal, one would expect negligible diffusion in the axial direction. It might therefore be more appropriate to consider the hexagonal crystals (see figure 6.1) as equivalent to infinite cylinders in which diffusion occurs only in the radial direction. It is shown appendix A that such a model leads to essentially similar expressions for the ZLC response curve and essentially the same diffusivity will be derived from both models if the equivalent

spherical radius is taken as 1.3 times the radius of the crystal. For consistency with previous data the spherical particle model has been used. Use of the cylindrical model would lead to diffusivity values that are increased by a factor of about 1.7.

To confirm the absence of extracrystalline resistance and thermal effects, measurements were carried out over a wide range of purge flow rates with different sample quantities. Representative results for methane at 298 K in 2.4 mg and 18.8 mg samples of DDR I are shown in figure 6.3. It is clear from figure 6.3a that the diffusional time constants (D/R^2) derived from the ZLC response curves are essentially invariant with purge flow rate and almost the same for the 2.4 and 18.8 mg samples. The values for $\text{CH}_4\text{-CO}_2$ are consistently higher than for $\text{CH}_4\text{-He}$. It follows from the definition of the parameter L (Eq 5.6) that, for measurements at a constant temperature with different sample quantities, a plot of $1/V_s L$ vs $1/F$ should yield a straight line through the origin with slope $3KD/R^2$. It is clear from figure 6.3b that the data for the 2.4 and 18.8 mg samples conform to this pattern showing consistency of both the equilibrium constants and the diffusivities between the two data sets. Although the diffusivity values for $\text{CH}_4\text{-CO}_2$ are consistently larger than the values for $\text{CH}_4\text{-He}$ (figure 6.3a) the product KD is essentially the same for both the He and CO_2 systems (figure 6.3b). This point is discussed in greater detail below.

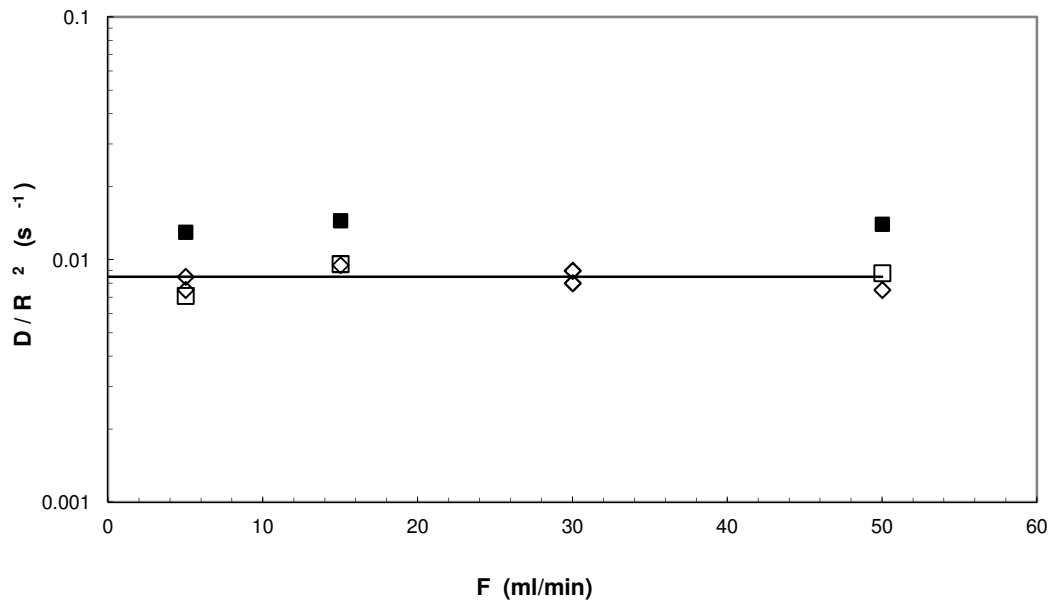


Figure 6.3. Comparison of Time Constants for Both Purge Gasses Comparing D/R^2 vs F . CH_4 - He (open symbols) and CH_4 - CO_2 (filled symbols) in 2.4 mg (◇) and 18.8 mg. (□, ■) samples of DDR I at 298K.

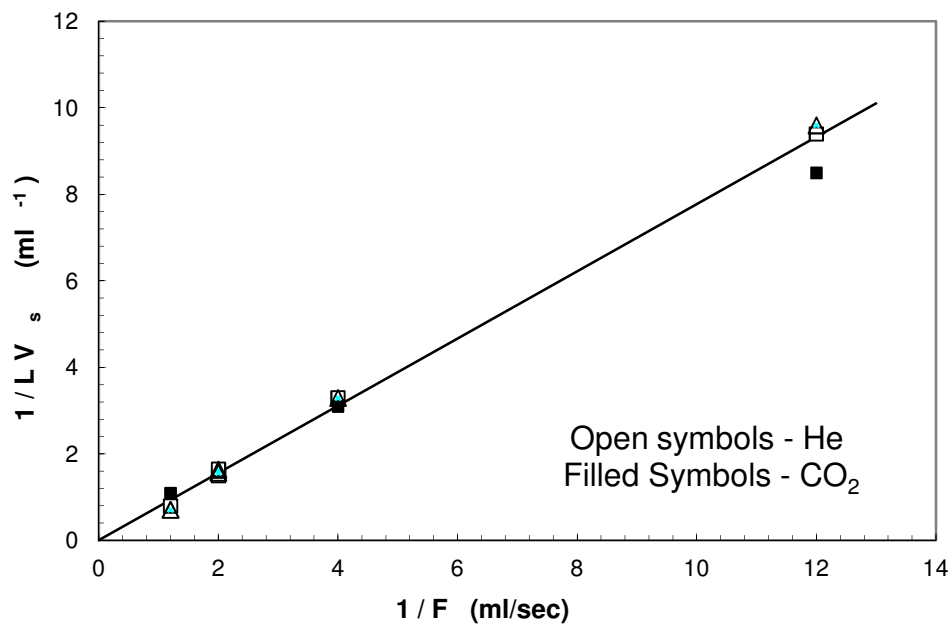


Figure 6.4. Comparison of Time Constants for Both Purge Gasses Comparing $1/LV_s$ vs $1/F$. CH_4 - He (open symbols) and CH_4 - CO_2 (filled symbols) in 2.4 mg (◇) and 18.8 mg. (□, ■) samples of DDR I at 298K. Confirming absence of any surface resistance as well as conformity between data for the different samples of DDR I and for He and CO_2 carriers.

6.3 CH₄/CO₂ Competitive Diffusion Results and Discussion

6.3.1 Diffusivity Data

The diffusivity values are summarized in Table 6.3 and as Arrhenius plots in Figure 6.4:

$$D_o = D_\infty e^{-E/RT} \quad (6.1)$$

The parameters D_∞ and E are given in Table 6.4. Note that the measured diffusivities are at very low loadings of the relevant sorbate so they should correspond to the limiting (zero loading) values (D_o). The symbols D and D_o are therefore used interchangeably. The diffusivity data of van den Bergh²³, derived from membrane permeation measurements are also included in Table 6.4.

Table 6.3 Summary of Diffusivities and Henry Constants for CH₄ – DDR.

T (K)	DDR I		DDR II			
	$D_{\text{CH}_4\text{-He}}$	$D_{\text{CH}_4\text{-CO}_2}$	$D_{\text{CH}_4\text{-He}}$	$D_{\text{CH}_4\text{-CO}_2}$	$K_{\text{CH}_4\text{-He}}$	$K_{\text{CH}_4\text{-CO}_2}$
273	0.29	1.5				
298	0.8	2.07	2.36	5.6	24	10.5
323	1.64	2.82	4.03	6.6	15.2	8.65
348	3.4	3.8	6.25	9.3	10.8	7.25
373			8.9	12	7.9	5.45
423			19	21	4.7	4.6

Diffusivities are in units of $10^{-12} \text{ m}^2 \text{ s}^{-1}$; K values are dimensionless.

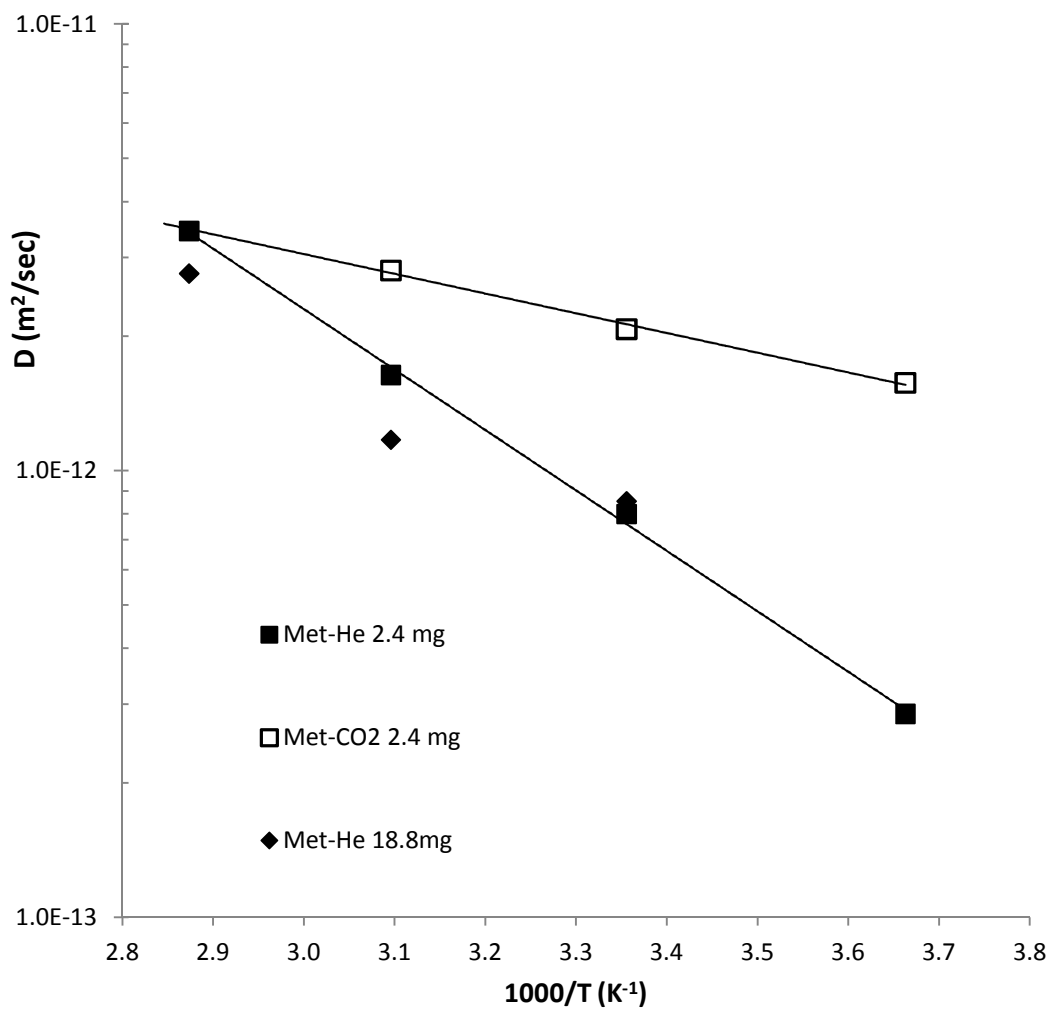


Figure 6.5. Arrhenius Plots Showing Temperature Dependence of Diffusivity in DDR I. (D_0) for methane in DD3R crystals as single components CH₄-He (■, 2.4 mg; ◆, 18.8 mg) and in the presence of one atmosphere of CO₂ for DDR I (□, 2.4 mg).

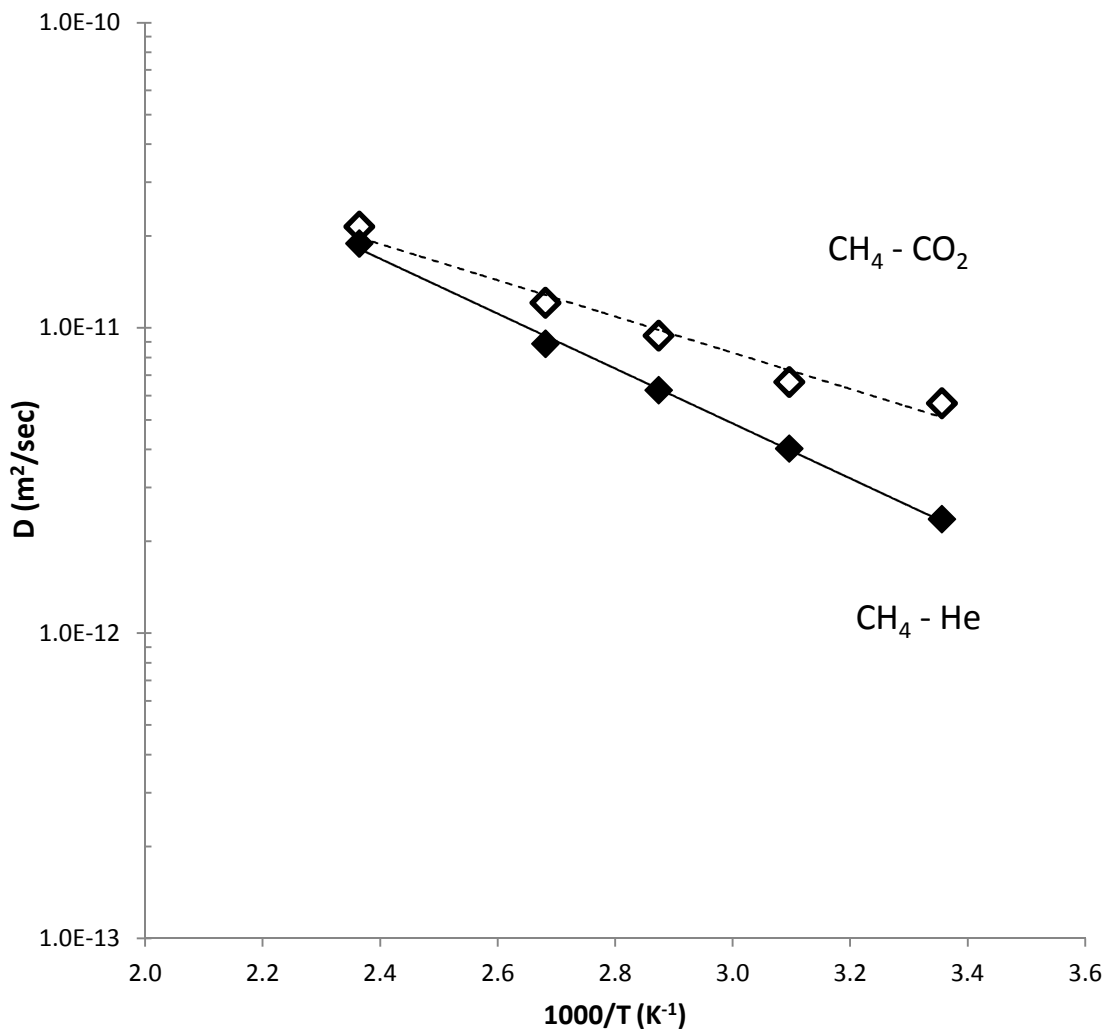


Figure 6.6. Arrhenius Plots Showing Temperature Dependence of Diffusivity in DDR II (D_0) for methane in DD3R crystals as single components ($\text{CH}_4\text{-He}$ (◆)) and in the presence of one atmosphere of CO_2 (◇) for DDR II. The broken line closely matches the $\text{CH}_4\text{-CO}_2$ diffusivity data is calculated as the product of $D_{\text{CH}_4\text{-He}}$ and the ratio ($K_{\text{CH}_4\text{-He}}/K_{\text{CH}_4\text{-CO}_2}$) as suggested by Eq. 6.6.

Measurements carried out with 2.4 mg and 18.8 mg samples (DDR I) yield consistent diffusivity values, thus confirming intracrystalline control and the absence of significant extra-crystalline resistances to mass and heat transfer. Since He is only very weakly adsorbed at these conditions the $\text{CH}_4\text{-He}$ measurements yield single component

diffusivities. CO₂ is, however, relatively strongly adsorbed so the CH₄-CO₂ data yield the diffusivities of CH₄ at low mole fractions in the binary adsorbed phase (containing mainly CO₂).

Table 6.4 Parameters giving Temperature Dependence of D and K according to Eqs. 6.1 and 6.2

	D_{∞} (m ² s ⁻¹)	E (kJ/mole)	K_{∞}	$-\Delta U$ (kJ/mole)
DDR I	1.9×10^{-8}	25.1		
DDR II	2.2×10^{-9}	17	0.116	13.1
Van den Bergh⁽²³⁾	4.7×10^{-11}	15.9	0.05	14.8

It is clear that, for both DD3R samples, the diffusivity of methane is significantly enhanced by the presence of CO₂. This is illustrated in Figure 6.3a and in Figure 6.4 as well as in Figure 6.5 in which representative ZLC response curves measured with He and CO₂ at the same temperature and flow rate are compared directly. This result appears at first sight to be surprising but such behavior is in fact consistent with transition state theory as discussed below.

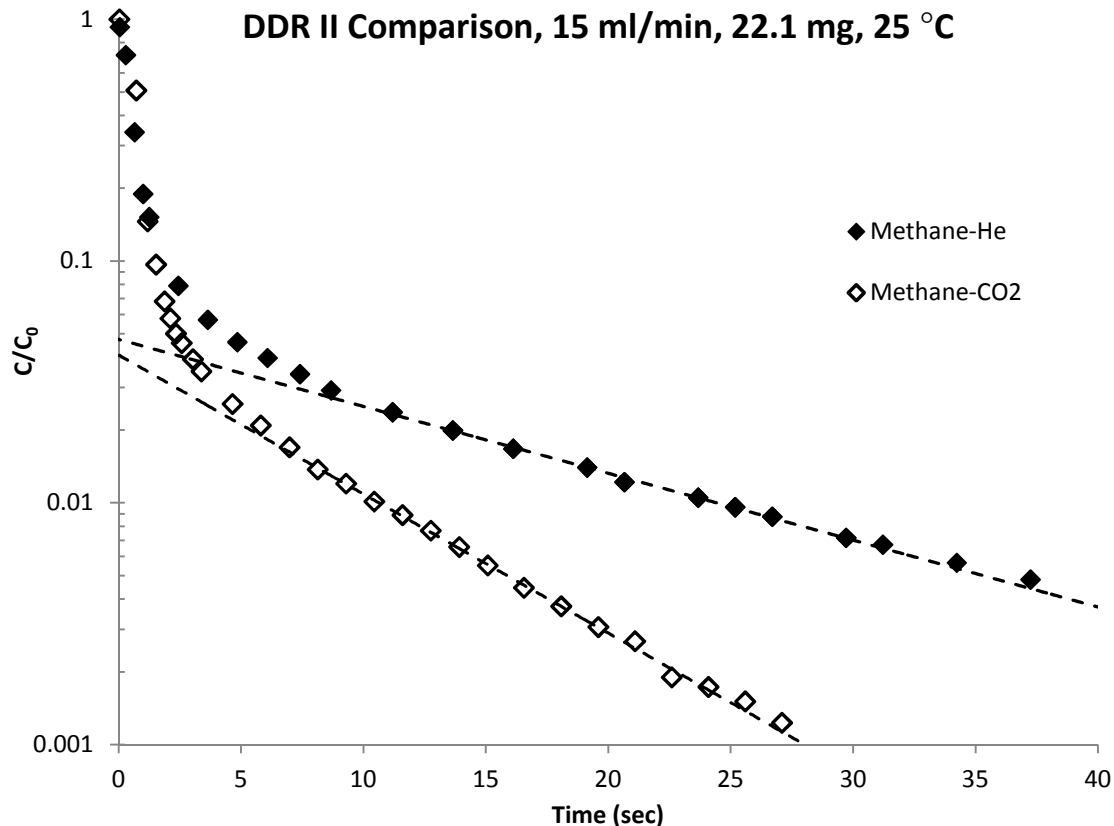


Figure 6.7. Comparison of ZLC Response Curves. For CH₄–He and CH₄–CO₂ measured with DDR II at 298K at purge flow rate F=15 ml/min (STP). The difference in the asymptotic slopes shows that diffusion is substantially faster in the presence of CO₂.

Some relevant comparisons with the data available from studies of other 8-ring systems (4A and 5A) and with the limited data from previous studies of DD3R are summarized in Table 6.5. The present (ZLC) diffusivity data for CH₄-DD3R are in good agreement with the measurements carried out at the ExxonMobil Laboratory (at 298K) by pulsed field gradient nuclear magnetic resonance (PFGNMR)²⁷. Our values are, however, an order of magnitude larger than the values reported by van den Bergh²³ which were derived from membrane permeance measurements. The extraction of diffusivities from membrane measurements is notoriously unreliable as it requires both accurate

equilibrium data and knowledge of the thickness of the active zeolite layer, which in a composite supported zeolite membrane is generally not accurately known. Our values are close to the values derived from the molecular simulations of Jee and Sholl³⁰ but substantially smaller (almost two orders of magnitude) than the values from the molecular dynamic simulations of Krishna and van Baten^{28,29}. The agreement with the work of Jee and Sholl is to be expected since they adjusted their repulsive potential to match the ExxonMobil measurements at low loadings^{3,6,27}. That the diffusivity of methane in DD3R is increased by the presence of CO₂ stands in marked contradiction of the prediction from these simulations that, in the binary system, the diffusivity of methane will be reduced as a result of the preferential occupation of the windows by CO₂. The binary diffusion data are discussed in greater detail below following consideration of the evidence from the equilibrium data.

Table 6.5 Comparative Data for Diffusion of CH₄ in 8-Ring Zeolites

Structure	Window (Å)	D ₀ at 298K (m ² .s ⁻¹)	E (kJ/mole)	Technique	Author
4A	3.8 x 4.2 (obstructed by Na ⁺)	5 x 10 ⁻¹⁵	24	Uptake Rate	Yucel ⁶⁷ Eagan ⁽⁶⁸⁾
DD3R	3.65 x 4.4	~ 10 ⁻¹³	15.9	Membrane	Van den Berg ⁽²³⁾
		1.5 -2x10 ⁻¹²	-	PFGNMR	Hedin ⁽²⁷⁾
		1.8x10 ⁻¹²	-	Simulation	Sholl ⁽³⁰⁾
	DDR I	8x10 ⁻¹³	25.5	ZLC	Present study
DDR II	2.3x10 ⁻¹²	17			
5A	4.3 x 4.6 (open)	10 ⁻⁹	4	PFGNMR	Caro ⁽⁶⁹⁾
		1.5x10 ⁻¹⁰	6	ZLC	Xu ⁽⁷⁰⁾

The diffusivity values fall in the expected sequence suggested by the window dimensions ($D_{4A} < D_{DDR} < D_{5A}$). However, the two to three orders of magnitude slower diffusion in DD3R compared with 5A, both of which have cation free 8-ring windows, must be attributed to the difference in the window shapes. Note that detailed XRD (synchrotron, PFGNMR) measurements show that, even in the symmetric 5A structure, the 8-rings are not exactly symmetric⁽³⁴⁾.

6.3.2 Equilibrium Data

The temperature dependence of the dimensionless Henry constant should conform to the familiar van't Hoff expression:

$$K = K_{\infty} e^{-\Delta U_o / RT} \quad (6.2)$$

where the internal energy of adsorption (ΔU_o) is related to the more commonly quoted enthalpy of adsorption by $\Delta U_o = \Delta H_o + RT_{av}$. The Henry constants derived from the ZLC data (for DDR II) are included in Table 6.3 and shown as van't Hoff plots in figure 6.6. The K values for DDR I (18.8 mg sample at 298 K) are evidently similar to the values for DDR II. It is evident that these values agree well with the values calculated from the equilibrium measurements reported by van den Bergh^{23,24}, which are indicated in the figure for comparison.

The effective Henry constants measured for the binary system CH₄-CO₂ are also included in Figure 6.6 for comparison with the true Henry constants (derived from the CH₄- He data). As is to be expected for competitive adsorption the K values for the binary system are smaller than the true Henry constants, with the difference being greater at lower temperatures as is to be expected if CH₄ and CO₂ are adsorbed competitively.

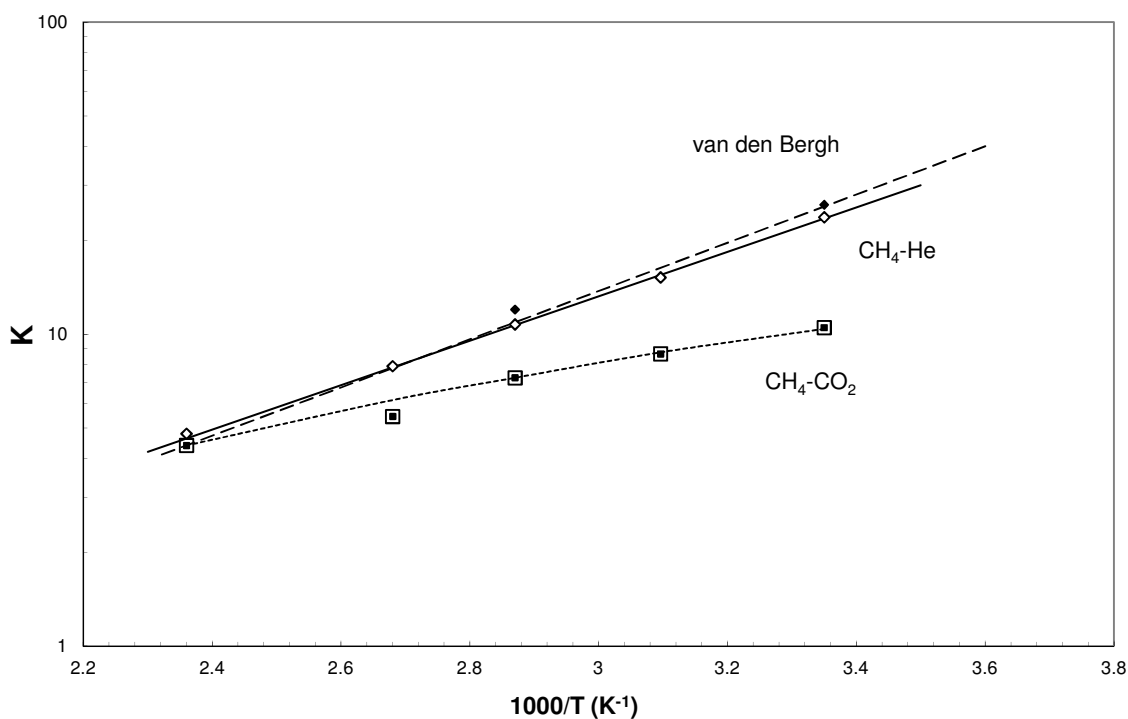


Figure 6.8. van't Hoff Plots Showing Temperature Dependence of Dimensionless Henry constants. Derived from ZLC response curves for CH₄-He (◇) and CH₄-CO₂ (□) in DDR II. Comparative values for CH₄-He (◆) and CH₄-CO₂ (■) in DDR I. The Henry constants calculated from the measured equilibrium data of van den Bergh^(23,24) (- - - -) are indicated for comparison.

6.3.3 Diffusion of Methane in Presence of CO₂

Although initially counter-intuitive, the observed increase in the diffusivity of CH₄ in DD3R in the presence of CO₂ can be understood from transition state theory as a natural consequence of competitive adsorption. We assume that the transition state corresponds to the molecule in the 8-ring window between two adjacent cages. According to transition state theory⁽⁷¹⁾ the limiting diffusivity is given by:

$$D_o = \frac{\ell^2 n}{h} \left(\frac{f^+}{f'_g} \right) \cdot \frac{e^{-V/kT}}{(q/p)_{eq}} \quad (6.3)$$

where f^+/f_g' represents the ratio of the reduced partition functions for the transition state and the free gas phase and V is the potential energy difference between the transition state and the gas phase, k is the Boltzmann constant, h is Planck's constant, ℓ and n represent the lattice spacing and site density respectively and q/p is the ratio of sorbate concentration to partial pressure. In a single component system this ratio is simply the Henry constant (K) while in a binary adsorbed phase this corresponds to the effective Henry constant (K'). In a competitive adsorption system these values will be different with K' being smaller than K . Eq.6.3 therefore shows that the diffusivity at infinite dilution in a binary adsorbed phase is expected to be reduced in comparison with the single component value.

If the equilibrium behavior can be represented by the binary Langmuir isotherm:

$$q_A = \frac{K_A p_A}{1 + b_A p_A + b_B p_B} \quad (6.4)$$

Because $p_A \ll p_B \approx 1$ atm we may assume that $b_A p_A \ll b_B p_B$ so that:

$$\frac{(q_A / p_A)_B}{(q_A / p_A)_{He}} = \frac{K'_A}{K_A} = \frac{1}{1 + (b p)_B} \quad (6.5)$$

Where, in the present case $A = \text{CH}_4$, $B = \text{CO}_2$ and $K_A = b_A q_s$. Therefore, if a methane molecule in the transition state is not affected by the presence of CO_2 it follows that:

$$\frac{D_{CH_4-CO_2}}{D_{CH_4-He}} = \frac{K_A}{K'_A} = 1 + b_B p_B \quad (6.6)$$

where $p_B = p_{CO_2} \approx 1$ atm. That is to say, at any given temperature, the products $(KD)_{CH_4-He}$ and $(K'D)_{CH_4-CO_2}$ should be equal. The experimental data shown in figure 6.3b conform to this behavior.

For an ideal Langmuir system Eq.6.6 provides a simple quantitative estimate of the enhancement factor for the diffusivity in the presence of CO_2 . Note that this factor depends on the product $b_B p_B$ and is independent of b_A . Therefore the same enhancement factor is to be expected for any binary Langmuirian system in which CO_2 is the diluent. The temperature dependence of b_B will be governed by a vant Hoff expression of the form of Eq.6.2 ($b = b_\infty \exp(-\Delta H_0/RT)$) so, in accordance with the experimental data, the ratio $(D_{CH_4-CO_2}/D_{CH_4-He})$ is expected to decrease with increasing temperature. This trend can be seen in table 6.6.

Table 6.6. Diffusivity ratio and product of diffusivity and Henry constant trending with temperature.

T (K)	D Ratio	K'D _{CH₄-CO₂} (m ² /sec)	KD _{CH₄-He} (m ² /sec)
298	2.40	5.98	5.63
323	1.65	6.23	6.16
348	1.51	6.85	6.76
373	1.36	7.20	7.03
423	1.14	10.58	11.66

D is in units of $10^{-12} \text{ m}^2\text{s}^{-1}$, K and K' are dimensionless

Although the qualitative trends of diffusivity and apparent equilibrium constant with temperature conform to the ideal Langmuir model the quantitative agreement is

poor. This is hardly surprising in view of the differences in size and shape between the CO₂ and CH₄ molecules. However, the correspondence between the diffusivity ratio ($D_{\text{CH}_4\text{-CO}_2}/D_{\text{CH}_4\text{-He}}$) and the inverse ratio of the K values ($K_{\text{CH}_4\text{-He}}/K_{\text{CH}_4\text{-CO}_2}$), as suggested by Eq. 6.6 should still apply regardless of whether or not the equilibrium isotherms conform to the Langmuir model. That is to say, assuming all terms in Eq. 6.3 except for D and K remain the same, the product of these two terms should remain constant. That this is indeed true for the present data is shown in figure 6.4 (and table 6.6) in which the dotted line, which lies close to the CH₄–CO₂ diffusivity data, is calculated from the CH₄-He diffusivities and the ratio of equilibrium constant in accordance with Eq.6.6 as well as in figure 6.10 which shows the diffusivity ratio ($D_{\text{CH}_4\text{-CO}_2}/D_{\text{CH}_4\text{-He}}$) plotted against the ratio of the equilibrium constants ($K_{\text{CH}_4\text{-He}}/K_{\text{CH}_4\text{-CO}_2}$) at the various temperatures. It is evident that the difference in diffusivity between the CH₄-He and the CH₄-CO₂ systems can be quantitatively accounted for by competitive adsorption of CO₂.

If both the CO₂ and CH₄ molecules are adsorbed competitively within the cages, then the presence of the more strongly adsorbed CO₂ will *increase* the potential energy of CH₄, thus *decreasing* the activation energy (the energy difference between the equilibrium state in the cage and the transition state for the molecule in transit through the window), thereby *increasing* the diffusivity. This is shown graphically in Figure 6.9, a schematic representation showing the decreased activation energy for the CH₄/CO₂ system as compared to the CH₄/He system. This effect can be seen quantitatively in table 6.7. Both DDR samples show a reduced activation energy for diffusion with CO₂ compared to He or pure-component CH₄.

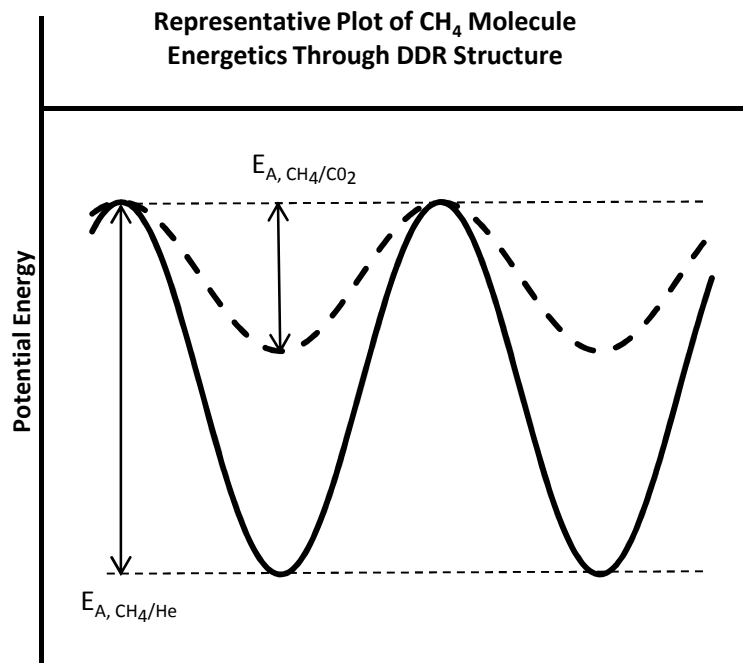


Figure 6.9 Representative Plot Describing Energy Levels of CH₄ in DDR Cage. As CH₄ transits through the DD3R cage with and without CO₂. It is assumed that the energy level of the CH₄ molecule within the window is the same for both systems.

Table 6.7. Data Showing Apparent Activation Energy of Diffusion for Methane in Both Sorbates Purged by Both He and CO₂.

Sorbent/Sorbate	E _A (KJ/mol)
DDR I , CH ₄ -He	25.9
DDR I , CH ₄ -CO ₂	8.5
DDR II,CH ₄ -He	17.2
DDR II, CH ₄ -CO ₂	11.4

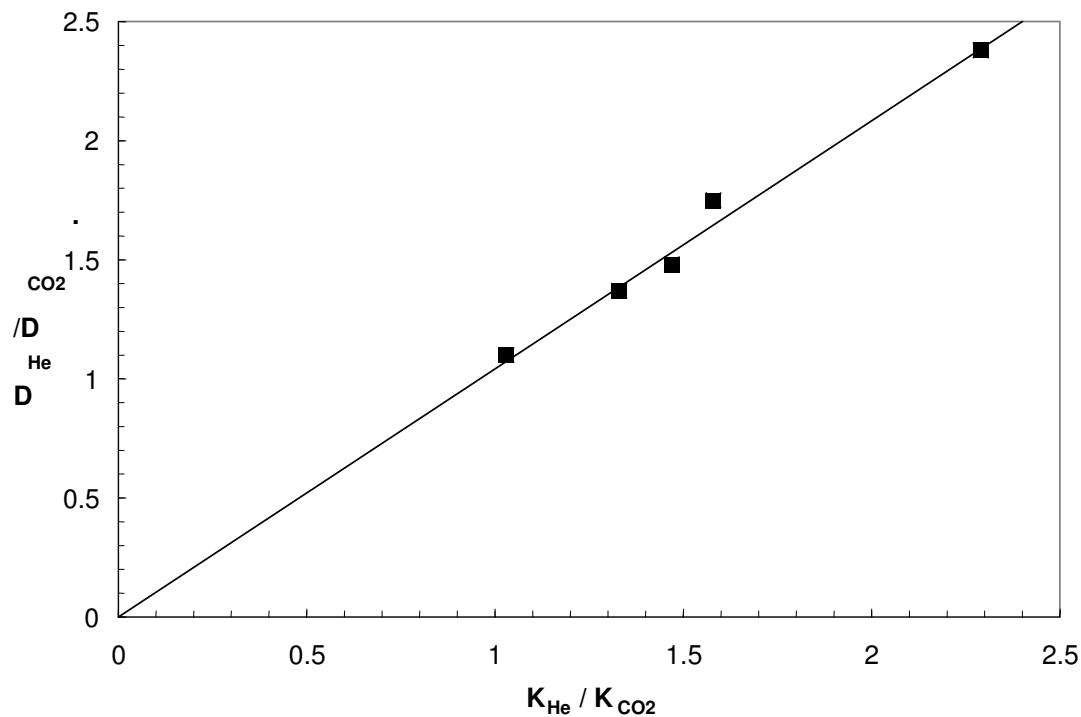


Figure 6.10. Plot of the ratio of measured diffusivities ($D_{\text{CH}_4\text{-CO}_2} / D_{\text{CH}_4\text{-He}}$) vs the ratio of measured equilibrium constants ($K_{\text{CH}_4\text{-He}} / K_{\text{CH}_4\text{-CO}_2}$). Plotted at various temperatures showing the close correlation between the diffusivities and apparent equilibrium constants for $\text{CH}_4\text{-He}$ and $\text{CH}_4\text{-CO}_2$ in DDR II.

6.4 DDR-Methane Conclusions

The ZLC data for both samples DDR I and DDR II conform to the simple model for an intracrystalline controlled system with no evidence of any significant surface resistance. Diffusion in the treated sample (DDR II) is however significantly faster than in the untreated sample (DDR I). The difference in diffusivity corresponds with the difference in activation energies although the pre-exponential factors for the two samples are not the same. This suggests that the sample treatment must have modified the dimensions of the 8-ring windows and cannot be explained as a simple cleaning of the external surface of the crystals.

In the presence of an atmosphere of CO₂ the equilibrium constant (K_{CH_4}) is reduced and the methane diffusivity is increased by the same factor. This result is consistent with transition state theory if it is assumed that CO₂ and CH₄ are adsorbed competitively and that the potential energy of the transition state (for methane) is not significantly affected by the presence of CO₂. That would be consistent with the usual model in which the transition state corresponds to a methane molecule in the 8-ring window between adjacent cages while the equilibrium state corresponds to molecules that are competitively adsorbed within the cages. However, these observations do not appear to be consistent with the Sholl model³⁰ which postulates preferential occupation of the windows by CO₂.

The observation that the intracrystalline diffusivity of methane is increased by the presence of CO₂ suggests that the assumption that the perm-selectivity for a CO₂ –CH₄ mixture will correspond to the value estimated from single component data must be treated with caution. Under the conditions of this study involving a small concentration of methane in an excess of CO₂ it was found that the methane diffusivity is increased by the same factor as the methane equilibrium constant is decreased so, according to the simple solution-diffusion model, the permeance, which corresponds to the product of the diffusivity and the equilibrium constant should remain constant! Whether or not this is true, especially at higher loadings beyond the linear region of the isotherm remains an open question.

CHAPTER 7
DIFFUSION OF ETHANE AND ETHYLENE IN DDR
ZEOLITES IN COMPETITION WITH CO₂

As a logical sequel to the methane studies described in the previous chapter, it was decided to investigate the kinetic behavior of C₂ hydrocarbons (C₂H₆ and C₂H₄) in DDR, both as single components and in the presence of CO₂. The results of this investigation show that the general patterns of behavior of C₂H₆ and C₂H₄ in DDR are similar but strikingly different from the behavior of methane.

7.1 Analysis of ZLC Response Curves

The standard approach to the analysis of ZLC response curves is based on the traditional model for a ZLC system in which it is the assessment that the desorption rate is controlled entirely by intracrystalline diffusion (Eq.5.8). However, ZLC desorption curves for C₂H₆ in DDR showed more complex behavior suggesting the presence of significant surface resistance. As demonstrated in section 5.5, when surface resistance is significant, the form of the ZLC response curve remains unchanged but the parameter L is replaced by L' where:

$$\frac{1}{L'} = \frac{1}{L} + \frac{D}{kR} = \frac{3KV_s}{F} \left(\frac{D}{R^2} \right) + \frac{D}{kR} \quad (7.1)$$

and L retains its original meaning (see Eq.5.6). This means that when L' is large ($L' > 10$) the slope of the long time asymptote ($-\pi^2 D/R^2$) is not affected by surface resistance; only

the intercept is modified in accordance with Eq. 5.19. Similarly, the plot of c/c_o vs $1/\sqrt{t}$, suggested by Eq.5.16 should yield $\sqrt{(\pi D/R^2)}$ and $1/L'$ for the x and y intercepts. Thus, provided measurements are made at $L > 10$, the ZLC response curves with and without surface resistance may be analyzed in exactly the same way. Measurements at different flow rates allow the magnitude of any surface resistance to be estimated from the variation of the parameter L' with flow rate in accordance with

Eq.5.19

Representative experimental ZLC ethane response curves showing conformity with both Eqs. 5.12 and 5.16 are shown in figure 7.1. The parameters derived from both the long time asymptote (Eq.5.12) and from the c/c_o vs $1/\sqrt{t}$ plot (Eq.5.16) are consistent; the average values of L' and D/R^2 are summarized in Table 7.1. If these curves are analyzed according to the traditional ZLC model consistent diffusivity values are obtained, but the apparent value of the Henry constant (K') increases monotonically with flow rate, as illustrated in Table 7.1. However, the values of $1/L'$ increase linearly with reciprocal flow rate in accordance with Eq.5.19 and the K values also calculated in accordance with Eq.5.21 are approximately independent of flow rate. A detailed analysis of the experimental values of L' is presented below .

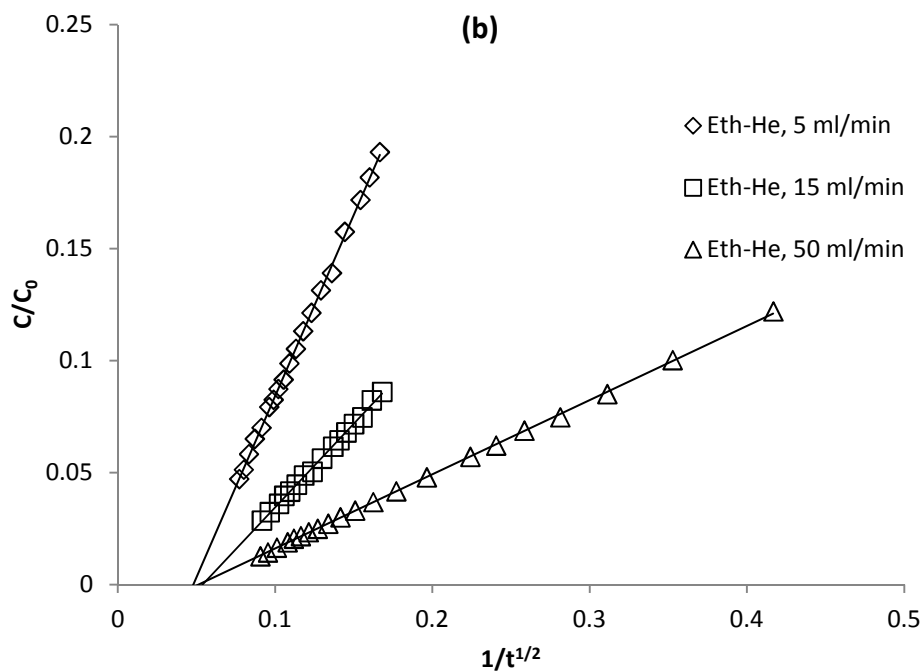
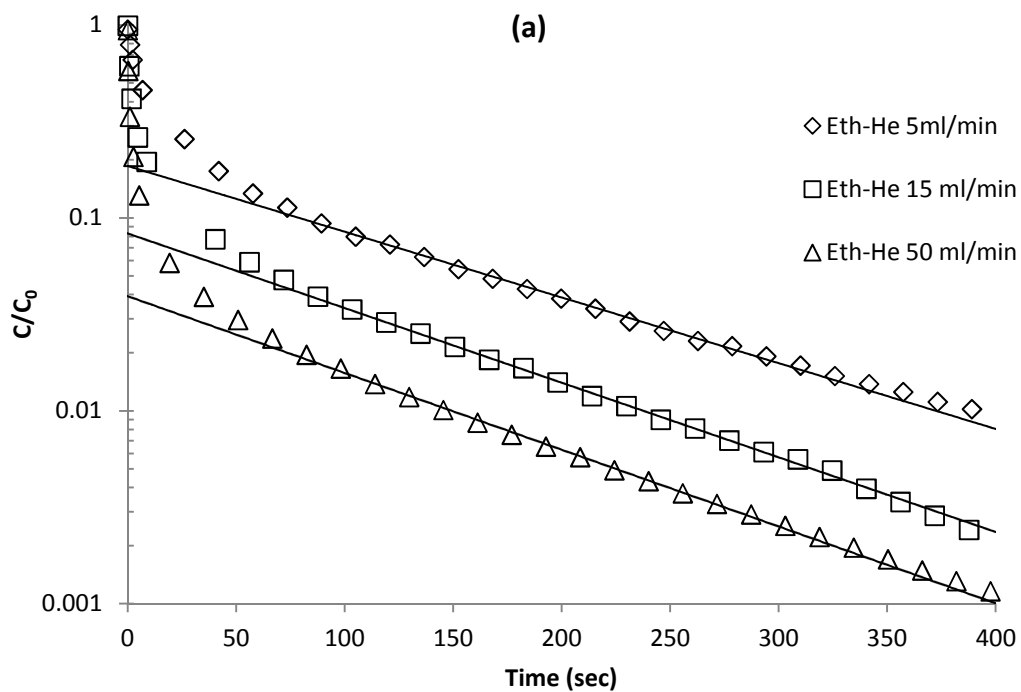


Figure 7.1 Representative ZLC response curves for C_2H_6 – He in DDR II. 22.1mg at 323K showing (a) Long Time Asymptotic Analysis (Eq.5.12) and (b) Intermediate Time Analysis (Eq. 5.16).

Table 7.1 Parameters Derived from Representative ZLC Response Curves.

System	F (ml/sec)	L'	D/kR	L	K'	K	D/R^2 (s^{-1})
C2H6-He DDR II 348 K	0.097	14		15	120	110	0.0015
	0.292	37	0.005	49	140	103	0.0014
	0.973	78		150	215	112	0.0014
C2H6-He DDR I (5.9 mg) 298 K	0.083	48		57	207	155	0.0008
	0.25	85	0.0035	120	344	180	0.0009
	0.5	128		232	485	189	0.001
	0.83	185		546	585	165	0.0008

Note: The response curves for DDR II are shown in figure 7.1.

7.2 Diffusion of Ethane in DDR

The diffusional time constants (D/R^2) derived from a series of replicate measurements with different sample quantities (DDR I) are summarized in Table 7.2. There is considerable experimental scatter ($\pm 20\%$) but there is no significant trend with sample mass, confirming the absence of any significant extracrystalline heat or mass transfer resistances.

Table 7.2 Comparison of Diffusional Time Constants for Ethane in DDR I at 298K. Values Reported as ($10^3 \times D/R^2 s^{-1}$)

	1.5 mg	2.4 mg		5.9 mg
He	0.81	1.2	0.85	1.0
CO₂	1.2	1.3	0.89	1.0

Figure 7.2 shows representative plots of diffusivity (for C₂H₆) vs the purge flow rate (F) for both He and CO₂ as purge gases in samples of DDR I and DDR II. Although the data show appreciable experimental scatter it is evident that there is no significant

trend with flow rate and the time constants for He and CO₂ purges are very similar. This implies that the diffusion of C₂H₆ is not significantly affected by the presence of CO₂, even in large excess. There is a substantial difference in diffusivities between DDR I and DDR II but differences between the three different samples of DDR I are minimal. These conclusions are supported by a direct comparison of the ZLC response curves measured with He and CO₂ at the same temperature and purge flow rate (see figure 7.3).

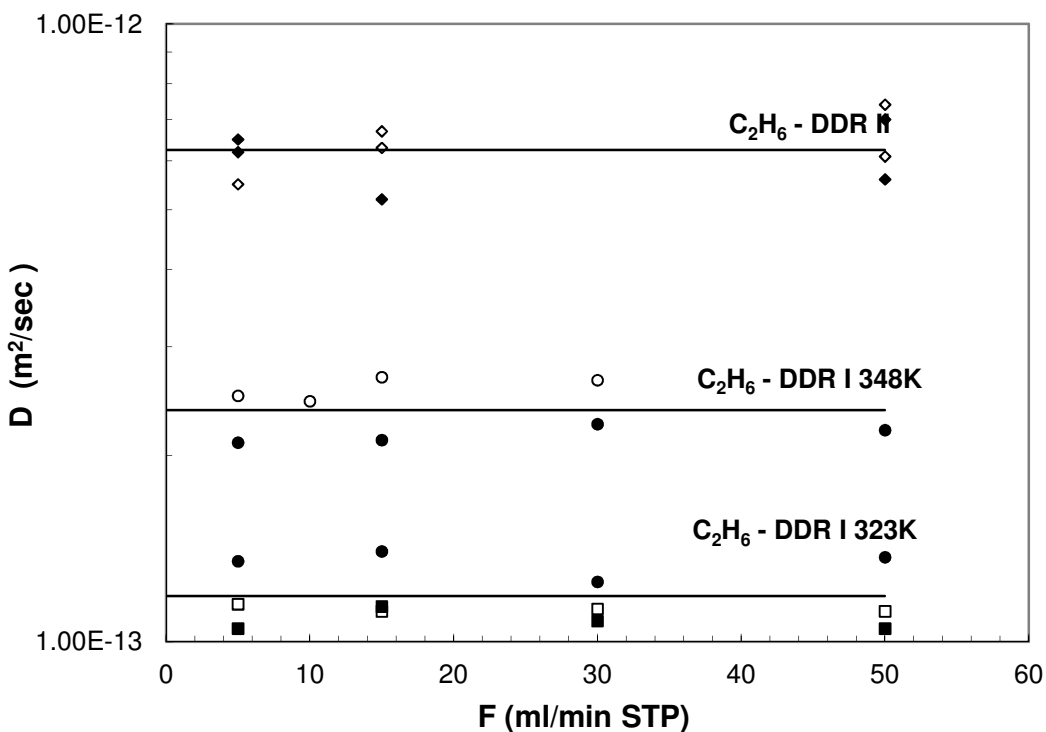


Figure 7.2. Variation of Experimental Diffusivities for C₂H₆ with Flow Rate. Showing comparison of data for DDR II (◇,◆) and DDR I (2.4 mg ○, ●; 5.9 mg □, ■) with He (filled symbols) and CO₂ (open symbols) as carrier. The lines denote the average values.

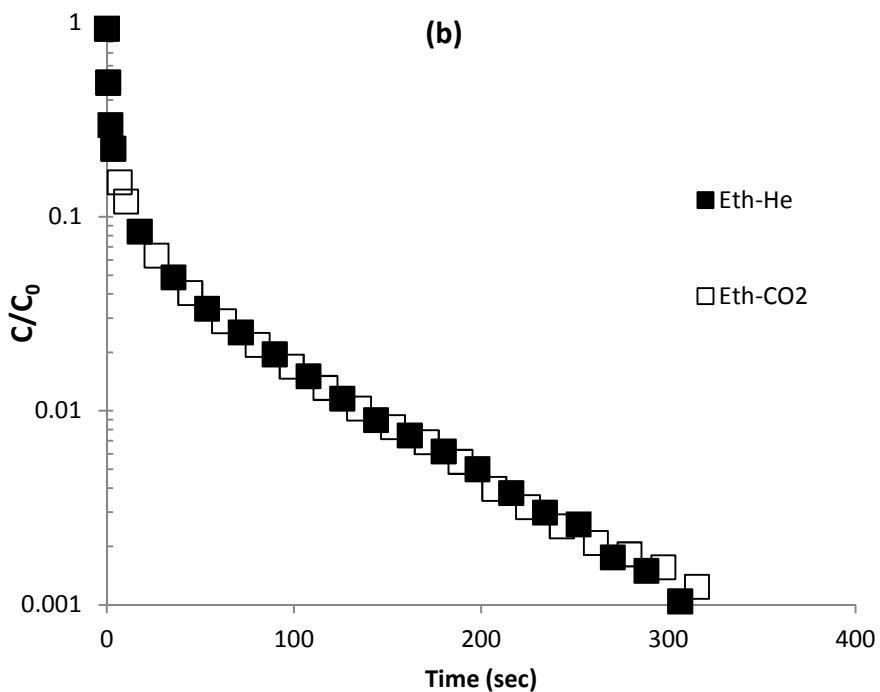
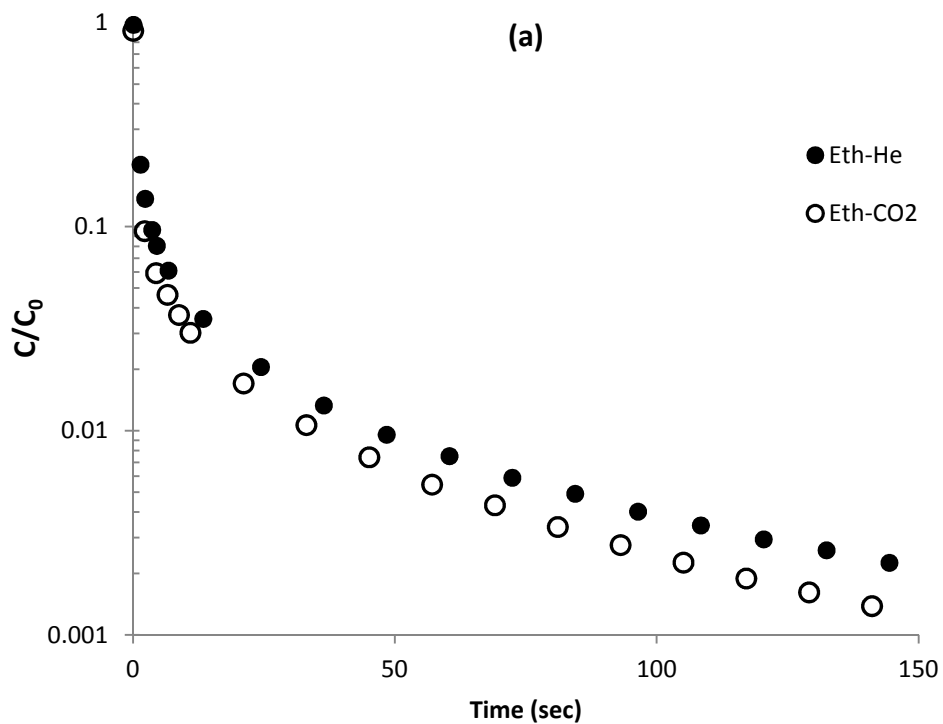


Figure 7.3. Comparison of Experimental ZLC Response Curves for C_2H_6 . Same temperature and purge flow rate) with He and CO_2 as the carrier gas. (a) DDR I at 323K; (b) DDR II at 348K.

The temperature dependence of D is shown in figure 7.4 plotted in accordance with the usual Arrhenius expression:

$$D = D_{\infty} e^{-E/RT} \quad (7.2)$$

The temperature dependence of the diffusivity is shown in Arrhenius form in figure 7.4 which includes the data obtained with both He and CO₂ as the purge gas. The Arrhenius parameters are summarized in Table 7.4. The data for DDR II are more consistent with less variation between replicate runs (as was seen in the methane experiments). For both DDR I and DDR II the diffusivities obtained with He and CO₂ are essentially the same (see figures 7.2 and 7.4) but the diffusivities for DDR II are about two to three times larger than the values for DDR I (at the same temperature). Remarkably the activation energy is also significantly larger for DDR II. This is somewhat unusual: more commonly different samples of the same zeolite show either a constant activation energy or, if the activation energy varies, the higher diffusivity is associated with a *lower* activation energy, as is the case for methane in DDR, seen in the previous chapter.

Published diffusivity data for ethane in DDR are scarce. At 301K Hedin et al⁶⁵ reported $1.5 \times 10^{-13} \text{ m}^2\text{s}^{-1}$ for the self-diffusivity of ethylene in DDR (measured by PFGNMR) and $4.8 \times 10^{-13} \text{ m}^2\text{s}^{-1}$ for ethane in Si-CHA (which has similar window dimensions). These values are of the same order as the present data for ethane in DDR.

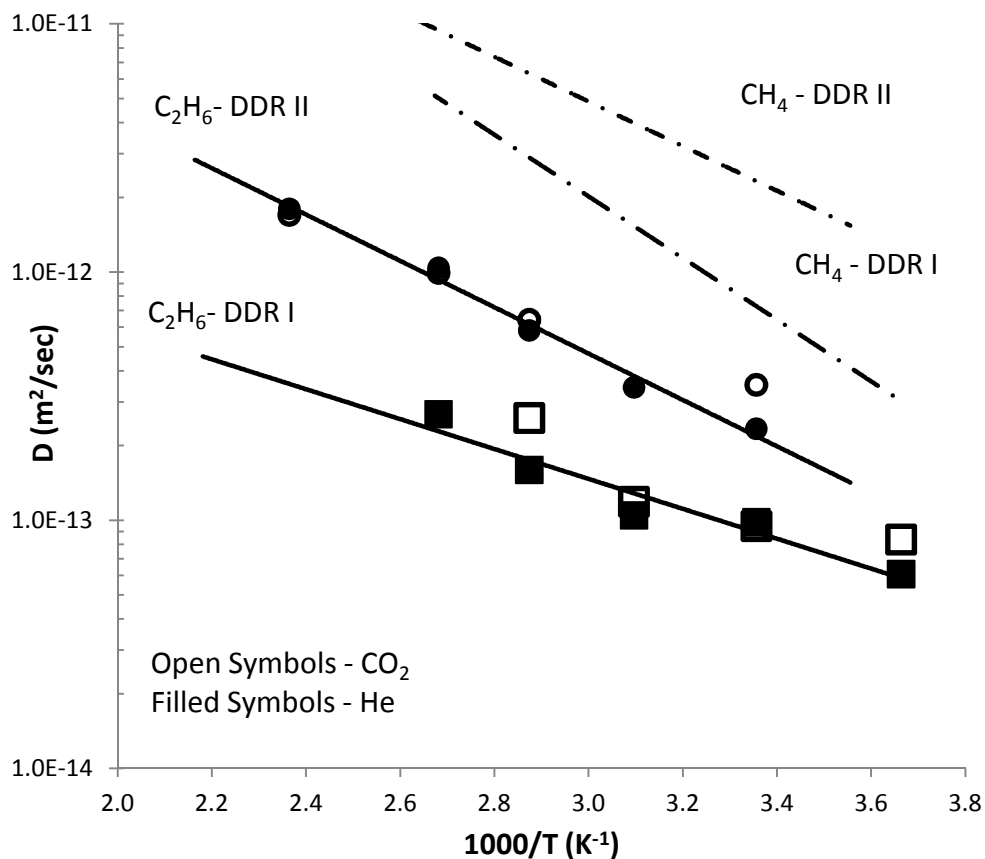


Figure 7.4. Arrhenius Plot Showing Temperature Dependence of Diffusivity for C₂H₆: Two different samples of DDR crystals (DDR I and DDR II). Data for CH₄ in the same DDR samples are indicated for comparison.

7.3 Diffusion of Ethylene in DDR

Diffusion of C₂H₄ in DDR was studied less extensively and only in DDR I. The diffusivity values measured at 298K are very close to the value reported by Hedin et al²⁷ from PFGNMR self-diffusivity measurements. The measured diffusivities are essentially independent of flow rate, as expected. As for C₂H₆, there appears to be little difference in diffusivity between the measurements with He and CO₂ and between the values for the 2.4 and 5.9 mg samples. This may be seen in figure 7.5 and from the direct comparison of

the ZLC response curves shown in figure 7.6 as well as from the Arrhenius plot shown in figure 7.7. Furthermore any difference in diffusivity between C_2H_4 and C_2H_6 appears to be minimal and within the range of experimental uncertainty.

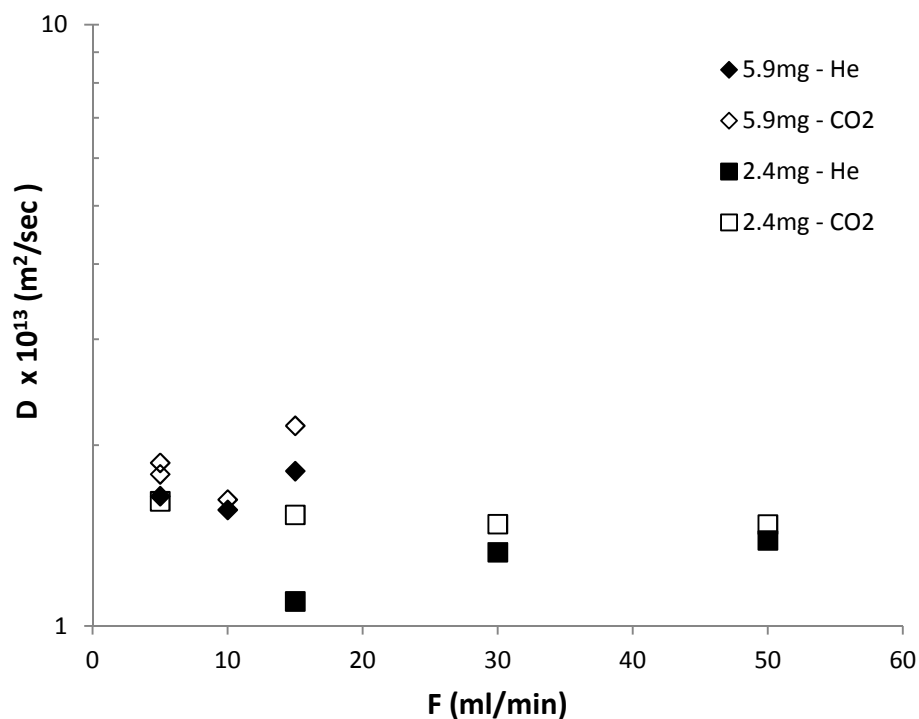


Figure 7.5. Diffusivity Data for C_2H_4 in DDR I. Showing comparison of data for two different samples (2.4 mg and 5.9 mg) with He and CO₂ purge.

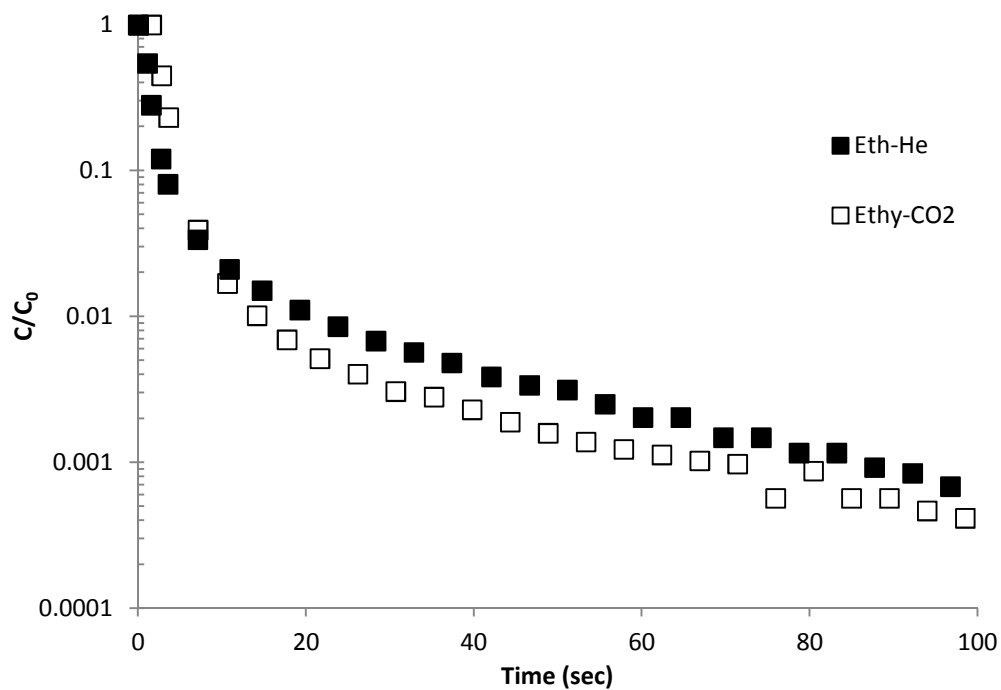


Figure 7.6. Direct Comparison of ZLC Response Curves for C_2H_4 . At 348 K, 15 ml/min showing similarity between data for He and CO_2 carriers.

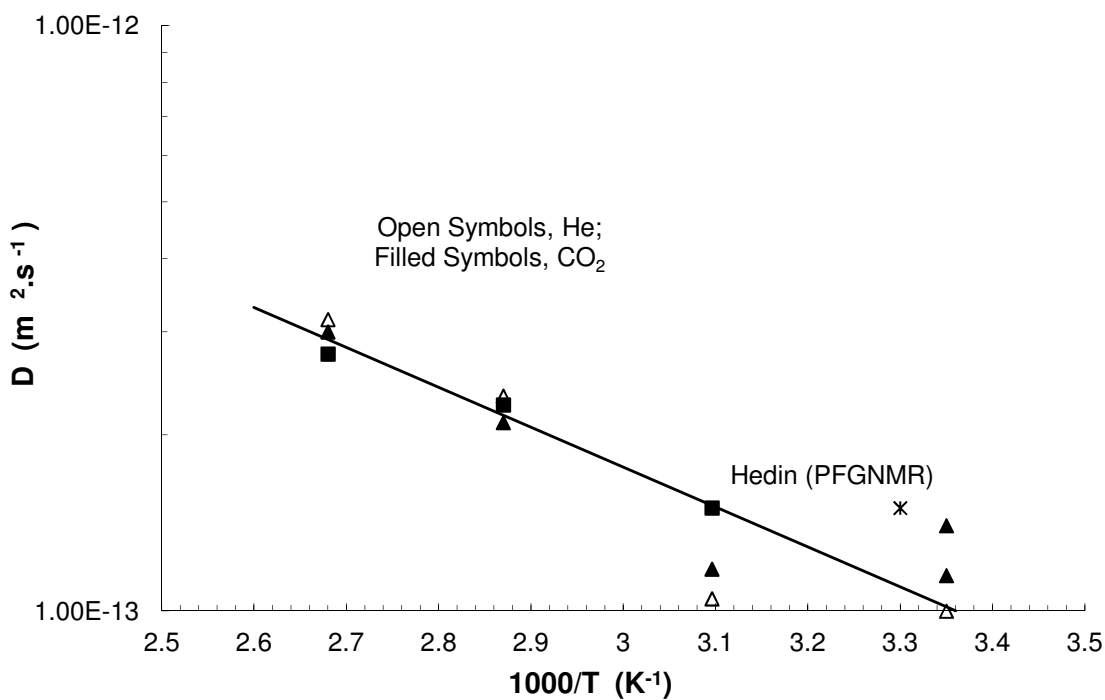


Figure 7.7 Arrhenius Plot Showing Temperature Dependence of Diffusivity for C_2H_4 .In DDR I,(5.9 mg Δ , \blacktriangle ; 2.4 mg \square). The line shows the average values for C_2H_6 in DDR I (see Figure 7.4).

7.4 Analysis of L Values: Surface Resistance

It follows from Eq 5.19 that a plot of $1/L'$ vs $1/F$ should yield a straight line with slope $3KV_sR^2/D$ and intercept D/kR . The intercept corresponds to the ratio of the time constants for intracrystalline diffusion and surface resistance and therefore measures the relative importance of these two resistances. A negligible intercept means no significant surface resistance (as seen for methane) and complete intracrystalline diffusion control while a large intercept would imply surface resistance control.

Representative plots $1/L'$ vs $1/F$ for C_2H_6 in DDR I and DDR II are shown in figure 7.8. The plots all show approximate conformity with Eq 5.19 but they show significant differences between the different samples. The behavior of DDR II and the 5.9 mg sample of DDR I (shown in Figure 7.8 a and b) is very similar. The intercepts are essentially constant (invariant with temperature) implying that the activation energies for surface resistance and intracrystalline diffusion are the same. This suggests that the surface barrier probably originates from complete blockage of a significant fraction of the pore entrances (rather than from partial obstruction of all the pore entrances). In contrast, for the 2.4 mg sample of DDR I, the intercept decreases regularly with temperature, as shown in Figure 7.8c, implying a higher activation energy for the surface resistance. Such behavior might suggest partial obstruction of the pore entrances, leading to a higher energy barrier at the crystal surface.

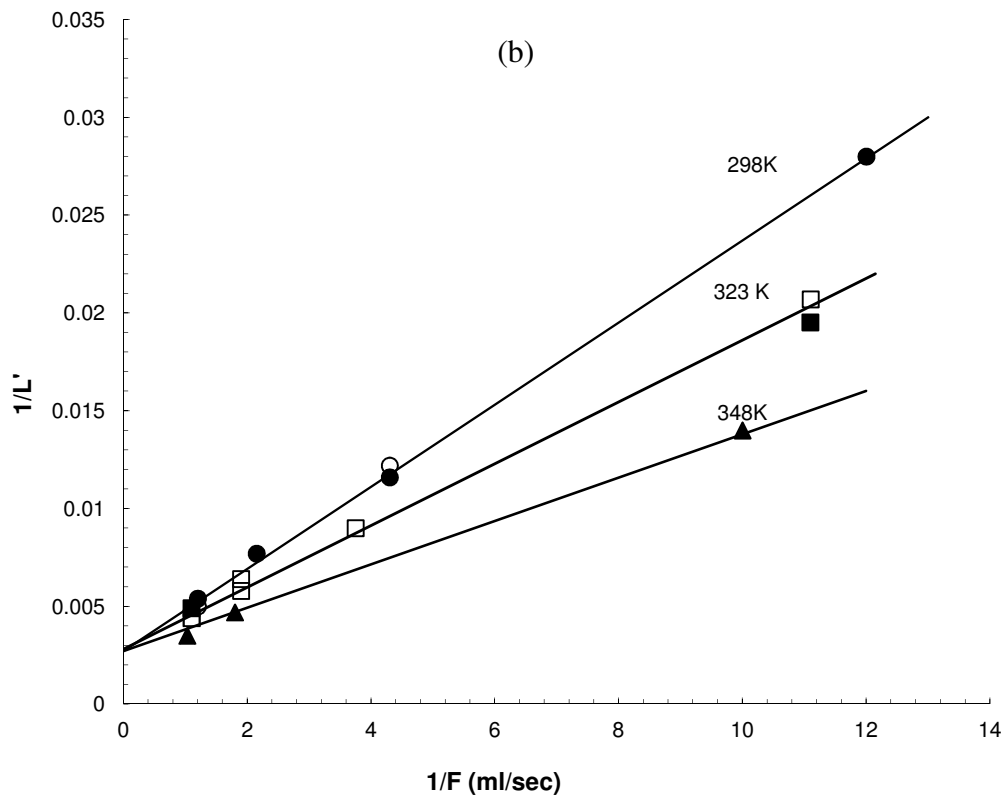
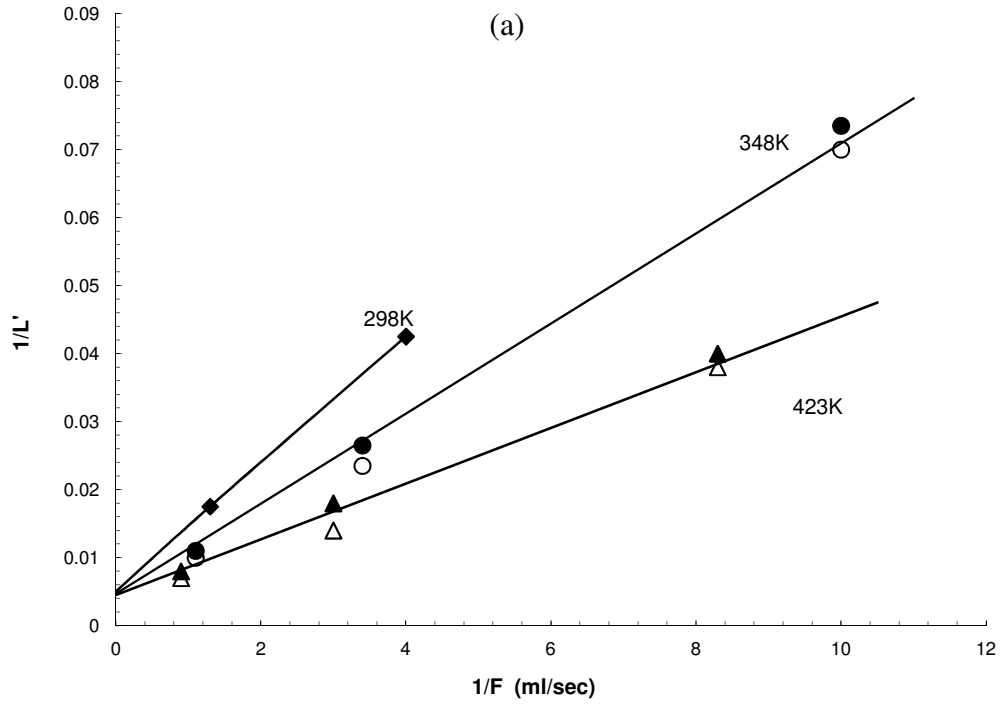


Figure 7.8. Relation of $1/L'$ v $1/F$ for C_2H_6 in Two Different Samples (a) DDR II; (b) DDR I (5.9 mg) Open symbols, He; filled symbols, CO_2 .

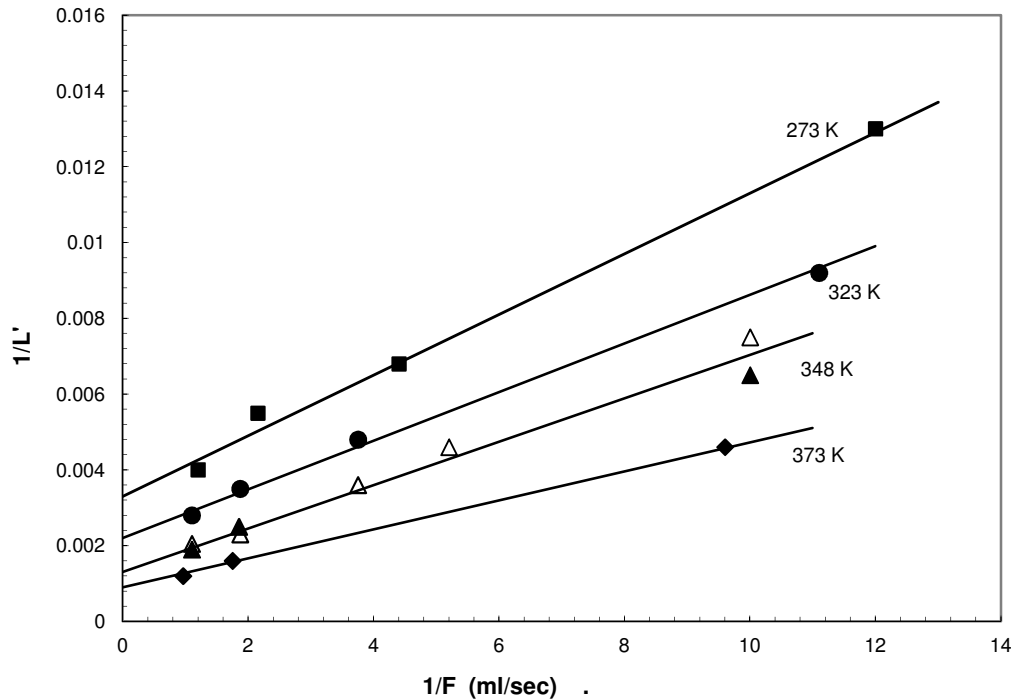


Figure 7.8 (continued...). Relation of $1/L'$ v $1/F$ for C_2H_6 in Two Different Samples (c) DDR I (2.4 mg) Open symbols, He; filled symbols, CO_2 .

In all cases, the intercepts are relatively small ($D/kR \sim 0.003-0.005$), implying that the contribution of surface resistance is minor except at the higher flow rates. To put this into context, the half-time for surface resistance control is given by $t_{surf} = (R/3k)\ln 2$ while the half time for internal diffusion is given by $t_{diff} = 0.03(R^2/D)$ so the ratio $t_{diff}/t_{surf} \approx 0.13(kR/D)$. With $D/Rk = 0.003$ this gives $t_{diff}/t_{surf} \approx 40$ so, by normal criteria, the system would be considered to be diffusion controlled. Nevertheless, even this small contribution from surface resistance leads to a significant variation of the apparent K value with flow rate, as may be seen from the data shown in Table 7.1. The analysis of the data for the 2.4 mg DDR I sample is summarized in Table 7.3.

Table 7.3 Analysis of L' Values for DDR I, 2.4 mg Sample.

T (K)	Int.=D/kR	k/R (s ⁻¹)	Slope	D/R ² (s ⁻¹)	K
273	0.0033	0.185	0.0008	0.00061	312
298	0.004	0.31	0.001	0.00124	192
323	0.0022	0.64	0.00063	0.0014	107
348	0.0014	1.52	0.00051	0.00213	57
373	0.0009	3	0.00039	0.0027	34

An Arrhenius plot of the surface rate coefficient (k/R vs $1/T$) yields about 28 kJ/mole for the activation energy, which is greater than the heat of adsorption (22 kJ/mole) and much greater than the diffusional activation energy (12.7 kJ/mole) - see Table 7.4. However, in view of the errors inherent in the estimation of the surface rate parameter this estimate of the activation energy should be treated with caution.

The differences in surface resistance between the samples, particularly the two samples of DDR I, suggest that the surface resistance is probably affected (or even determined) by the sample history rather than by the original synthesis. The obvious suspect would be surface coke deposition.

The experimental data for C_2H_4 are less consistent, with greater differences between replicate measurements. As a result the plots of $1/L'$ vs $1/F$ were too scattered to provide any useful information.

7.5 Ethane and Ethylene Henry Constants

The temperature dependence of K (figure 7.9) plotted in accordance with the usual van't Hoff expression:

$$K = K_{\infty} e^{-\Delta U / RT} \quad (7.3)$$

The K values for the two samples of DDR I are essentially the same and very similar to the values derived from the equilibrium isotherms for C_2H_6 on DDR reported by Zhu et al. The values for DDR II are slightly larger. The parameters K_{∞} and $(-\Delta U)$ correlating the temperature dependence are given in Table 7.4 which includes also the kinetic parameters.

Since it was not possible to derive reliable K values for C_2H_4 from plots of $1/L'$ vs $1/F$ the values included in figure 7.9 were estimated directly from the ZLC response curves at the lowest purge flow rate (5 ml/min) at which the effect of surface resistance is minimal. These values are very close to the values for C_2H_6 . This is consistent with the equilibrium data of Zhu et al⁽²⁶⁾ which show that the Henry constants for C_2H_4 and C_2H_6 in DDR are essentially the same.

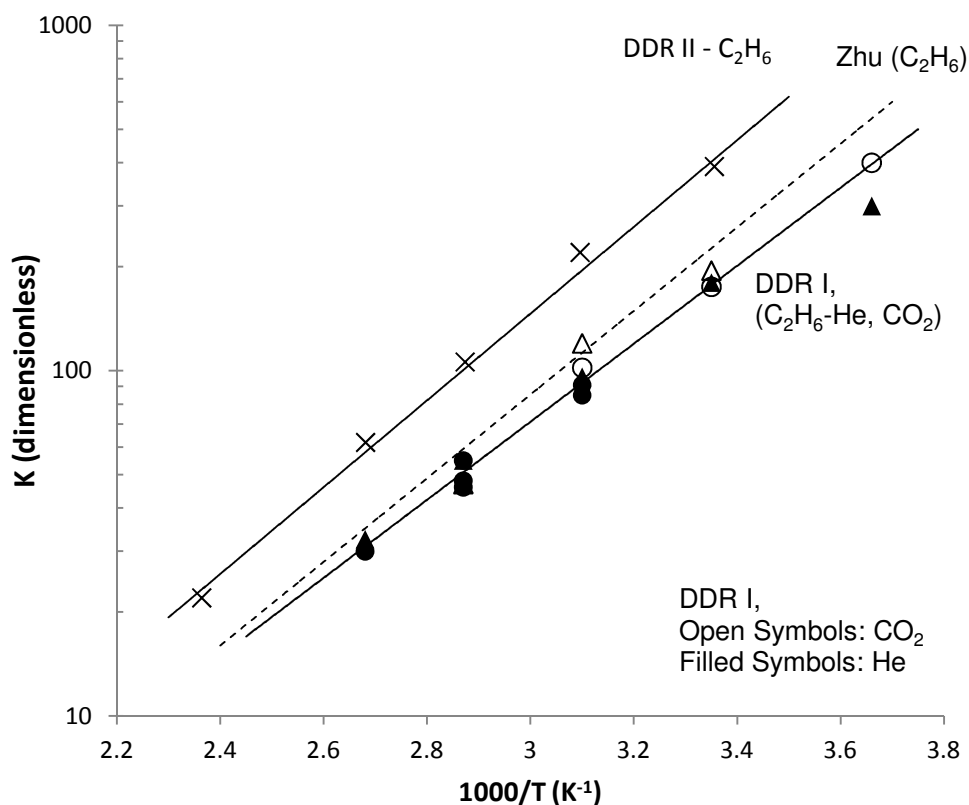


Figure 7.9. van't Hoff plot for C_2H_6 –He and C_2H_6 – CO_2 in DDR. Showing variation of dimensionless Henry constant (K) with temperature. Measurements with different samples of DDR I are indicated by different symbols. The dashed line indicates the values calculated from the equilibrium isotherms presented by Zhu²⁶.

Table 7.4 Summary of Kinetic and Equilibrium Parameters for C_2H_6 and CH_4 in DDR

	D_∞ ($m^2 s^{-1}$)	E (kJ/mole)	K_∞	$-\Delta U$ (kJ/mole)	D/kR
C_2H_6					
DDR II	2.6×10^{-10}	17.5	0.025	24	0.0047
DDR I (5.9mg)	1.75×10^{-11}	12.7	0.025	22	0.0028
DDR I (2.4mg)					0.001- 0.0033
Zhu ⁽⁵⁶⁾	-	-	0.026	22.5	
CH_4					
DDR II	2.2×10^{-9}	17	0.116	13.1	0
DDR I	2.2×10^{-8}	25.5	0.116	13.1	0

7.6 Ethane and Ethylene Discussion of Results

The substantial difference in both diffusivity and diffusional activation energy between the original (untreated) DDR I sample and the treated DDR II sample means that the proprietary treatment must have caused a significant modification of the internal structure rather than simply a modification of the external surface. The precise structural difference between the samples is, however, far from clear.

The diffusional and equilibrium behavior of ethane and ethylene are very similar and do not appear to reflect the slightly smaller critical diameter of the ethylene molecule. For DDR I the equilibrium constants for both ethane and ethylene agree well with the isotherm data of Zhu et al.²⁶, and the ethylene diffusivity data are consistent with the self-diffusivity of ethylene (at 300K) measured by PFGNMR²⁷ (See figure 7.7). The DDR sample used in those studies was not subjected to any treatment and was presumably similar to DDR I.

The pattern of behavior shown by the C₂ species is quite different from that shown by CH₄. Our study of the diffusion of methane in DDR showed that the diffusivity is substantially enhanced and the equilibrium constant is correspondingly reduced in the presence of an atmosphere of CO₂. That pattern of behavior is to be expected from transition state theory as a consequence of competitive adsorption. In contrast, for both ethane and ethylene in both DDR samples, both the diffusivity and the equilibrium constant appear to be essentially unaffected by the presence of CO₂. That result implies that the adsorption of C₂ hydrocarbons and CO₂ is non-competitive. A similar result was reported by Guimaraes et al.⁷² who showed that the diffusivity of C₄-

C₁₀ linear alkanes in silicalite was not affected by the presence of CO₂. For those systems such a result is not unexpected since the linear paraffins are located preferentially in the straight channel segments whereas CO₂ molecules prefer the channel intersections, thus making adsorption non-competitive.

However, in DDR both the C₂ hydrocarbons and CO₂ may be expected to be competitively adsorbed within the large cages leading to a competitive adsorption situation. The equilibrium isotherms at higher loadings show clearly that CO₂ occupies the large cages since the saturation capacity corresponds closely to the quotient of the specific micropore volume and the molecular volume of CO₂. However, the isotherms for ethane and ethylene provide some tentative evidence that these molecules may prefer the window sites. The saturation capacities for both ethane and ethylene in DDR, derived from the isotherms of Zhu et al.³³ correspond to approximately 1.5 molecules per cage. Each cage contains three windows (shared with the adjacent cage) so if the C₂ hydrocarbons preferentially occupy the window sites the apparent saturation limit of 1.5 molecules per cage and the non-competitive adsorption of CO₂ would be explained.

It is surprising that, for ethane, the higher diffusivity adsorbent (DDR II) also has a higher diffusional activation energy than DDR I, whereas for methane the activation energy shows the expected trend, being smaller for DDR II. It is also surprising that the diffusional activation energies of methane and ethane in DDR II are essentially the same (see Table 7.4). Even more surprising is the observation that the diffusional activation energy for DDR I is substantially smaller for ethane than for methane (12.7 vs 25.5 kJ/mole). This suggests, somewhat counter-intuitively, that the energy barrier to intracrystalline diffusion of ethane is not determined by the molecular diameter. Both

these observations could be considered as consistent with the preferential occupation of the windows by the C₂ hydrocarbons since the energy barrier would then correspond to the higher energy region in the centre of the cage which would be much less sensitive to small differences in molecular diameter. Of course any such hypothesis is highly speculative and would require validation by either detailed experimental studies with a CO₂ sensitive detector or molecular simulations.

From a practical perspective it is interesting to consider the product KD since this determines the permeance of a DDR membrane. Table 7.5 shows a comparison of the KD values for methane and ethane in DDR II, calculated from the data given in Table 7.4.

Table 7.5: Comparison of KD (m²s⁻¹) for Methane and Ethane in DDR II

T (K)	(KD) _{CH₄}	(KD) _{C₂H₆}
298	5.25x10 ⁻¹¹	9x10 ⁻¹¹
373	7.23x10 ⁻¹¹	5.3x10 ⁻¹¹

It is clear that the values for methane and ethane are very similar suggesting that a DDR membrane will show similar permeances for these species.

7.7 Conclusions

The results from this study lead to some important conclusions having both practical and theoretical implications. The usefulness of the ZLC technique and its ability to distinguish between internal and surface resistance to mass transfer is clearly confirmed. The value of the asymptotic analysis which can yield an accurate value for

the diffusional time constant, even in the presence of surface resistance is also confirmed. However, to avoid errors in this approach a very stable baseline is necessary.

The proprietary treatment to which sample DDR II was subjected clearly induces a significant structural change although the nature of this change is not at all clear.

Ethane and ethylene appear to behave very similarly in DDR but the difference in the patterns of behavior between CH_4 and the C_2 hydrocarbons is striking. Whereas the data for methane show no evidence of surface resistance in either of the DDR samples studied, the C_2 hydrocarbons show clear evidence of a small but significant contribution from surface resistance. Both the kinetic and equilibrium data imply that the C_2 hydrocarbons are adsorbed non-competitively with CO_2 whereas CH_4 and CO_2 are clearly adsorbed competitively. This, together with the anomalous differences in activation energy between methane and ethane or ethylene, might be explained by preferential occupation of the window sites by the dumbbell shaped C_2 molecules but any such hypothesis is obviously speculative.

From the practical point of view the data suggest that as a result of the compensation between diffusivity and equilibrium the permeances of methane and ethane in a DDR membrane will be very similar.

CHAPTER 8
DIFFUSION OF PROPYLENE IN DDR ZEOLITES
IN COMPETITION WITH CO₂

The previous two chapters described studies of the diffusion of methane, ethane and ethylene in DD3R. In view of the potential application of DDR for molecular sieve separation of C₃H₆ / C₃H₈²² we decided to extend our study to these species. The measurements were carried out and the response curves were analyzed in the same way as described in chapters 5-7. However the diffusivities for the C₃ hydrocarbons are substantially smaller, requiring a substantially longer equilibration time. Measurements were carried out only with the DDR I sample since for the larger DDR II crystals the required time scale is too long for convenient study, except at higher temperatures at which polymerization reactions are likely to become problematic.

8.1 Propane/Propylene Results and Discussion

Representative ZLC response curves are shown in figures 8.1 and 8.2. The experimental curves conform closely to the expected form. The parameters K and D/R² were derived from the slopes and intercepts of such plots according to Eqs 5.12 and 5.16. The values of D and K derived from both expressions were consistent within a few percent. The mean values at each temperature are shown in figures 8.3 and 8.4.

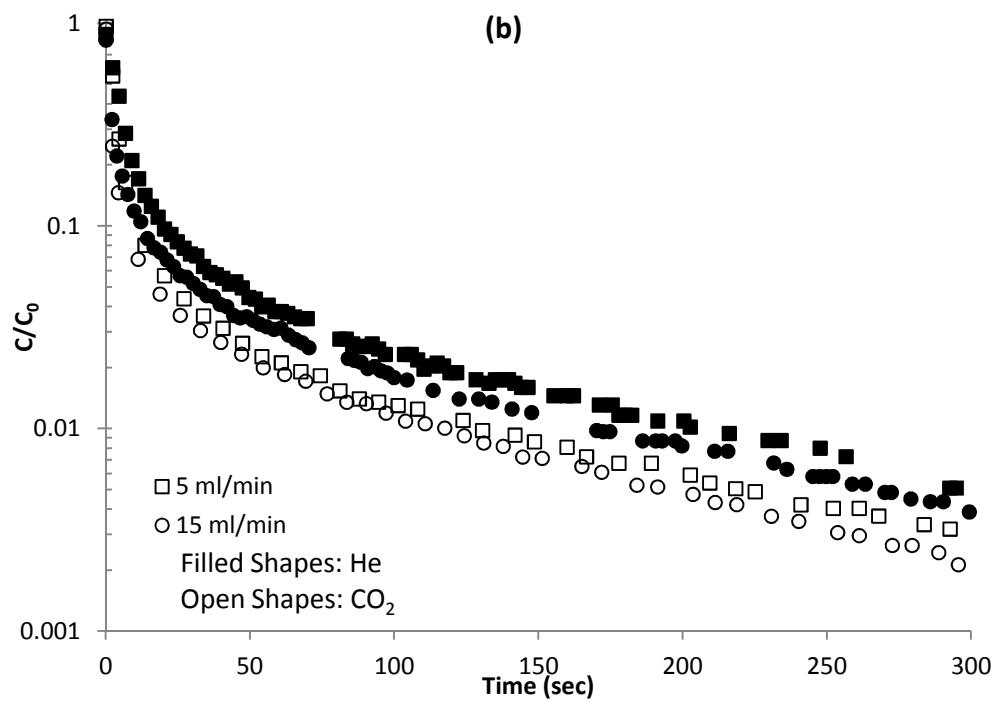
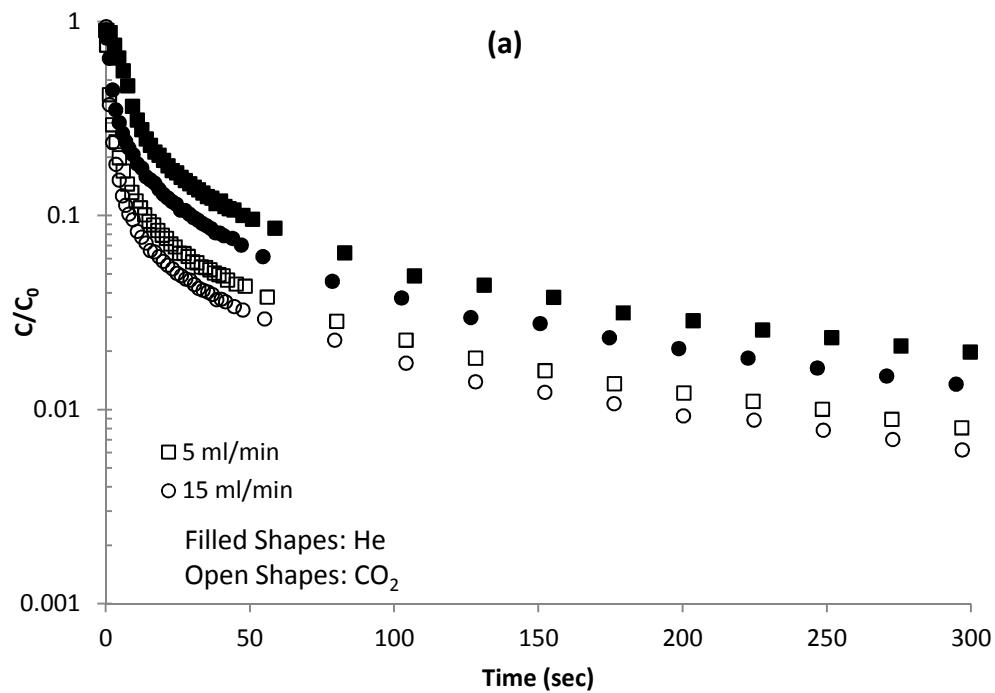


Figure 8.1 Representative ZLC response curves for C_3H_6 –He and C_3H_6 –CO₂. Purge rates of 5 and 15 ml/min plotted as $\log(c/c_0)$ vs t (in accordance with Eq. 5.12): (a) 323K (b) 373K.

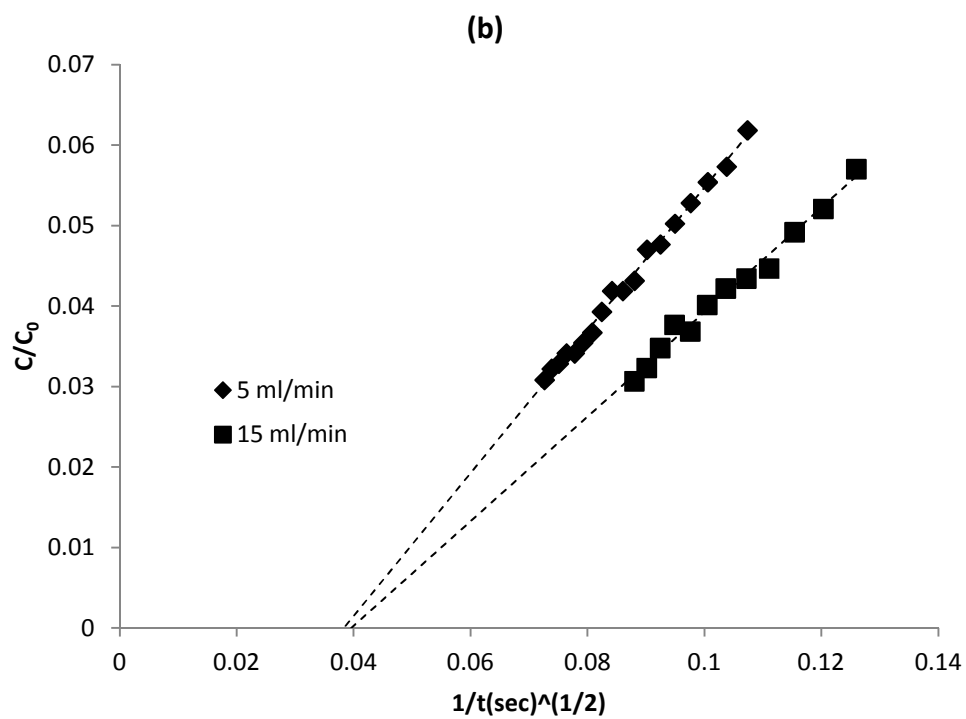
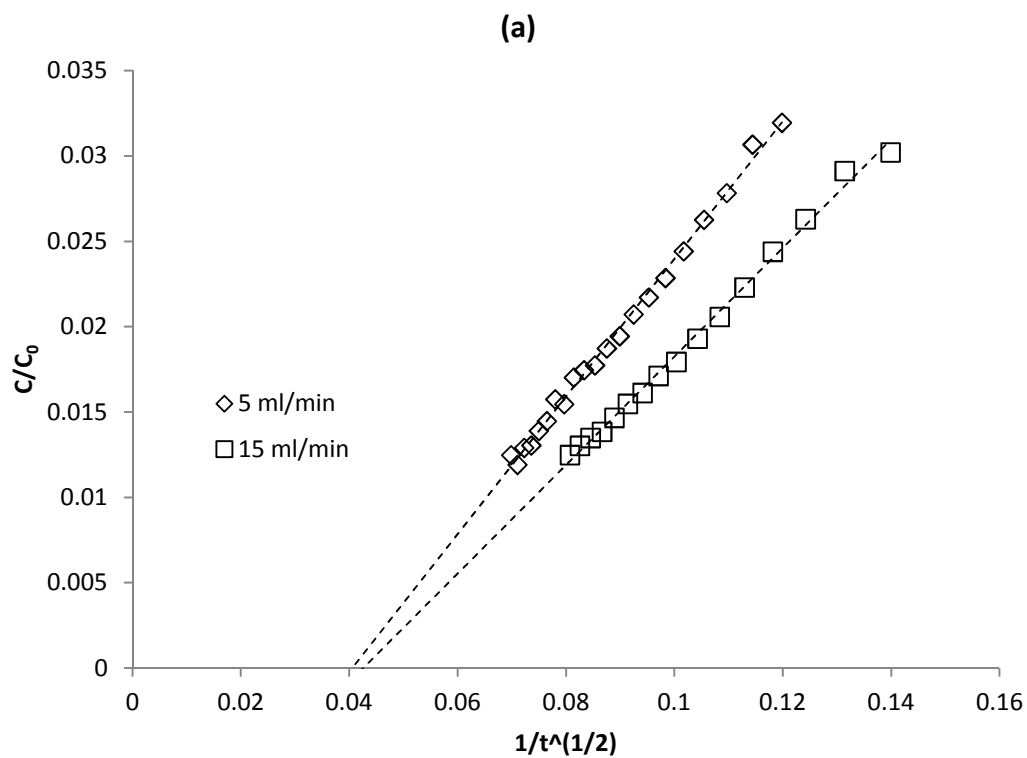


Figure 8.2 Representative Intermediate Time Analysis ZLC Data for C_3H_6 in DDR. (a) $\text{C}_3\text{H}_6\text{-CO}_2$, (b) $\text{C}_3\text{H}_6\text{-He}$.

It is evident from Figure 8.1 (and Eq. 5.12) that with CO₂ as the carrier gas, under otherwise similar conditions, the response is faster (higher asymptotic slope) and the equilibrium less favorable (lower intercept on the y axis). This is also evident from figures 8.3 and 8.4 from which it is clear that the mean diffusivities for the C₃H₆ -CO₂ system are consistently larger and the K values correspondingly smaller than the values for the C₃H₆ – He system.

The diffusivities for ethane in the same sample of DDR crystals are also indicated in Figure 3. As expected propylene diffuses less rapidly than ethane but, as a consequence of the higher activation energy, it appears that this would be reversed at temperatures above about 400K but that is beyond the range of the ethane measurements. This pattern of behavior, which was also observed for methane in DDR as detailed in chapter 6, is as expected from transition state theory for a competitively adsorbed carrier⁷¹. In contrast, the data represented in the previous chapter for ethane (and ethylene) suggest that, for those species, there is no significant difference between the diffusivities (or equilibria) measured with He or CO₂, implying non-competitive adsorption.

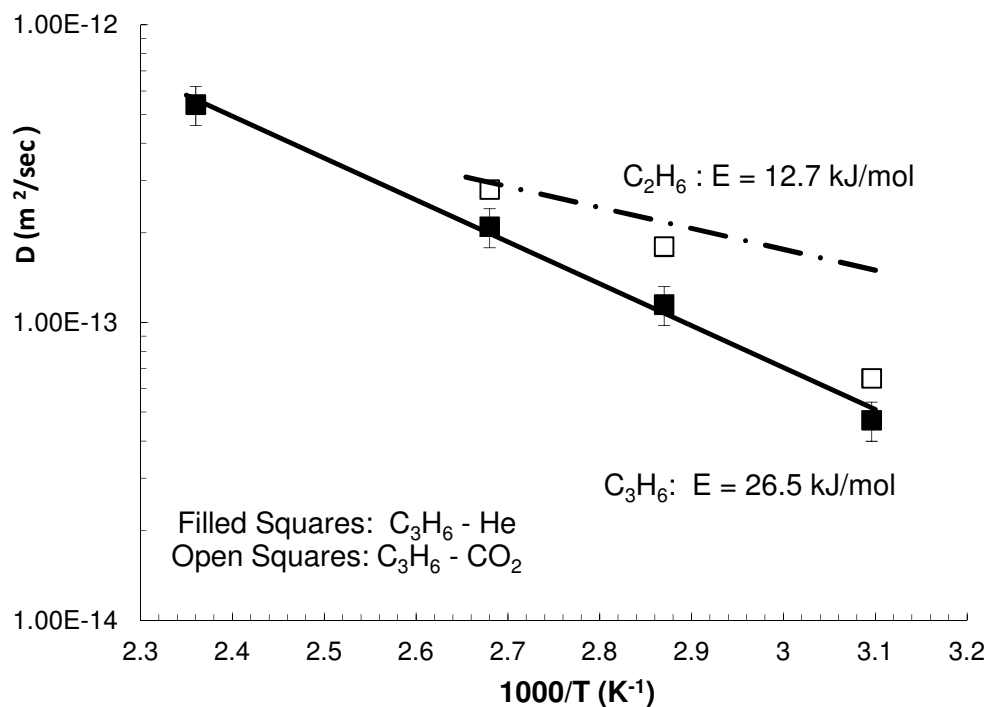


Figure 8.3. Arrhenius Plot for C₃H₆ in DD3R. Showing temperature dependence of diffusivity for C₃H₆ in DD3R crystals.

The K values derived from the ZLC response curves are compared in Figure 8.4 with the values derived from the equilibrium isotherms of Zhu et al.³³. At the higher temperatures there is good agreement but at lower temperatures the values derived from the ZLC measurements appear to be too low. This is probably because, as a result of slow diffusion at the lower temperatures, the adsorbent was not fully equilibrated prior to the ZLC desorption runs.

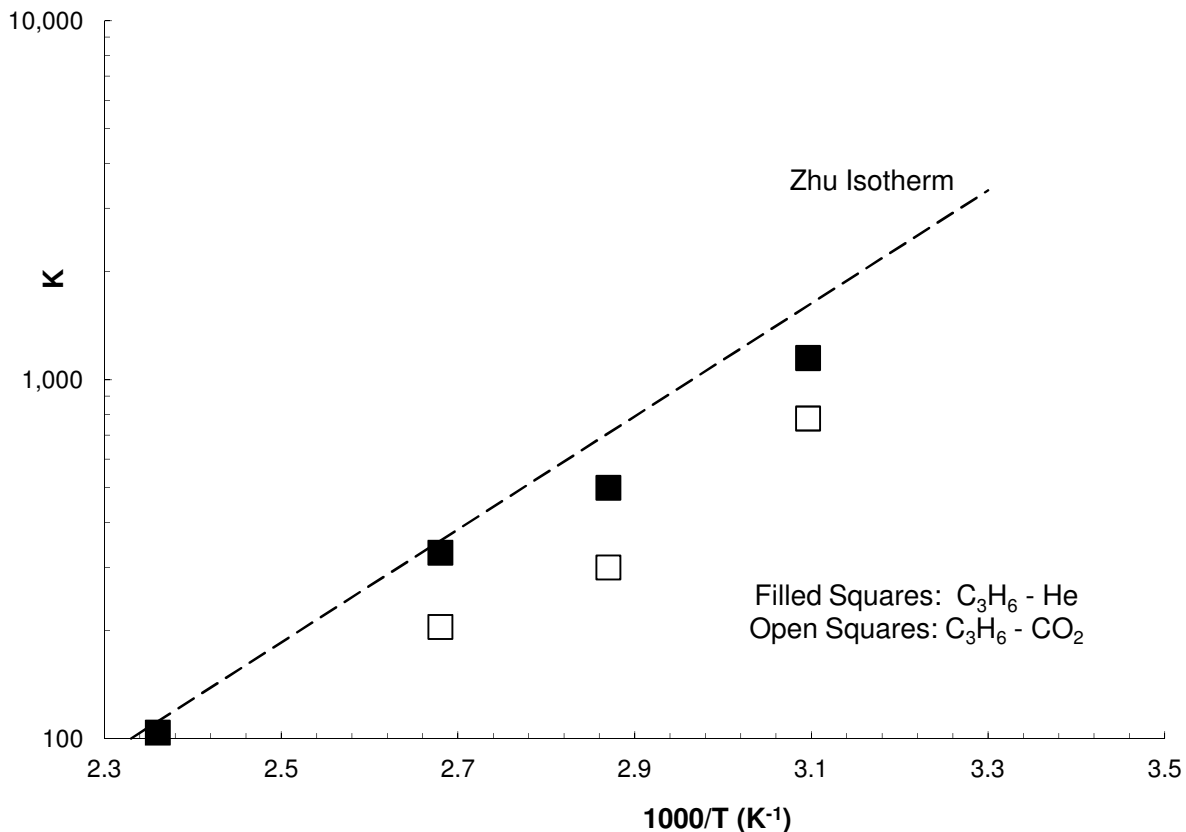


Figure 8.4. van't Hoff plot for C_3H_6 in DDR. Showing temperature dependence of equilibrium constant for C_3H_6 in DDR crystals.

The Arrhenius and van't Hoff parameters giving the temperature dependence of K and D are summarized in Table 8.1.

Table 8.1: Parameters giving Temperature Dependence of D and K

	D_∞ (m ² s ⁻¹)	E (kJ/mole)	K_∞	$-\Delta U$ (kJ/mole)
C_3H_6	1.04×10^{-9}	26.5	0.0084	33
C_2H_6/C_2H_4	1.75×10^{-11}	12.7	0.025	22

Temperature dependence is given by $D = D_\infty e^{-E/RT}$; $K = K_\infty e^{-\Delta U/RT}$

Typical ZLC response curves for propane at 323 and 373 K are shown in figure 8.5. These curves show the classic form of a blank response indicating negligible desorption on the relevant time scale. The small capacity indicated by the minor deviation from the detector response can be easily accounted for by adsorption on the external surface of the crystals. A similar conclusion was reached by Zhu et al.³³

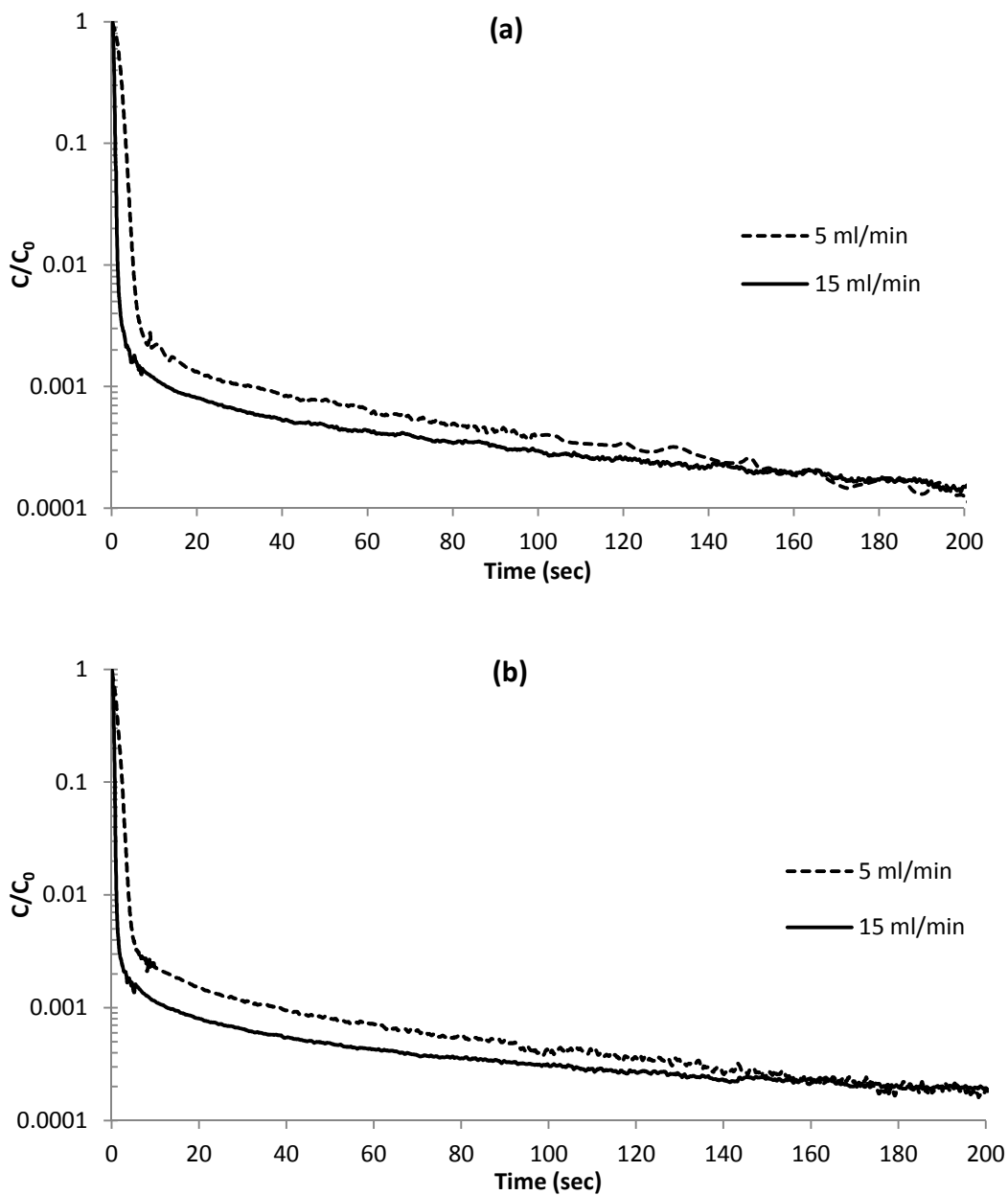


Figure 8.5. Representative ZLC Data for C_3H_8 in DDR Samples (a) 323 K (b) 373 K.

8.2 Propane/Propylene Conclusions

The diffusional behavior of C₃H₆ in DDR crystals shows the expected trends. In the temperature range 323K – 423K the diffusivities are of order 10⁻¹³ m²s⁻¹ and the diffusional activation energy is about 26.5 kJ/mole. Over the experimental range the diffusivities for C₃H₆ are somewhat lower than the values for ethane (in the same DDR crystals) but, since the activation energy for propylene is larger than that for ethane, a crossover may occur at higher temperatures.

The diffusivity of C₃H₆ is enhanced by the presence of CO₂, suggesting competitive adsorption. Similar behavior was observed for methane but, surprisingly, ethane showed no such effect implying non-competitive adsorption.

Diffusion of propane in DDR is too slow to measure in crystals of this size at the temperatures covered by this study. This supports the conclusion that DD3R is a potentially attractive adsorbent for the molecular sieve separation of propylene/propane.

CHAPTER 9

CONCLUSIONS AND RECOMMENDATIONS

On account of their unique molecular sieve properties a great deal of research has been directed towards understanding the adsorption and diffusion behavior of the small pore zeolites. Recently, as noted in chapters 1-4, attention has been focused largely on the silica rich zeolite analogs such as Si-CHA and DDR. The present study has been concerned mainly with the adsorption and diffusion of methane in DDR in the presence and absence of CO₂ but similar studies have also been carried out for other light hydrocarbons. Additional measurements were also carried out for the light olefins, especially for propylene, in view of the potential application of DDR for the molecular sieve separation of C₃H₆ and C₃H₈.

9.1 General Considerations

Measurements were made mainly by the ZLC technique which depends on following the response curve for a small pre-equilibrated sample of adsorbent purged by a non-adsorbing carrier gas stream (generally He). By analyzing the desorption curve, diffusivity and equilibrium data can be extracted, and as it became evident, in some cases the surface mass transfer resistance. The ZLC does have some limitations; it is difficult to study sorbates that are either too weakly or too strongly adsorbed. Furthermore, it is difficult to analyze data outside the linear adsorption range, the maximum sorbate pressure depends on the particular species and the temperature.

9.2 Effect of Hydroxyl Concentration on CO₂ Adsorption

High silica zeolites show promising potential as selective adsorbents for light alkane purification. Zeolites are usually prepared using a template synthesis process which results in residual hydroxyls attached to the internal surface. Evidence has shown that these hydroxyls may affect the adsorption of polar and quadrupolar molecules such as water and possibly CO₂. Various high silica MFI and DDR samples were studied to determine the magnitude of effect of these hydroxyls on CO₂ sorption.

¹H NMR was used in order to determine the amount of hydroxyls present within each sample; the zeolite samples were prepared by different methods resulting in varying hydroxyl concentrations. The samples were then subjected to CO₂ adsorption equilibrium tests using a pure gas volumetric device. Using this method accurate equilibrium isotherms were generated for 4 to 760 mmHg at three different temperatures. This allowed the calculation of heats of adsorption and equilibrium constants.

It was determined that for the MFI structures the heats of adsorption were not significantly affected by the presence of hydroxyls. However, two of the DDR samples showed a significant effect from the presence of the hydroxyls on CO₂ sorption at very low loading. When this was accounted for, a clear trend of increased CO₂ capacity with increasing hydroxyl content still remained. The heats of adsorption for the four DDR samples were not greatly altered, indicating that the increased amount of hydroxyls did little in the way of changing the energetics of adsorption, rather the adsorption capacity or site density was increased. This potentially could be caused by the increased hydroxyl content creating a more open structure allowing access of CO₂ to regions within the

structure which in less strongly hydroxylated samples may be closed. Opening of some of the smaller cages is an possibility.

9.3 Extended ZLC Model Incorporating Surface Resistance

With recent advances in microscopy, it has been established that many zeolite crystals show clear evidence of significant mass transfer resistance at the particle surface. In such samples sorption are controlled by a combination of intraparticle diffusion and surface resistance. Previous work has been conducted to account for surface resistance as the dominant effect. However in the present study, it was determined that both effects may have similar magnitudes. Therefore the standard ZLC model was extended in order to account for both resistances.

This model was developed and used with the Ethane-DDR data reported in chapter 7. While the effect of the surface resistance was only one-tenth that of diffusion, it still must be accounted for in order to avoid wildly varying and unrealistic apparent K values. In the presence of surface resistance the intercept of the long time asymptote is decreased. The magnitude of the error in the apparent K value increases with increasing flow rate. This phenomenon allows direct experimental detection of whether or not surface resistance is significant. If surface resistance is significant its magnitude can be determined with reasonable accuracy.

9.4 Adsorption and Diffusion of Methane Within DDR in Competition with CO₂

DD3R has shown considerable promise for application to CO₂ removal from light alkanes, particularly methane, based on size selective properties. Single component diffusion and equilibrium data suggest that, in DDR, CO₂ diffuses much faster than methane, making it potentially useful as a molecular sieve adsorbent material to separate these species. However, there is scant data on how these two species behave in a binary mixture. One hypothesis proposed by van Den Bergh postulated that the presence of CO₂ could increase the diffusivity of methane within DDR, but his data were based on permeance measurements, which for a zeolite system, do not always yield reliable diffusivity values. Another hypothesis proposed by Jee and Sholl suggested that the diffusion of methane would be reduced. Their conclusion was based on molecular simulations that may not properly represent the behavior of the real system.

The ZLC system is well suited for measuring both diffusivities and equilibrium properties in both single component and multicomponent systems, in order to resolve these conflicting theories. Using different sample quantities and flow rates, data could be collected while eliminating the concern of possible intrusion of extracrystalline mass transfer or heat effects from altering the data. Diffusion of methane was studied in a single component system and in a binary system with CO₂.

The data show clearly that CO₂ enhances the diffusivity of methane within the DDR system. CO₂ was also found to be competitively adsorbing with methane as shown by the reduction in the adsorption equilibrium constants in the binary system. This result suggests that CO₂ and methane are competitively adsorbed in DDR, competing for the same sites within the cage structure. Since CO₂ is the more strongly adsorbing species, it

follows from transition state theory that the diffusivity of methane will be increased as a consequence of its weakened adsorption (equilibrium) in the presence of CO₂. That is to say that methane stays in a somewhat energized state within the cage allowing it to pass through the cage window with a reduced energy penalty as compared to methane in a single component system. The increased diffusivity values were confirmed using a second sample of DDR that had undergone a proprietary treatment. This treated sample showed increased diffusion of methane compared with the first DDR sample; but the relative effect of CO₂ was the same, with an increased diffusivity of methane in the presence of CO₂ compared with the single component system.

However the prediction from transition state theory that the product of KD remains constant suggests that the increased diffusivity of methane in the presence of CO₂ may have little effect on the overall perm-selective or kinetic selectivity.

9.5 Adsorption and Diffusion of Ethane, Ethylene and Propylene within DDR in Competition with CO₂

As a logical next step in evaluating DDR's potential to purify light alkanes, the diffusion of ethane, ethylene propane and propylene in DDR was also studied. The results from ZLC measurements with these sorbates were generally similar to methane but there were also some striking differences.

The initial data yielded apparent K values, that increased strongly with flow rate. This was subsequently explained and accounted for using the extended ZLC model that accounts for both internal diffusion and surface resistance effects.

Both ethane and ethylene have similar diffusivities and Henry constants. Methane showed no detectable surface resistance, but more importantly, the C₂ hydrocarbons appear to adsorb non-competitively with CO₂. The preferential occupation of different sites by both CO₂ and C₂ alkanes might indicate that these dumbbell shaped molecules reside preferentially between cages within the windows, whereas CO₂ primarily remains within the free volume of the cage itself. This hypothesis is supported by coincidental isotherm data; but further more detailed measurements would be needed to verify this hypothesis.

Interestingly propylene appears to behave similarly to methane showing the expected increase in diffusivity and corresponding decrease in equilibrium constant in the presence of CO₂. The kinetic selectivity for C₃H₆ /C₃H₈ appears to be very large making DDR an ideal adsorbent for this separation.

9.6 Modified MFI Zeolites, Adsorption and Diffusion with Light Alkanes

Another approach to utilizing zeolites as a selective membrane is to take a currently existing zeolite that is easily made and modify the structure with functional groups to alter its properties. That is the approach that collaborators are using at the Georgia Institute of Technology. Using an MFI structure, they have replaced the surface hydroxyls with a variety of functional groups in an effort to modify their chemistry; we were subsequently provided with several samples in order to characterize how these materials interact with light alkanes.

The functional groups characterized were: Butanol, Hexanol and Phenylamine, additionally a non-functionalized sample was analyzed in order to provide a baseline.

Using the ZLC method at varying flow rates, at 50 °C, equilibrium and diffusivity values were determined for four samples with four different gasses. Furthermore it was possible to back out isotherms from the equilibrium controlled runs.

It was shown that the functionalized materials all showed a reduced equilibrium constant. The trend becomes more apparent as the molecular size of the alkane increases. Diffusivity had a different, more nebulous trend; methane could not be measured accurately and ethane showed a surprising increase in diffusivity. Propane either increased or decreased depending on the functional group and butane showed a decrease in diffusivity for all functional groups.

The functionalized materials show promise as a way to tailor the behavior of zeolite materials for a specific application. Furthermore, using ZLC measurements to screen these materials for both equilibrium and diffusive effects proved to be a useful approach. To gain a greater understanding of how these materials function with different sorbates, it might be advisable to alter the temperature as well, but that also gives an additional degree of freedom in the screening process which would make the testing of multiple sorbates quite time consuming.

9.7 Recommendations

The focus of this study was on the use of the ZLC method in order to characterize zeolites as selective adsorbents for CO₂/CH₄ and olefin/paraffin separations. This has been accomplished; however, it would be prudent to extend these studies. One obvious extension would be to further examine the interaction of methane, CO₂ and DDR. This

could be done in a variety of ways, including altering the partial pressure of CO₂, examining other treatments and also reducing the temperature and flow rate in order to further study the material in the equilibrium controlled regime, particularly with methane.

Another logical extension to this study would be to introduce a system that could detect CO₂. Using a sensitive mass-spectrometer or another species sensitive detector, it would be possible to examine the effect of methane on CO₂ diffusion as a logical complement to the present study in which an FID was used to study the effect of CO₂ on diffusion of CH₄. The behavior of CO₂ in the presence of other light alkanes also merits further experimental study.

A similar study to measure the diffusivity of CO₂ in the presence of C₂H₆ or C₂H₄ would even be more interesting. If the hypothesis that the C₂ hydrocarbons occupy preferentially the windows is correct the diffusivity of CO₂ should be reduced dramatically in the presence of ethane or ethylene. Thus such measurements have the potential to verify or disprove this hypothesis.

REFERENCES

1. D.L. MacClean, S. Lerner, V. Malik. *Gas Sep. & Pur.*, 1987: 77.
2. Breck, D.W. *Zeolite Molecular Sieves-Structure, Chemistry, and Use*. New York City: John Wiley & Sons, 1977.
3. R.R.Chance and E.W.Corcoran *Diffusion Fundamentals 1*, Leipzig University (2005)
4. T.E. Clark, H.W. Deckman, D.M. Cox and R.R. Chance *J. Membrane Sci.* **230**, 94 (2004)
5. H.W. Deckman, R. Chance, E. Corcoran, G.De Martin, S.Reyes, N.Hedin, C.Yoon and T.Clark *North American Membrane Society*, Annual Meeting (2006)
6. R.R.Chance 229th ACS National Meeting, San Diego, CA, Mar 13-17 (2005)
7. R.M.Milton U.S.Patents 2,882,243 and 2,882, 244 (1959) to Union Carbide inc.
8. D.W.Breck, W.G.Eversole, R.M.Milton and T.B.Reed *J.Am. Chem.Soc.* **78**, 5963 (1956)
9. C.W. Skarstrom U.S. Patent 2,944,627 (July 12, 1960) to Esso Research and Engineering
10. P.G.de Montgareuil and D.Domine U.S. Patent 3,155,468 (1964) to Air Liquide.
11. W.J. Asher et al. U.S. Patent 3,070,542 (1962) to Esso Research and Engineering
12. W.J.Asher, M.L.Campbell, W.R. Epperly and J.L. Robertson *Hydrocarbon Processing* **48** (1) 134 (1964)
13. Ch. Baerlocher, L.B.McKusker, D.H.Olson *Atlas of Zeolite Structures* (6th Edition), Elsevier Science, Amsterdam (2007)
14. G.T.Kokotailo and W.M.Meier p.33 in *Properties and Applications of Zeolites* R.P.Townsend, ed. Special Publ. No. 33 Chem. Soc. London (1979)
15. H.Gies *Z.Kristallogr.* **175**, 93-104 (1986)
16. R.M.Barrer *Zeolites and Clay Minerals as Sorbents and Molecular Sieves* Academic Press, London (1978)

17. J.Cejka, H.van Bekkum, A.Corma and F.Schueth *Introduction to Zeolite Science and Practice* Chapter 2 *Studies in Surface Science and Catalysis* **168** Elsevier, Amsterdam, (2007).
18. Caro, J. *Adsorption*, 2005: 215-227
19. C. Cheng, T. Bae, B. McCool, R. Chance, S. Nair, C. Jones *J. Phys. Chem C*, **112**, 3543-3551 (2008)
20. D.M.Ruthven and S.C.Reyes *Microporous Mesoporous Mats.* **104**, 59-66 (2007)
21. D.H.Olson U.S.Patent 6,488,741 (Dec. 3, 2002)
22. D.H.Olson, M.A.Camblor, L.A.Villaescusa and G.H.Kuehl *Microporous Mesoporous Mats.* **67**, 27-33 (2004)
23. J.van den Bergh *PhD Thesis*, University of Delft (2010)
24. J.van den Bergh, W.Zhu, J.Gascon, J.A.Moulijn and F.Kapteijn *J.Membrane Sci.* **316**, 35-45 (2008)
25. J.van den Bergh, A.Tihaya and F.Kapteijn *Microporous Mesoporous Mats.* **132**, 137-147 (2010).
26. W.Zhu, F.Kapteijn, J.A.Moulijn, M.C.den Exter and J.C.Jansen *Langmuir* **16**, 3322-3329 (2000)
27. N.Hedin, G.J.DeMartin, W.J.Roth, K.G.Strohmaier and S.C. Reyes *Microporous Mesoporous Mats.* **109**, 327-334 (2008)
28. R.Krishna and J.M.van Baten *Sep.Purif. Technol.* **61**, 414-423 (2008)
29. R.Krishna and J.M.van Baten *Microporous and Mesoporous Mats.* **137**, 83-91 (2011)
30. S.E.Jee and D.S.Sholl *J.Am.Chem.Soc.* **131**, 7896-7904 (2009).
31. T.Tomita, K.Nakayama and H.Sakai *Microporous mesoporous Mats.* **68**, 71, (2004)
32. M.J. den Exter, J.C.Jensen and H.van Bekkum in *Zeolites and Related Microporous Material: State of the Art 1994.* **84**, 1139 (1994)
33. W.Zhu, F.Kapteijn and J.A.Moulijn *Chem. Commun.* 2453, (1999) Adsorbents
34. D.M.Ruthven and S.Reyes *Microporous Mesoporous Mats* **104**, 59-66 (2007)

35. A.F. Kapteijn, W.J.W. Bakker, J. van der Graaf, G. Zheng, J. Poppe and J.A. Moulijn *Catal. Today* **25**, 213, (1995)
36. A.J. van den Bergh, W. Zhu, J. Gascon, J.A. Moulijn and F. Kapteijn *J. Membrane Sci.* **316**, 34-45, (2008)
37. A. Neimark and P. Ravikovitch, *Langmuir*, **13**, 5145-5160 (1997)
38. S. Himeno, T. Komatsu, S. Fujita, T. Tomita, K. Suzuki, K. Nakayama and S. Yoshida *Microporous Mesoporous Mats.* **98**, 62-69 (2007)
39. D.M. Ruthven *Principles of Adsorption and Adsorption processes* p.70, John Wiley, New York
40. R.M. Barrer and J.A. Davies *Proc. Roy. Soc. London* **A320**, 289 (1970)
41. F.R. Siperstein and A.L. Myers, *AIChE Jl.* **47** 1141-159 (2001)
42. P. Wu, A. Debebe and Y.H. Ma *Zeolites*, **3**, 118-122 (1983)
43. M.J. den Exter, J.C. Jansen, H. van Bekkum, A. Zikanova, J. Dubsy and M. Kocirik *Coll. Czech. Chem. Commun.* **62**, 1-14 (1997).
44. M. Eic and D.M. Ruthven *Zeolites* **8**, 472 (1988)
45. J. Crank *Mathematics of Diffusion* p73 Oxford University Press, London (1956)
46. D.M. Ruthven, S. Brandani and M. Eic in *Molecular Sieves* Vol 7, 45- 84 H.G. Karge and J. Weitkamp eds. Springer Verlag, Berlin, Heidelberg (2008)
47. D.M. Ruthven and S. Brandani, "Measurement of Diffusion in Porous Solids by ZLC Methods", pp. 187-212, in *Recent Advances in Gas Separation by Microporous Ceramic Membranes*, N. K. Kanellopoulos, Ed., Elsevier, Amsterdam (2000)
48. J. Kärger and D.M. Ruthven *Diffusion in Zeolites and other Microporous Solids* pp328-333 John Wiley, New York (1992)
49. S. Brandani and D.M. Ruthven *Adsorption* **2**, 133-143 (1996).
50. M. Eic and D.M. Ruthven *Zeolites* **8**, 472 (1988)
51. D.M. Ruthven and M. Eic *Am. Chem. Soc. Symp. Ser.* **368**, 362 (1988)

52. D.M. Ruthven and S. Brandani, pp. 187-212, in *Recent Advances in Gas Separation by Microporous Ceramic Membranes*, N. K. Kanellopoulos, Ed., Elsevier, Amsterdam (2000)
53. P. Kortunov, C. Chmelik, J. Kärger, R.A. Rakoczy, D.M. Ruthven, Y. Traa, S. Vasenkov and J. Weitkamp; *Adsorption* **11**, 235-244, (2005)
54. L. Heinke, P. Kortunov, D. Tzoulaki, J. Kärger *Adsorption* **13**, (2007) 215-223
55. D.M.Ruthven, L.Heinke and J.Kaerger *Microporous Mesoporous Mats.* **132**, 94-102 (2010).
57. F.Brandani and D.M.Ruthven *Adsorption* **11**, 31-35 (2005)
58. J.Kärger and D.M.Ruthven Ch. 12 *Diffusion in Zeolites and other Microporous Solids* John Wiley, New York (1992)
59. D.M. Ruthven *Microporous and Mesoporous Mats.* Submitted for publication Oct 25 2010
60. S.C.Reyes, K.V.Venkatesan, G.J.DeMartin, J.H.Sinfelt, K.G.Strohmaier, J.G.Santiesteban, US Patent 730,142, May 4, 2004
61. S.C.Reyes, V.K.Krishnan, G.J.DeMartin, J.H.Sinfelt, K.G.Strohmaier, J.G.Santiesteban, US Patent 6.733,572, May 11, 2004
62. D.H.Olson US Patent 6,488,741, Dec3, 2002
63. R.Krishna and J.M.van Baten *Sep.Purif. Technol.* **61**, 414-423 (2008)
64. R.Krishna and J.M.van Baten *Microporous and Mesoporous Mats.* **137**, 83-91 (2011)
65. N.Hedin, G.J.DeMartin, K.G.Strohmaier and S.C. Reyes *Microporous Mesoporous Mats.* **98**, 182-188 (2007)
66. D.M.Ruthven, S.Brandani and M.Eic in *Molecular Sieves* Vol 7 , 45- 84 H.G.Karge and J.Weitkamp eds. Springer Verlag, Berlin, Heidelberg (2008)
67. H.Yucel and D.M.Ruthven *J.Chem. Soc. Faraday Trans. I* **76**, 60-70 (1980)
68. J.D.Eagan and R.B.Anderson *J.Colloid and Interface Sci.* **50**, 419-433 (1975)
69. J. Caro, J.Kaerger, G.Finger, H.Pfeifer and R.Schoellner *Z.Phys. Chem,((Leipzig)* **256**, 698 (1975) and **257**, 903 (1976).

70. Z.Xu, M.Eic and D.M.Ruthven *9th International Zeolite Conf.*, Montreal (1992) Proceedings Vol.2 p147-155 R. von Ballmoos, J.B. Higgins and M.M.J. Treacy eds., Butterworth, Stoneham MA (1993)
71. J.Kärger and D.M.Ruthven *Diffusion in Zeolites and other Microporous Solids* pp 107-111, John Wiley, New York (1992)
72. A.P.Guimaraes, A.Moeller, R.Staudt, D.C.S.de Azvedo, S.M.P. Lucena and C.L.Cavalcante *Adsorption* **16**, 29-36 (2010).
73. Doelle, H.-J.; Heering, **J.**; Riekert, L.; Marosi, L. *J. Catalysis*. **71**, 27-40 (1981)
74. Eic, M.; Ruthven, D. M. Intracrystalline Diffusion of Linear Paraffins and Benzene in Silicalite Studied by the ZLC Method. In *Zeolites: Facts, Figures, Future*; Jacobs, P. A., Santen, R. A., Eds.; Elsevier: Amsterdam, **49**, p 897 (1989)
75. R.E. Richards and L.V.C. Rees, *Langmuir* **3**, 335 (1987)
76. J. Caro, M. Bülow, W. Schirmer, J. Kärger, W. Heink, and H. Pfeifer, *J. Chem Soc. Faraday Trans. I*. **81**, 2541 (1985)
77. J. Kärger, W. Krause and H. Pfeifer, *Z. Phys. Chem. (Lepzig)* **264**, 838 (1982)
78. D.T Hayhurst and A. Paravar, *Zeolites* **8**, 27 (1988)
79. K. Jobic, M. Bee, and A.J. Dianoux, *J. Chem. Soc. Faraday Trans. I* **84**, 2347 (1988)
80. M. Bülow, H. Schlodder, L.V.C. Rees, and R.E. Richards, in *Proc. 7th Internat. Conf. on Zeolites*, Tokyo (1986)
81. N. Van Den Begin, L.V.C. Rees, J. Caro, and M. Bülow, *Zeolites* **9**, 287 (1989)

APPENDIX A

ZLC RESPONSE FOR A CYLINDRICAL PARTICLE

The transient sorption curve for an infinite cylindrical adsorbent, in which equilibrium is linear and the kinetics are controlled by the combined effects of surface resistance and internal diffusional resistance, subjected to a step change in the ambient sorbate concentration at time zero, is given by⁴⁵:

$$\frac{\bar{q}}{q_o} = 1 - 4L^2 \sum_{n=1}^{\infty} \frac{\exp(-\beta_n^2 Dt / R^2)}{\beta_n^2 (\beta_n^2 + L^2)} \quad (\text{A.1})$$

where β_n is given by the roots of:

$$\beta J_1(\beta) = LJ_0(\beta); \quad L = \frac{FR^2}{2KV_s D} \quad (\text{A.2})$$

and J_0 and J_1 are the zero and first order Bessel functions.

The ZLC response curve for such a system is given by:

$$\frac{c}{c_o} = -\frac{KV_s}{F} \frac{d}{dt} \left(\frac{\bar{q}}{q_o} \right) = 2L \sum_{n=1}^{\infty} \frac{\exp(-\beta_n^2 Dt / R^2)}{(\beta_n^2 + L^2)} \quad (\text{A.3})$$

and the long time asymptote is given by:

$$\ln\left(\frac{c}{c_o}\right) = \ln\left(\frac{2L}{\beta_1^2 + L^2}\right) - \beta_1^2 Dt / R^2 \quad (\text{A.4})$$

Comparison with Eq. 5.13 shows that approximately the same values of D will be obtained from both models if $R_{\text{sphere}} = 1.3R_{\text{cylinder}}$. If the same values of R are used in the two models D_{cylinder} (the value of D derived from matching the response curve to the cylinder model) will be about 1.7 times the value derived from the spherical particle model.

For consistency with previous studies the spherical particle model has been used throughout the present work, even though the cylindrical particle model may be regarded as a more appropriate description of the DDR pore structure.

APPENDIX B

CHARACTERIZATION OF MODIFIED SILICALITE ADSORBENTS

As part of the present GOALI research project a research program was also carried out at the Georgia Institute of Technology (Prof. Nair and M. Kasee) to investigate the potential of modified silicalite as a size selective adsorbent. The underlying concept was to modify the internal surface and the effective pore size by attaching various function groups. In order to characterize the modified adsorbents ZLC measurements were performed (at the University of Maine) with methane, ethane, propane and butane yielding values for the Henry constants, the equilibrium isotherms and intracrystalline diffusivities; a summary of these results is included here.

B.1 Materials

The silicalite crystals had an average length of 10 μm with a width 5 μm of and a thickness of about 2 μm . Three different functionalized samples were prepared by treatment with phenyldiamine (PDA), n-butanol and n-hexanol as the untreated parent material were studied with CH_4 , C_2H_6 , C_3H_8 and C_4H_{10} as the test sorbates. The sample preparation procedure has been reported in detail by Cheng¹⁹.

B.2 ZLC Measurements

The ZLC response curves were measured at 50 °C at several different purge flow rates. At the higher flow-rates the shapes of the response curves suggest diffusion control

but, at the lower flow rates, equilibrium control appears to be approached. This was confirmed by comparing the ZLC desorption curves plotted as c/c_0 vs Ft , where F is the purge flow rate. Under equilibrium controlled conditions the curves for the different flow rates should coincide when plotted this way (see eqn. 5.14).

B.3 Henry Constants

The Henry constants may be determined from the ZLC response curves by two different methods:

i. Directly from the slope of the response curve under equilibrium controlled conditions. For a linear system, the ZLC response curve will be given by Eqn. 5.14:

$$\frac{C}{C_0} \approx \exp\left(\frac{-Ft}{KV_s}\right) \quad (5.14)$$

ii. Alternatively the equilibrium isotherm may be calculated by integration of the response curve and the Henry constant may then be derived from the initial slope of the isotherm. This approach is preferable for measurements at higher loading beyond the Henry's law region. The values extracted in both these ways are reasonably consistent, as may be seen from Table B.1 and B.2. The resulting isotherms are shown in figures B.1 – B.6

Table B.1. Resulting Kinetic and Equilibrium Data for Methane and Ethane

	Flow Rate	Methane				Ethane			
		Bare	Butanol	PDA	Hexanol	Bare	Butanol	PDA	Hexanol
Isotherm Henry Constant (K) (dimensionless)	5 ml/min	64	66	43	44	516	256	282	365
	15 ml/min	55	50	33	26	584	315	396	393
ZLC Calculation Henry Constant (K) (dimensionless)	5 ml/min	213	36	62	40	505	349	351	350
	15 ml/min	155	26	43	32	406	324	447	345
D/r^2 (sec ⁻¹)	100 ml/min	-	-	-	-	0.0072	0.0272	0.0208	-
	200 ml/min	-	-	-	-	0.0096	0.0226	0.0144	-
Diffusivity \mathcal{D} (m ² /sec) <i>Assuming $r = 10 \mu m$</i>	100 ml/min	-	-	-	-	7.2E-13	3E-12	2E-12	-
	200 ml/min	-	-	-	-	9.64E-13	2E-12	1E-12	-

Table B.2. Resulting Kinetic and Equilibrium Data for Propane and Butane

	Flow Rate	Propane				Butane			
		Bare	Butanol	PDA	Hexanol	Bare	Butanol	PDA	Hexanol
Isotherm Henry Constant (K) (dimensionless)	5 ml/min	3524	1866	1984	2004	-	-	-	-
	15 ml/min	3254	1736	2433	2923	-	-	-	-
ZLC Calculation Henry Constant (K) (dimensionless)	5 ml/min	1458	817	1470	1682	-	-	-	-
	15 ml/min	1305	1349	2205	1471	-	-	-	-
D/r^2 (sec ⁻¹)	100 ml/min	0.0067	0.0019	-	0.0159	0.0062	0.0020	0.0021	0.0038
	200 ml/min	0.0048	0.0028	0.0098	-	0.0064	0.0026	0.0018	0.0035
Diffusivity \mathcal{D} (m ² /sec) <i>Assuming $r = 10 \mu m$</i>	100 ml/min	6.7E-13	1.93E-13	-	2E-12	6.24E-13	2E-13	-	3.8E-13
	200 ml/min	4.8E-13	2.84E-13	9.82E-13	-	6.42E-13	3E-13	2E-13	3.5E-13

As may be seen from the above data, the Henry constant is clearly affected by the grafting of the functional groups into the MFI structure.

Diffusion time constants were determined from the slope of the long time linear asymptotes of the ZLC response curves, plotted on $\log(c/c_0)$ vs t , as suggested by Eq. 5.12.

The data for butane suggest a marked reduction in diffusivity for the treated samples (in comparison with the parent material). The propane data show a mixed trend while surprisingly we see a significant increase in the diffusivity for ethane in the functionalized material.

B.4 Modified Silicalite Discussion of Results

Some of the data can be compared with other values found in literature which have been tabulated in Tables B.3 and B.4. The published values of equilibrium constants and diffusivity vary widely between the different samples. This may be a function of the method of preparation or the chemical composition of the MFI materials. The Si/Al ratios were not reported and this could be an important variable for both the equilibrium and kinetic effects. However, it is evident that our diffusivity values are of the same order as the literature values. Similarly, a comparison of the equilibrium data shows that our values for the bare adsorbent are within the range of the reported values.

Table B.3. Published values for Henry Constants for Ethane and Propane in Silicalite; Doelle et al.⁷³ & Eic et al.⁷⁴, The methods used to determine stated values are noted).

Literature Values K (dimensionless)			
Ethane		Propane	
Gravimetric (Doelle et al), T=293 K, r= 0.5 μm	2705	Gravimetric (Doelle et al), T=293 K, r= 0.5 μm	65,851
Gravimetric (Doelle et al), T=293 K, r= 0.5 μm	1411	Gravimetric (Doelle et al), T=293 K, r= 0.5 μm	30,009
Gravimetric (Eic et al), T=324.7 K,	88.94	Gravimetric (Eic et al), T=324.7 K,	1732

Table B.4. Published values for Diffusivity for Methane, Ethane and Propane In Silicalite. The methods used to determine stated values are noted. Data from R.E. Richards⁷⁵, J. Caro et al.⁷⁶, J. Karger et al.⁷⁷, Hayhurst & Paravar⁷⁸, K. Jobic et al.⁷⁹, M. Bülow et al.⁸⁰, & N. van den Begin et al.⁸¹

Literature Values \mathcal{D} (m^2/sec)					
Methane		Ethane		Propane	
NMR (R.E. Richards), T=334, r= 20-30 μm	1.00E-08	NMR (J. Caro et al.) (PFG), T=334, r= 20-30 μm	1.10E-10	NMR (R.E. Richards), T=334, r= 20-30 μm	3.00E-09
NMR (J. Caro et al.) (PFG), T=334, r= 20-30 μm	7.00E-09	FR (Jobic et al.), T=334, r= ~20 μm	1.60E-11	FR, (Jobic et al.) T=334, r= ~20 μm	1.50E-11
Membrane (J. Karger et al.) T=334, r= 300 μm	1.10E-10	Square Wave, (M. Bülow et al.) T=334, r= 35 μm	4.00E-09	Square Wave (M. Bülow et al.), T=334, r= 35 μm	2.50E-09
Neutron Scattering, (Hayhurst & Paravar) T=250 K, r= 14 μm	3.10E-09	Membrane, (J. Karger et al.) T=334, r= 300 μm	2.20E-11	ZLC (van den Begin) , T=334, r= 27 μm	1.20E-11
				Membrane (J. Karger et al.) , T=334, r= 300 μm	7.30E-12

The isotherms derived by integrating the ZLC response curves are shown in figures B.2-B.8. Comparing the isotherms for the same sorbate against the different samples allows for a direct comparison of the different functionalizations. Comparisons made at the same purge flow rates (5 ml/min & 15 ml/min) also appear to be more reliable. Included is a compilation of all of the isotherms at two different flow rates,

showing that there is reasonable agreement between the two data sets. It may be seen that effect of functionalization appears to increase with increasing size of sorbate molecule – possibly a kinetic effect. The propane isotherms are clearly more reliable than the isotherms for methane and ethane for the reasons noted above.

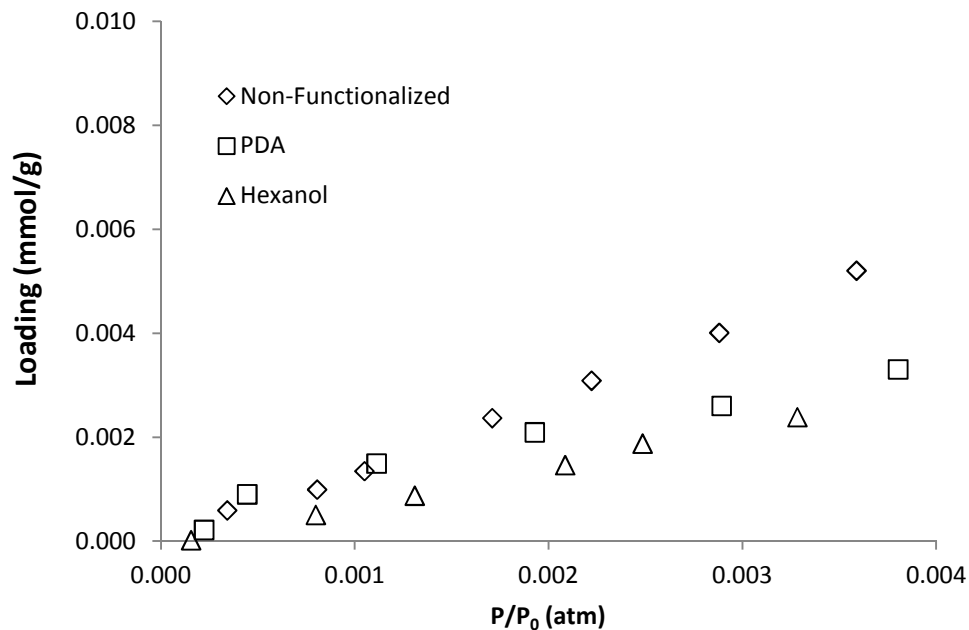


Figure B.1. Comparative Methane Isotherms at 5 ml/min, 50 °C.

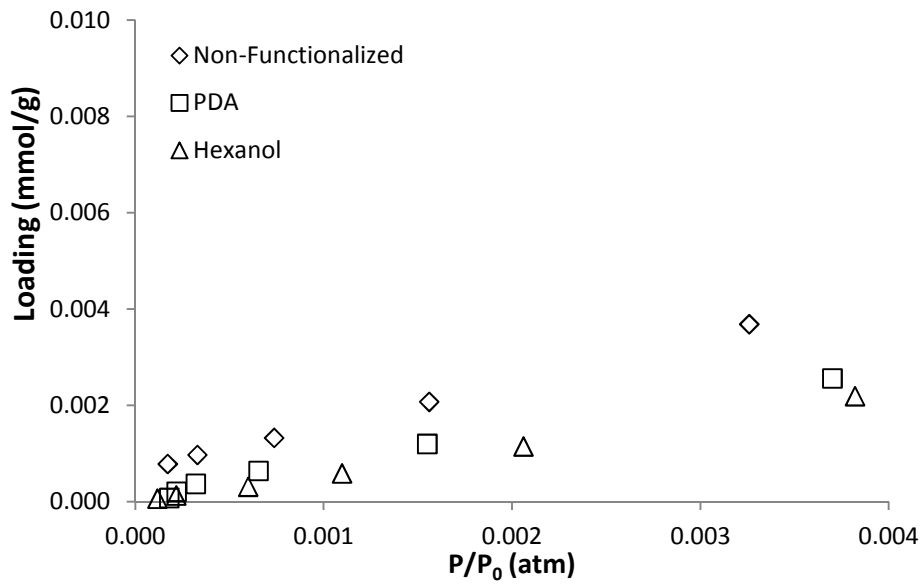


Figure B.2. Comparative Methane Isotherms at 15 ml/min, 50 °C.

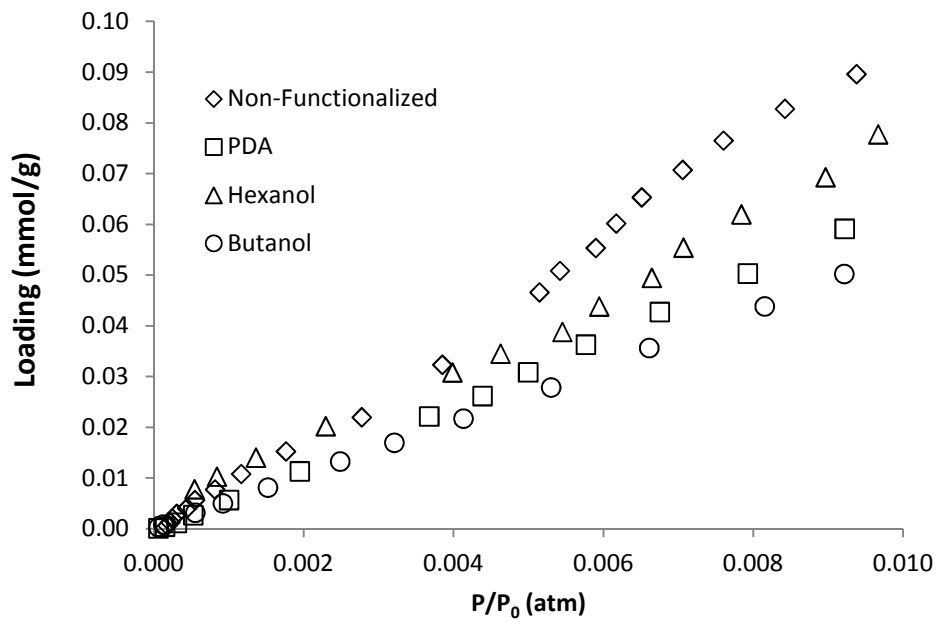


Figure B.3. Comparative Ethane Isotherms at 5 ml/min, 50 °C.

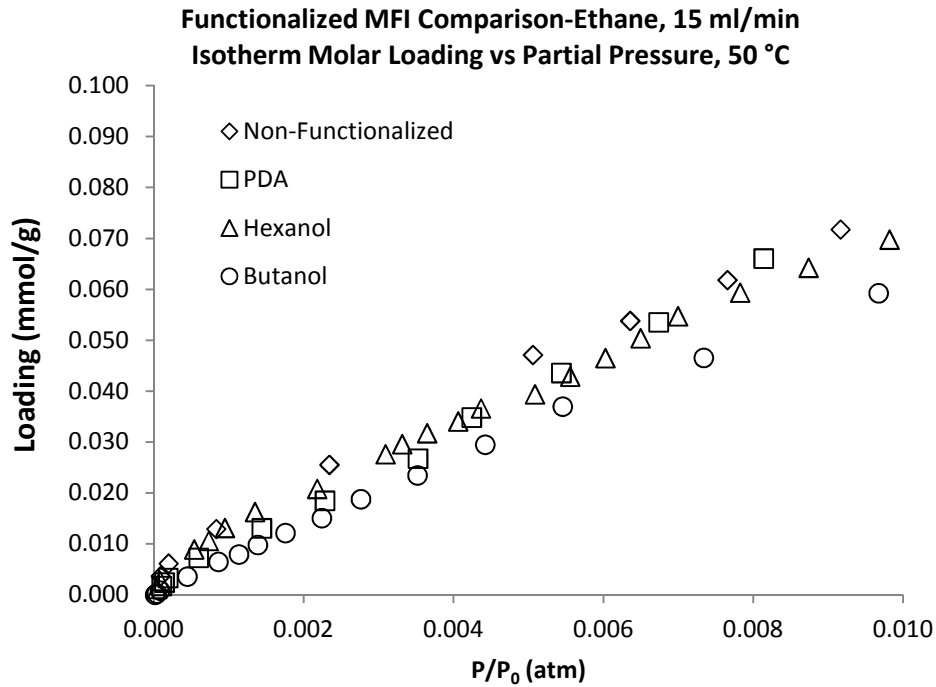


Figure B.4. Comparative Ethane Isotherms at 15 ml/min, 50 °C.

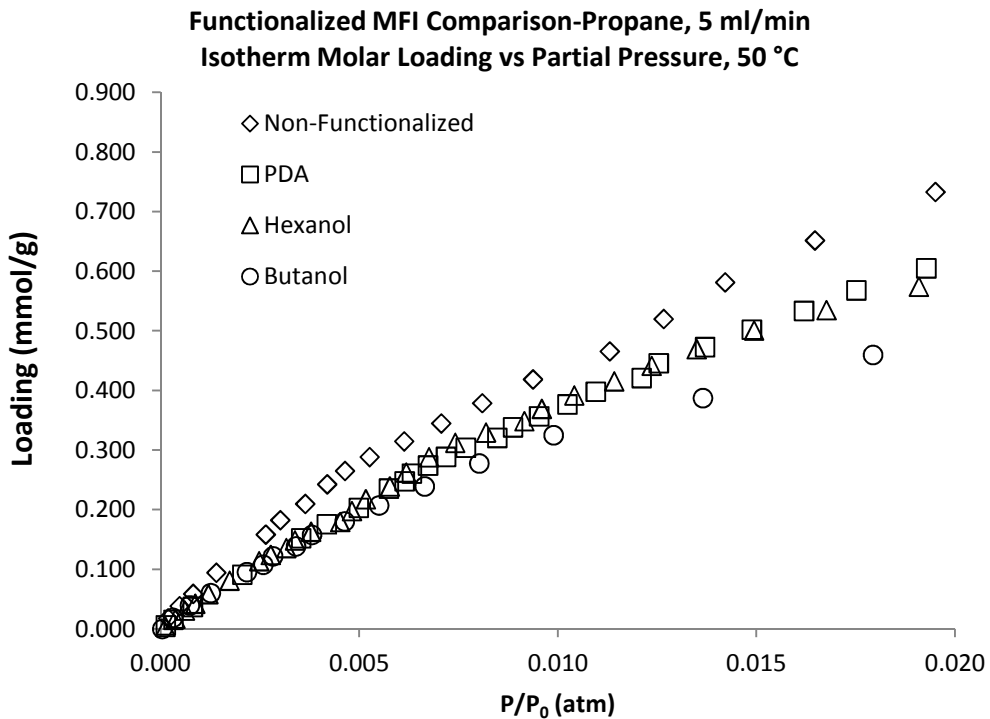


Figure B.5. Comparative Propane Isotherms at 5 ml/min, 50 °C.

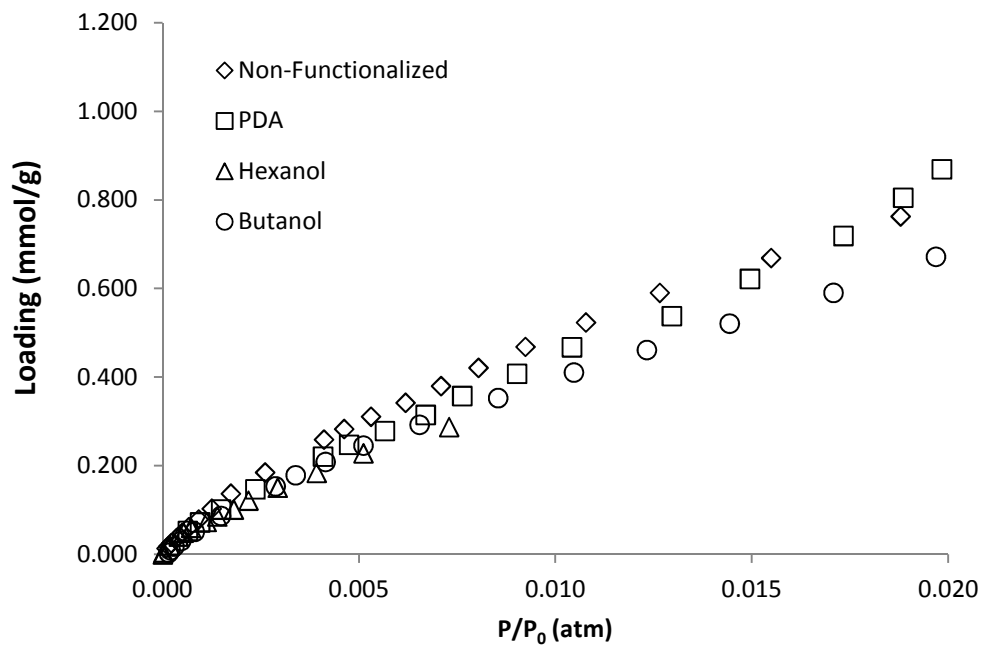


Figure B.6. Comparative Propane Isotherms at 15 ml/min, 50 °C.

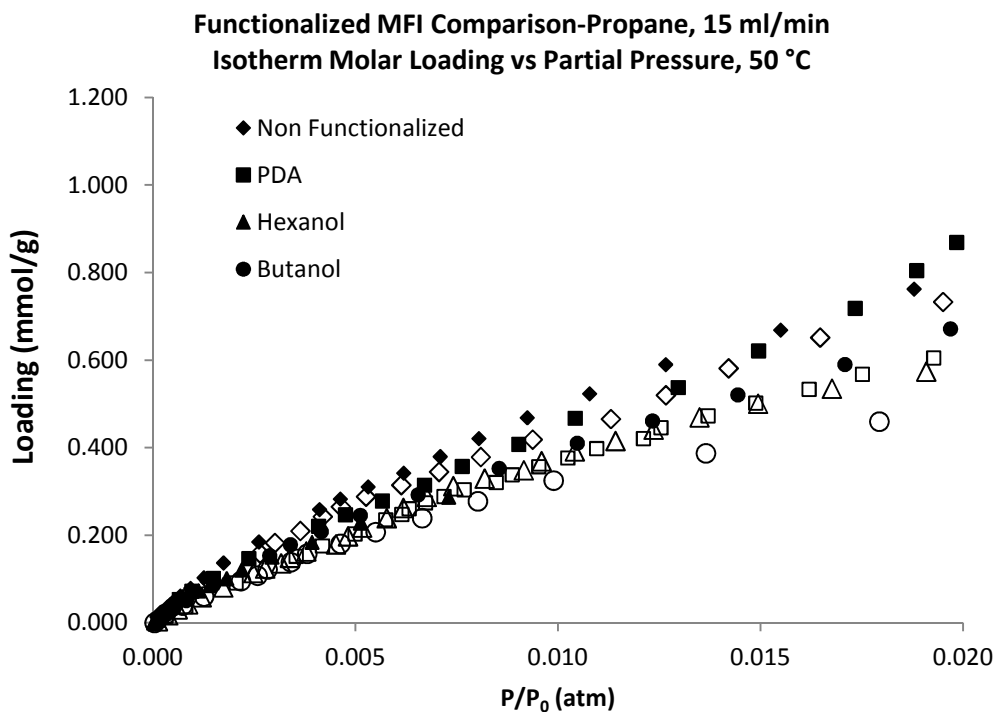


Figure B.7 Comparative Propane Isotherms at 5 ml/min & 15 ml/min, 50 °C. 5 ml/min (open shapes) & 15 ml/min (filled shapes) showing agreement between the two different flow rates

B.5 Conclusions

The above data suggest that there is a relationship between functionality and MFI-hydrocarbon interactions. Both the equilibrium and diffusional behavior are affected by the functionalization of the MFI framework. As may be seen from the isotherms the affinity for the hydrocarbons was reduced by functionalization although the differences from the bare sample were relatively modest. This effect is more pronounced for the heavier sorbates. This phenomenon is also demonstrated numerically in the tabulated data. The three hydrocarbons all showed a reduced Henry constant between the non-functionalized MFI material and the three functionalized samples. A more thorough analysis would be needed in order to establish the quantitative effects of the various functional groups.

In the functionalized samples the diffusivity of butane is reduced while the diffusivity of ethane is increased. Propane shows both trends depending on the functional groups.

BIOGRAPHY OF THE AUTHOR

Adam Vidoni was born in Denver, Colorado on April 16, 1982. Growing up in Denver, he graduated from Thomas Jefferson High School (Denver, CO) in 2000. After high school, he attended Bucknell University in Lewisburg, Pennsylvania and graduated in 2004 with a Bachelor of Science in Chemical Engineering degree. He was employed by Mitsui & Co., Engineering Polymers Division from 2005 to 2007 in New York, New York. He entered the Chemical Engineering graduate program at the University of Maine in the fall of 2007. As a part of his research, Adam was a research intern for ExxonMobil in Annandale, NJ in the summer of 2008. He is a candidate for the Doctor of Philosophy degree in Chemical Engineering from the University of Maine in December, 2011.

REFERENCES

1. D.L. MacClean, S. Lerner, V. Malik. *Gas Sep. & Pur.*, 1987: 77.
- 2 Breck, D.W. *Zeolite Molecular Sieves-Structure, Chemistry, and Use*. New York City: John Wiley & Sons, 1977.
- 3 R.R.Chance and E.W.Corcoran *Diffusion Fundamentals 1*, Leipzig University (2005)
- 4 T.E. Clark, H.W. Deckman, D.M. Cox and R.R. Chance *J. Membrane Sci.* **230**, 94 (2004)
- 5 H.W. Deckman, R. Chance, E. Corcoran, G.De Martin, S.Reyes, N.Hedin, C.Yoon and T.Clark *North American Membrane Society, Annual Meeting* (2006)
- 6 R.R.Chance 229th ACS National Meeting, San Diego, CA, Mar 13-17 (2005)
- 7 R.M.Milton U.S.Patents 2,882,243 and 2,882, 244 (1959) to Union Carbide inc.
- 8 D.W.Breck, W.G.Eversole, R.M.Milton and T.B.Reed *J.Am. Chem.Soc.* **78**, 5963 (1956)
- 9 C.W. Skarstrom U.S. Patent 2,944,627 (July 12, 1960) to Esso Research and Engineering
- 10 P.G.de Montgareuil and D.Domine U.S. Patent 3,155,468 (1964) to Air Liquide.
- 11 W.J. Asher et al. U.S. Patent 3,070,542 (1962) to Esso Research and Engineering
- 12 W.J.Asher, M.L.Campbell, W.R. Epperly and J.L. Robertson *Hydrocarbon Processing* **48** (1) 134 (1964)
- 13 Ch. Baerlocher, L.B.McKusker, D.H.Olson *Atlas of Zeolite Structures* (6th Edition), Elsevier Science, Amsterdam (2007)
- 14 G.T.Kokotailo and W.M.Meier p.33 in *Properties and Applications of Zeolites* R.P.Townsend, ed. Special Publ. No. 33 Chem. Soc. London (1979)
- 15 H.Gies *Z.Kristallogr.* **175**, 93-104 (1986)
- 16 R.M.Barrer *Zeolites and Clay Minerals as Sorbents and Molecular Sieves* Academic Press, London (1978).
- 17 J.Cejka, H.van Bekkum, A.Corma and F.Schueth *Introduction to Zeolite Science and Practice* Chapter 2 *Studies in Surface Science and Catalysis* **168** Elsevier,

-
- Amsterdam, (2007).
- 18 Caro, J. *Adsorption*, 2005: 215-227
- 19 C. Cheng, T. Bae, B. McCool, R. Chance, S. Nair, C. Jones *J. Phys. Chem C*, **112**, 3543-3551 (2008)
- 20 D.M.Ruthven and S.C.Reyes *Microporous Mesoporous Mats.* **104**, 59-66 (2007)
- 21 D.H.Olson U.S.Patent 6,488,741 (Dec. 3, 2002)
- 22 D.H.Olson, M.A.Cambor, L.A.Villaescusa and G.H.Kuehl *Microporous Mesoporous Mats.* **67**, 27-33 (2004)
- 23 J.van den Bergh *PhD Thesis*, University of Delft (2010)
- 24 J.van den Bergh, W.Zhu, J.Gascon, J.A.Moulijn and F.Kapteijn *J.Membrane Sci.* **316**, 35- 45 (2008)
- 25 J.van den Bergh, A.Tihaya and F.Kapteijn *Microporous Mesoporous Mats.* **132**, 137-147 (2010).
- 26 W.Zhu, F.Kapteijn, J.A.Moulijn, M.C.den Exter and J.C.Jansen *Langmuir* **16**, 3322-3329 (2000).
- 27 N.Hedin, G.J.DeMartin, W.J.Roth, K.G.Strohmaier and S.C. Reyes *Microporous Mesoporous Mats.* **109**, 327-334 (2008)
- 28 R.Krishna and J.M.van Baten *Sep.Purif. Technol.* **61**, 414-423 (2008)
- 29 R.Krishna and J.M.van Baten *Microporous and Mesoporous Mats.* **137**, 83-91 (2011)
- 30 S.E.Jee and D.S.Sholl *J.Am.Chem.Soc.* **131**, 7896-7904 (2009).
- 31 T.Tomita, K.Nakayama and H.Sakai *Microporous mesoporous Mats.* **68**, 71, (2004)
- 32 M.J. den Exter, J.C.Jensen and H.van Bekkum in *Zeolites and Related Microporous Material: State of the Art 1994.* **84**, 1139 (1994)
- 33 W.Zhu, F.Kapteijn and J.A.Moulijn *Chem. Commun.* 2453, (1999) Adsorbents
- 34 D.M.Ruthven and S.Reyes *Microporous Mesoporous Mats* **104**, 59-66 (2007)
- 35 A F.Kapteijn, W.J.W.Bakker, J.van der Graaf, G.Zheng, J.Poppe and J.A.Moulijn *Catal. Today* **25**, 213, (1995)

-
- 36 A.J. van den Bergh, W. Zhu, J. Gascon, J.A. Moulijn and F. Kapteijn *J. Membrane Sci.* **316**, 34-45, (2008).
- 37 A. Neimark and P. Ravikovitch, *Langmuir*, **13**, 5145-5160 (1997)
- 38 S. Himeno, T. Komatsu, S. Fujita, T. Tomita, K. Suzuki, K. Nakayama and S. Yoshida *Microporous Mesoporous Mats.* **98**, 62-69 (2007)
- 39 D.M. Ruthven *Principles of Adsorption and Adsorption processes* p.70, John Wiley, New York
- 40 R.M. Barrer and J.A. Davies *Proc. Roy. Soc. London* **A320**, 289 (1970)
- 41 F.R. Siperstein and A.L. Myers, *AIChE Jl.* **47** 1141-159 (2001)
- 42 P. Wu, A. Debebe and Y.H. Ma *Zeolites*, **3**, 118-122 (1983)
- 43 M.J. den Exter, J.C. Jansen, H. van Bekkum, A. Zikanova, J. Dubsky and M. Kocirik *Coll. Czech. Chem. Commun.* **62**, 1-14 (1997).
- 44 M. Eic and D.M. Ruthven *Zeolites* **8**, 472 (1988)
- 45 J. Crank *Mathematics of Diffusion* p73 Oxford University Press, London (1956)
- 46 D.M. Ruthven, S. Brandani and M. Eic in *Molecular Sieves Vol 7*, 45- 84 H.G. Karge and J. Weitkamp eds. Springer Verlag, Berlin, Heidelberg (2008)
- 47 D.M. Ruthven and S. Brandani, "Measurement of Diffusion in Porous Solids by ZLC Methods", pp. 187-212, in *Recent Advances in Gas Separation by Microporous Ceramic Membranes*, N. K. Kanellopoulos, Ed., Elsevier, Amsterdam (2000)
- 48 J. Kärger and D.M. Ruthven *Diffusion in Zeolites and other Microporous Solids* pp328- 333 John Wiley, New York (1992)
- 49 S. Brandani and D.M. Ruthven *Adsorption* **2**, 133-143 (1996).
- 50 M. Eic and D.M. Ruthven *Zeolites* **8**, 472 (1988)
- 51 D.M. Ruthven and M. Eic *Am. Chem. Soc. Symp. Ser.* **368**, 362 (1988)
- 52 D.M. Ruthven and S. Brandani, pp. 187-212, in *Recent Advances in Gas Separation by Microporous Ceramic Membranes*, N. K. Kanellopoulos, Ed., Elsevier, Amsterdam (2000).
- 53 P. Kortunov, C. Chmelik, J. Kärger, R.A. Rakoczy, D.M. Ruthven, Y. Traa, S. Vasenkov and J. Weitkamp; *Adsorption* **11**, 235-244, (2005)

-
- 54 L. Heinke, P. Kortunov, D. Tzoulaki, J. Kärger *Adsorption* **13**, (2007) 215-223
- 55 D.M.Ruthven, L.Heinke and J.Kaerger *Microporous Mesoporous Mats.* **132**, 94-102 (2010).
- 57 F.Brandani and D.M.Ruthven *Adsorption* **11**, 31-35 (2005)
- 58 J.Kärger and D.M.Ruthven Ch. 12 *Diffusion in Zeolites and other Microporous Solids* John Wiley, New York (1992)
- 59 D.M. Ruthven *Microporous and Mesoporous Mats.* Submitted for publication Oct 25 2010
- 60 S.C.Reyes, K.V.Venkatesan, G.J.DeMartin, J.H.Sinfelt, K.G.Strohmaier, J.G.Santiestebau, US Patent 730,142, May 4, 2004
- 61 S.C.Reyes, V.K.Krishnan, G.J.DeMartin, J.H.Sinfelt, K.G.Strohmaier, J.G.Santiestebau, US Patent 6.733,572, May 11, 2004
- 62 D.H.Olson US Patent 6,488,741, Dec3, 2002
- 63 R.Krishna and J.M.van Baten *Sep.Purif. Technol.* **61**, 414-423 (2008)
- 64 R.Krishna and J.M.van Baten *Microporous and Mesoporous Mats.* **137**, 83-91 (2011)
- 65 N.Hedin, G.J.DeMartin, K.G.Strohmaier and S.C. Reyes *Microporous Mesoporous Mats.* **98**, 182-188 (2007)
- 66 D.M.Ruthven, S.Brandani and M.Eic in *Molecular Sieves* Vol 7 , 45- 84 H.G.Karge and J.Weitkamp eds. Springer Verlag, Berlin, Heidelberg (2008)
- 67 H.Yucel and D.M.Ruthven *J.Chem. Soc. Faraday Trans. I* **76**, 60-70 (1980)
- 68 J.D.Eagan and R.B.Anderson *J.Colloid and Interface Sci.* **50**, 419-433 (1975)
- 69 J. Caro, J.Kaerger, G.Finger, H.Pfeifer and R.Schoellner *Z.Phys. Chem,((Leipzig)* **256**, 698 (1975) and **257**, 903 (1976).
- 70 Z.Xu, M.Eic and D.M.Ruthven *9th International Zeolite Conf.*, Montreal (1992) Proceedings Vol.2 p147-155 R. von Ballmoos, J.B. Higgins and M.M.J. Treacy eds., Butterworth, Stoneham MA (1993)
- 71 J.Kärger and D.M.Ruthven *Diffusion in Zeolites and other Microporous Solids* pp 107-111, John Wiley, New York (1992)

-
- 72 A.P.Guimaraes, A.Moeller, R.Staudt, D.C.S.de Azvedo, S.M.P. Lucena and C.L.Cavalcante
Adsorption **16**, 29-36 (2010).
- 73 Doelle, H.-J.; Heering, J.; Riekert, L.; Marosi, L. *J. Catalysis*. **71**, 27-40 (1981)
- 74 Eic, M.; Ruthven, D. M. Intracrystalline Diffusion of Linear Paraffins and Benzene in Silicalite Studied by the ZLC Method. In *Zeolites: Facts, Figures, Future*; Jacobs, P. A., Santen, R. A., Eds.; Elsevier: Amsterdam, **49**, p 897 (1989)
- 75 R.E. Richards and L.V.C. Rees, *Langmuir* **3**, 335 (1987)
- 76 J. Caro, M. Bülow, W. Schirmer, J. Kärger, W. Heink, and H. Pfeifer, *J. Chem Soc. Faraday Trans. I* **81**, 2541 (1985)
- 77 J. Kärger, W. Krause and H. Pfeifer, *Z. Phys. Chem. (Lepzig)* **264**, 838 (1982)
- 78 D.T Hayhurst and A. Paravar, *Zeolites* **8**, 27 (1988)
- 79 K. Jobic, M. Bee, and A.J. Dianoux, *J. Chem. Soc. Faraday Trans. I* **84**, 2347 (1988)
- 80 M. Bülow, H. Schlodder, L.V.C. Rees, and R.E. Richards, in *Proc. 7th Internat. Conf. on Zeolites*, Tokyo (1986)
- 81 N. Van Den Begin, L.V.C. Rees, J. Caro, and M. Bülow, *Zeolites* **9**, 287 (1989)